20

NORTHROP

Research and Technology Center

(20)

SECURITY CLASSIFICATION OF THIS PAGE (When Data Entered)

REPORT DOCUMENTATION PAGE

READ INSTRUCTIONS BEFORE COMPLETING FORM

1. REPORT NUMBER
2. GOVT ACCESSION NO.
3. RECIPIENT'S CATALOG NUMBER

4. TITLE (and Subtitle)

(6) OPTICAL COATINGS 2-6 MICRONS

5. TYPE OF REPORT & PERIOD COVERED

(9) Final Technical Report, June 1976-through December 1977

6. PERFORMING ORG. REPORT NUMBER

(14) NRTC-78-13R

7. AUTHOR(s)

(10) P./Kraatz

8. CONTRACT OR GRANT NUMBER(s)

(15) N00123-76-C-1321

9. PERFORMING ORGANIZATION NAME AND ADDRESS

Northrop Corporation Northrop Research and Technology Center One Research Park Palos Verdes Peninsula, California 90274

10. PROGRAM ELEMENT, PROJECT, TASK AREA & WORK UNIT NUMBERS

11. CONTROLLING OFFICE NAME AND ADDRESS

DARPA (MATS) 1400 W. Wilson Blvd. Arlington, VA 22209 Att'n. Capt. H. Winsor

12. REPORT DATE

(11) 7 April 1978

13. NUMBER OF PAGES

181 (12) 195 p.

14. MONITORING AGENCY NAME & ADDRESS (if different from Controlling Office)

U. S. Naval Weapons Center Code 3815 China Lake, CA 93555

Att'n. Dr. R. S. Hughes

15. SECURITY CLASS. (of this report)

Unclassified

15a. DECLASSIFICATION/DOWNGRADING SCHEDULE

16. DISTRIBUTION STATEMENT (of this Report)

Distribution Unlimited.

DISTRIBUTION STATEMENT A
Approved for public release; Distribution Unlimited

17. DISTRIBUTION STATEMENT (of the abstract entered in Block 20, if different from Report)

DDC RECEIVED APR 25 1978 B

18. SUPPLEMENTARY NOTES

19. KEY WORDS (Continue on reverse side if necessary and identify by block number)

optical coatings, optical materials, infrared laser windows, coating absorption, coating crystal structure, coating preferred orientation, substrate crystal orientation, substrate absorption, substrate surface absorption, substrate surface chemistry, substrate surface finish, optical polishing, laser calorimetry, x-ray diffraction, Auger electron spectroscopy, HF environment.

20. ABSTRACT (Continue on reverse side if necessary and identify by block number)

This report presents and discusses results of an investigation of optical coating materials for the mid infrared with emphasis on the 3.8 μm (DF) and 5.3 μm (CO) wavelength regions. A data base of experimental information generated under the contract, comprising crystal structure and preferred orientation, deposition parameters, relative growth rates, refractive indices, and absorption coefficients of ten candidate optical thin film materials is presented. This listing of properties is utilized to identify five coating materials, ThF_4, PbF_2, →

next page

DD FORM 1 JAN 73 1473 EDITION OF 1 NOV 65 IS OBSOLETE

SECURITY CLASSIFICATION OF THIS PAGE

20. Abstract (continued)

SiO, ZnSe, and ZnS for intensive study and application in fabricating laser optics. Intensive studies include optimization of deposition conditions, absorptance and film thickness, effects of polycrystalline substrates upon coating structure and absorptance, and determination of survivability in an HF environment. Results of these investigations and of measurements of absorptance, structure, and preferred orientation in multilayer coatings employing these materials are presented and discussed. In addition, the relative merits of CaF_2 and SrF_2 substrates, critical chemical characteristics of substrate surfaces and cleaning procedures, and effects of substrate crystallographic orientation upon single layer film properties are discussed in detail.

OPTICAL COATINGS
2 - 6 MICRONS

Final Technical Report
7 April 1978

Prepared For

U. S. Naval Weapons Center
Code 3815
China Lake, California 93555

Under Contract No. N00123-76-C-1321
Sponsored by DARPA (MATS)
1400 Wilson Blvd.
Arlington, VA 22209

By

Northrop Corporation
Northrop Research and Technology Center
One Research Park
Palos Verdes Peninsula, California 90274

TABLE OF CONTENTS

TABLE OF CONTENTS (Cont.)

LIST OF ILLUSTRATIONS

LIST OF ILLUSTRATIONS (Cont.)

LIST OF TABLES

LIST OF TABLES (Cont.)

LIST OF TABLES (Cont.)

LIST OF TABLES (Cont.)

LIST OF TABLES (Cont.)

PREFACE

This final Technical Report describes work performed on Contract Number N00123-76-C-1321, entitled "Optical Coatings 2 - 6 Microns" during the period from 1 June 1976 to 1 December 1977.

The following investigators performed work on the contract and/or contributed to this report: Mr. M. Evangelista, Research Assistant; Mr. S. J. Holmes, Member Senior Technical Staff; Mr. A. Klugman, Member Senior Technical Staff; Dr. P. Kraatz, Principal Investigator; Mr. F. Kuller, Research Assistant; Dr. J. M. Rowe, Member Senior Technical Staff; Dr. J. L. Stanford, Code 3818, Michelson Labs. NWC.; Mr. F. W. Towns, Research Assistant.

This report covers all work performed and results obtained under the contract, whether previously reported or not.

1.0 INTRODUCTION

The past five years has seen a rapid increase in research on growth and properties of bulk and thin film materials for application to infrared laser optical components. This research has been primarily directed toward control of material absorptance, homogeneity, chemical purity, and mechanical properties by more or less empirical means. Very little research has been directed toward elucidating structure or growth characteristics and relating them to physical properties of bulk crystalline materials or thin films.

From published data,[1-6] it is evident that thin films not only differ widely from bulk materials in their principal parameters, but also show considerable variations in properties according to conditions used for their preparation. Moreover, it is becoming increasingly clear that these variations originate to a large extent in structural differences,[4, 6] which in turn are related, to the numerous factors involved in film deposition.

Much of the recent and current research in the field of optical thin films indicates that key physical characteristics may be controlled within limits acceptable for medium power laser use merely by careful standardization of preparation procedures. Selection of the best procedure is invariably based on experiments correlating directly to the physical property of interest with variables such as deposition rate, total ambient pressure, substrate preparation, and temperature. Such correlations, however useful from a practical standpoint, cannot provide meaningful physical interpretations, nor lead finally to optimization of film properties for high power laser applications of the present and future. In the absence of structural data, these efforts can become empirical exercises based largely on intuition and extrapolation from well known conditions and behavior.

The primary objective of this program was to generate a data base comprising crystal structure, deposition conditions, growth characteristics, optical properties, and environmental tolerance of ten candidate optical thin film materials for the DF (3.8 μm) and CO (5.3μm) wavelength regions, sufficient to identify optimum materials and processes for fabrication of coated optics for high power DF and CO lasers. As a "parallel technology" effort supported by DARPA, this program was formulated in a manner to compliment and supplement the technology being developed on other fluoride laser window programs. Data from this effort pertaining to thin film coating and substrate optical properties have been provided in a timely manner for use in these parallel programs. In addition, the state-of-the-art samples which were fabricatad, evaluated and tested as part of this program can be made available at the discretion of the Defense Advanced Research Projects Agency, to various government laboratories for additional testing and evaluation. One set of such samples was provided to Dr. John Detrio of UDRI for damage testing during September, 1977.

Secondary objectives of the program included determining effects of the crystallographic orientation of the substrate upon thin film refractive index, absorptance, crystal structure, and preferred orientation, identification of critical chemical characteristics of substrate surfaces and procedures used to clean them, and effects of polycrystalline substrates and multilayer coating designs upon film structure and properties.

The procedures employed and results attained during the contractual effort (1 June 1976 to 1 December 1977) to achieve these objectives are described in detail in this report. The report itself is divided into seven sections. Section 2 covers all experimental methods and techniques utilized in the investigation including x-ray diffraction, substrate polishing and cleaning, coating deposition methods and materials, optical properties determination, and absorptance measurement by laser calorimetry.

Section 3 embodies the major thrust of the report, the experimental results. It is divided into five subsections covering substrate structure, orientation, and surface finish, substrate absorptance, structure and properties of coating materials, deposition techniques and their optimization for selected materials, results of absorptance vs. film thickness investigations (βL vs. L), effects of polycrystalline substrates on coating structure and properties, tolerance of various coatings to an HF environment, and structure and properties of multilayer coatings. Section 3.3 is a focal point of the report for optical designers, laser engineers, optical coaters, and materials scientists, in that it provides a self-contained coating materials reference source comprising composition, structure, preferred orientation, refractive index, absorptance, HF environment tolerance, and comments on deposition and applications of the ten coating materials studied at two wavelengths (3.8 μm and 5.3 μm).

Section 4 is a summary in tabular or matrix format, of the coating structures preferred orientations, refractive indices, absorption coefficients, and relative growth rates determined under the program. It should be of major interest to designers, engineers, and coaters desiring a quick reference for comparison of materials for the two wavelength regions. Although it is less detailed than section 3.3, much of the essential information is retained in the summary, with some comments on choices of materials for specific purposes.

Conclusions and recommendations based on the information gathered are presented in section 5 and references are cited in section 6. Section 7 is an appendix consisting of the text of a technical paper on CaF_2 substrate surface chemistry and absorptance, employing parallel Auger electron spectroscopy and laser calorimetry studies at 2.7 μm (HF), 3.9 μm (DF), and 5.3 μm (CO) wavelengths.

2.0 EXPERIMENTAL PROCEDURES

The specific laboratory procedures and experimental methods employed in this investigation are described in this section in sufficient detail to allow verification by other investigators. Most of the techniques are well established, so that exhaustive discussion is not required.

2.1 X-Ray Determination of Composition, Structure, and Preferred Orientation.

Standard diffractometer (powder) patterns were employed in the determination of composition and structure of coating raw materials as well as for study of structure and preferred orientation of the same materials, deposited as thin films on CaF_2 and SrF_2 substrates. For films in the range of physical thickness encountered in this investigation (6000-10,000Å), x-rays provide information on the entire thickness of the film as well as yielding diffraction peaks from the substrates. Electron diffraction, using either transmission or reflection techniques, provides information on film structure complementing that obtained from x-ray.[7] Transmission electron diffraction (TEM) would provide the greatest amount of information on the structure and orientation of the films studied under the program. However, this method requires removal of films from substrates, with minimal damage to the films.[7] Since all of the coating materials studied adhere very strongly to the substrates, which are not readily soluble, separation of films from substrates for TEM analysis is not readily achieved. Reflection electron diffraction (RED) , with the electron beam incident at a glancing angle[8] is an effective technique for this situation which has been employed previously.[6] Unfortunately, it only provides information on material near the top surface of the film and is thus of limited utility in a study of this type. Hence we relied exclusively upon x-ray diffraction in the present work.

The x-ray machine employed is a General Electric XRD-6 diffractometer, equipped with copper or chromium target x-ray tubes and appropriate auxiliary equipment, including a pole figure device for obtaining more detailed information on preferred orientation in polycrystalline materials and a Laue camera for determining the orientation of single crystals. Radiation from a copper-target tube operated at 35 kV, 18 mA and filtered through nickel foil was used in all cases; nominal wavelength is $CuK_{\alpha 1}$ or 1.5405Å. A scan speed of 2°(2θ) per minute was employed with 1° soller slits at the tube, a 0.1° slit at the detector and a counter time constant of 0.5 sec, in a G.E. XRD-6 x-ray diffractometer. When greater intensity was required for poorly crystallized films, a 3° slit at the tube and 0.2° at the detector were employed.

To eliminate misidentification of spurious peaks arising from the substrate as arising from the various thin film materials, uncoated substrates were run in the diffractometer. The predominant crystallographic orientation of the central area of polycrystalline substrates was also established in this way. Orientation of single crystal substrates was determined by the back reflection Laue method.

2.2 Substrate Surface Preparation

All of the 1.00 inch and 1.52 inch diameter single crystal CaF_2 and SrF_2 samples were polished and characterized using Nomarski microscopy. The optical finishing technique is basically a three-step process in which the window substrate is initially ground flat on a cast iron lap using 9 μm Al_2O_3 abrasive in a water vehicle. To remove the light scratches and pits remaining from the grinding operation, the window substrate is given a rough polish on a pitch lap with 1 μm Al_2O_3 (Linde C) in a water vehicle. The surface is considered ready for the final polishing when visual inspection with a 7x loupe reveals that all grinding marks have been removed.

The window is then finished to the required flatness and surface quality on a medium hard pitch lap (Swiss pitch #73) with 0.3 μm Al_2O_3 (Linde A) in de-ionized water using a recirculating slurry system (a modified bowl feed technique). The window is polished until optimum surface finish is obtained as judged by Nomarski microscopy examination.

In a previous study,[6] it was found that when substrates having (100), (110), and (111) orientations are polished simultaneously on the same, effectively rigid block, the (100) and (110) surfaces polish well and the (111) surface exhibits appreciable scratching. It was postulated that the observed differences in surface quality resulted from different rates of material removal from the (111) and (100) or (110) surfaces, the rate of removal from the (111) surface being most rapid, due to the natural cleavage in this plane. In that study, segregating and blocking substrates according to orientation was suggested as a solution to this problem.[6] This procedure was followed in the present work and results (sec. 3.1) indicate that the problem was eliminated.

2.3 Substrate Cleaning and Surface Chemistry

Cleaning of substrate surfaces following polishing and preceding coating is a critical step in fabrication of a coated optical component. Effective removal of contaminant materials from substrate surfaces is necessary to (1) eliminate barriers to thin film adhesion, (2) prevent nucleation of film defects (inclusions, pinholes) at particulate contaminant sites, and (3) reduce overall absorptance of the coating/substrate interface. Two separate and distinct processes may be used to achieve this end: (1) solvent cleaning and (2) glow discharge cleaning *in situ* in the coating chamber. A solvent cleaning procedure which had been found satisfactory in previous work[4, 6], was employed in the present studies, with very minor modification. This procedure is summarized below:

Solvent Cleaning Procedure

(1) Soak in acetone (30 minutes).
(2) Rinse with warm tap water.
(3) Wash with warm tap water and liquid detergent.
(4) Rinse with distilled water.
(5) Rinse with reagent grade alcohol.
(6) Blow dry with nitrogen gas.

The minor modification, employed consistently prior to calorimetric absorptance measurement, involved the substitution of lens tissue, drawn slowly across the substrate surface wet with a few drops of reagent grade methanol, for steps 5 and 6.

Glow discharge cleaning in the coating system immediately prior to the film deposition was employed as a final cleaning process in a majority of the depositions carried out under this program. Details of the procedure are summarized below:

Glow Discharge Cleaning Procedure

(1) Solvent clean, as above, place in vacuum chamber.
(2) Pump out chamber to $\sim 5 \times 10^{-6}$ Torr (1 Hr.). Heater on (200° C).
(3) Glow discharge 3 minutes at 200 mA in 2×10^{-2} Torr of Argon.
(4) Evaporate coating material when chamber pressure has returned to $\sim 5 \times 10^{-6}$ Torr (< 1 minute).
(5) Heater off. Valve shut. (10^{-4} Torr range).
(6) Sample cools to ambient (1 Hr.).
(7) Remove sample from glow discharge chamber, place in laser calorimeter following equilibration to room temperature (20-30 min.).
(8) Pump out calorimeter.

To test the effects of this procedure upon substrate surface absorptance, step 4 (coating deposition) was eliminated and absorptance was measured.[9] These measurements indicated a strong decrease in general, but conflicts among the results and lack of a satisfactory explanation for them led to a more detailed investigation. This investigation comprised parallel Auger

Electron Spectroscopy and laser calorimetry studies on single crystal CaF_2 surfaces oriented parallel to (110) and (111). Results were presented at the Topical Meeting on Optical Phenomena in Infrared Materials (December, 1976) sponsored by the Optical Society of America and will be submttted to Applied Optics for publication. A copy of the manuscript is appended to this report, detailing procedures and results. In general, it was found that absorptance of substrates subjected to glow discharge cleaning varied significantly with (1) the ambient medium (Argon or oxygen) employed in the chamber, (2) time of exposure to external atmosphere (air) between glow discharge and absorptance measurement, and (3) crystallographic orientation of the substrate. These effects are still not perfectly understood. Hence, in later stages of the program, this cleaning operation was eliminated from some series of coating depositions in order to isolate other variables (e.g. β vs. L in section 3.4.2).

2.4 Coating Deposition and Materials

Successful deposition of thin film coatings requires careful control of the evaporation technique and the associated parameters. Currently, thermal evaporation in a high vacuum is the technique that is most frequently used to deposit film coatings. Thermal evaporation in a high vacuum has been extensively developed, and two of the most common modes of evaporation are resistance heating and electron-beam heating. Both modes of evaporation are widely used, and it is relatively easy to produce good optical coatings. In spite of this favorable aspect, results of investigations of the properties of evaporated films have not always shown the expected consistency. The cause of these discrepancies probably does not lie in the method of evaporation itself, but rather in the lack of control of the many experimental parameters.

Evaporation from directly heated crucibles is widely and successfully used. By far the simplest and most common method is to make use of a boat of refractory metal which performs the dual function of a crucible and, when an electric current is passed through it, a heater. The selection of crucible materials, shapes, and designs is quite extensive. A great variety of crucibles suited to individual materials is produced and sold by specialized companies. Baffles sources, for example, are used to evaporate and minimize the danger of spitting of SiO. Materials like ZnS can be evaporated from a howitzer source which is particularly useful in the infrared as its capacity can be very great.[10]

However, it has been found that some materials and to some extent the rather stable fluoride materials may react with the crucible used for their evaporation and this reaction may result in films having appreciable absorption.[11] The chance of a crucible reaction causing the deposited films to be absorbing is even greater for the oxide materials. For these materials there is also a good probability that dissociation causing absorption occurs due to overheating, especially if the evaporations are performed at very high temperatures to obtain high deposition rates.

If the material does not decompose at the evaporation temperature, then there are two main factors which govern the choice of crucible and heating method. The first is the temperature itself, and second is the tendency of the material to react with the crucible material. Materials which sublime at not too high a temperature can be heated in a crucible of alumina or even fused silica by radiation from above. A tungsten spiral, just above the surface of the material, can produce enough heat to vaporize it. Tantalum, molybdenum, and tungsten are all suitable for the manufacture of crucibles. Tantalum is the most frequently used and a wide range of materials can be evaporated from it. However, some materials react with it, (cerium oxide for example) and with molybdenum, and require the less reactive, but

rather more difficult tungsten. PbF_2 will be reduced by hot tantalum, tungsten, or molybdenum crucibles, and it has to be evaporated from platinum or ceramic crucibles.

A method of evaporation which avoids many of the difficulties associated with directly and indirectly heated crucibles is electron-beam heating. In this method, the evaporant is contained in a suitable crucible or hearth of electrically conducting material, and is bombarded with a beam of electrons to heat and vaporize it. The portion of the evaporant which is heated is in the center of the exposed surface, and there is a reasonably long thermal conduction path through the evaporant to the hearth, which can be held at a rather lower temperature than the melting point of the evaporant without prohibitive heat loss. This means that reaction between the evaporant and hearth can be inhibited; the hearth is frequently water-cooled to ensure this. Materials as reactive as silicon can be evaporated in this manner. The electrons are emitted by a hot tungsten filament and are attracted to the evaporant by a potential of several kilovolts. If the power is limited to the order of a kilowatt or so, it will be necessary to use an electrostatic or electromagnetic field to focus the electron-beam to a very small spot size in order to achieve reasonable evaporating rates. In this case, the temperature of the evaporant is extremely high and some evaporants can decompose at these elevated temperatures, causing absorption to appear in the condensed films. Decomposition of easily dissociating compounds can be prevented by increasing the spot size and increasing the power to achieve a reasonable rate of evaporation. However, this requires much high power approaching 10 kW, and possible disadvantages in this are the charging of the substrates and ionization of the evaporant material.[2] Therefore, some experimentation is required to establish the desired deposition rates which will allow the deposition of low absorbing films. A considerable amount of material has been written on electron-beam technology. Airco-Temescal has written a very informative thirty page booklet on this subject.[12]

The preparation of the materials to be evaporated is of considerable importance for the deposition of high quality optical coatings. Crucial properties are purity, gas content, and grain size. It is highly recommended that one use vacuum sintered and outgassed materials or even pieces of solid crystals to avoid gas outbursts and spattering during the evaporation process. Powders are normally not suitable, since they have too much adsorbed gas which is desorbed during the heating and leads to pressure rise and spattering of the materials.

The quality of the optical coating materials depends on the purity of the starting materials and the method of preparation. Since impurities can increase optical absorption as well as initiate a variety of macroscopic or structural defects, commercial materials of highest purity must be used. The purity is frequently given in percentage of the main material, up to 99.9999%; the remainder consisting of unknown impurities. Although this number indicates ultrapure material, it still contains a great number of impurity atoms per cubic centimeter. It is, therefore, necessary to know the kind and concentration of all impurities. A variety of methods exist for the detection and determination of impurity concentration.[13] The most important are x-ray, optical absorption, and mass spectroscopy. Knowing the impurities present, it is essential to determine which ones actually influence the respective properties. These impurities must be removed or at least reduced in concentration.

Coating materials of desired purity are only available when a material has attained broad application. In most cases, it has to be purified; this is quite an involved operation. Drying is very essential if the material is contaminated by water in any form. The effects of absorbed moisture are so pronounced that they completely mask the normal aging and the basic loss mechanism. Absorbed or trapped water or hydroxyl ions can be eliminated by drying under vacuum and slowly increasing the temperature to the

level at which the loosely bound water is removed by diffusion and evaporation. True oxide or hydroxide compounds in solid form are not removable by this means, but require chemical reaction in some form, (i.e., scavenging by a reactive atmosphere).

Coating materials employed in the program are listed and identified as to source and nominal purity in Table I. In all cases, these materials represent the highest purity commercially available. No attempt was made to further purify any of these materials. In the vacuum deposition of thin films by an evaporation process, knowledge of the substrate temperature and its control is often very important. In fact, the substrate temperature plays an especially important role for the whole condensation process. It controls the surface mobility of the condensing atoms or molecules and determines the degree of disorder of the growing film. Film adhesion and durability are improved by heating the substrates prior to and during deposition. Of paramount importance is the removal of adsorbed gases from the substrate. Thus water removal is one of the main reasons for heating substrates prior to deposition.

In practice a wide range of substrate temperatures is employed. The deposition of metal oxides requires substrate temperatures of approximately 300°C to obtain optimal film properties.[11] On the other hand, zinc sulfide should be deposited at a substrate temperature below 180°C to provide a compromise between reevaporation and film durability.[14] If a low substrate temperature is required to obtain a desired film property such as minimal scattering, and if this temperature is too low to remove water vapor from the substrate, then the substrate can be preheated to remove the water vapor and subsequently cooled to the required deposition temperature. Glow discharge cleaning can also be used in this situation.

TABLE 1. COATING MATERIALS

Al_2O_3	Random Chunks of UV-Grade Sapphire, Union Carbide Corporation, San Diego, Calif.
LaF_3	Hot-Pressed Tablets, 99.9% Purity, Balzers High Vacuum Corp., Santa, Ana, Calif.
MgF_2	Fused Granules, 99.99% Purity, Balzers High Vacuum Corp., Santa Ana, Calif.
MgO	Hot-Pressed Tablets, 99.95% Purity, Balzers High Vacuum Corp., Santa Ana, Calif.
PbF_2	Fused Granules, 99.99% Purity, Balzers High Vacuum Corp., Santa Ana, Calif.
SiO	Linde Select Grade, R. D. Mathis Company, Long Beach, California.
SrF_2	Random Chunks, Optical Grade, EMCO Sales, Anaheim, California.
ThF_4	Fused Granules, 99.9% Purity, CERAC, Milwaukee, Wisconsin.
ThF_4	Fused Granules, 99.9% Purity, Balzers, High Vacuum Corp., Santa, Ana, Calif.
ZnS	Hot-Pressed Tablets, 99% Purity, Balzers High Vacuum Corp., Santa Ana, Calif.
ZnSe	Granules, 99.99% Purity, Balzers High Vacuum Corp., Santa Ana, Calif.
ZnSe	Random Chunks, CVD, Ratheon Research Division, Waltham, Massachusetts.

Since the index of refraction of the films and film structure are a function of substrate temperature, it is important that both substrates and monitoring pieces be maintained at a uniform and constant temperature and throughout the deposit cycle. A typical substrate heater is described by Mattauch[15] and the measurement and control of substrate temperature is discussed by Hanson, et. al.[16]

The objective in vacuum evaporation is nearly always to deposit films to certain specifications. If the specification is primarily one of thickness, it is sufficient to determine when the accumulated deposit has reached the desired value so that the deposition process can be terminated. However, intensive film properties such as density, stress, crystallinity, and index of refraction depend on the rates at which the evaporant and residual gas molecules arrive at the substrate. It is therefore necessary to maintain specified evaporation rates. The influence of the deposition rates on the index of refraction of SiO has been studied by Hass, et. al.[17] A high rate of deposition corresponds to a high index of refraction, whereas, a slow rate of deposition corresponds to a low index of refraction.

Reviews of thickness and rate monitors have been given by Steckelmacher[18] and Behrndt.[19] The control of evaporation rate is a more complex task than thickness control because it requires adjustment of the source temperature.

All coating depositions required for this program were carried out in a commercial vacuum system (Balzers Model 710) which is equipped with an oil diffusion pump and a liquid nitrogen trap. This system is capable of routinely maintaining pressures of the order of 10^{-6} Torr and is equipped with a substrate heater and a thin film monitor to control deposition rate and film thickness. Proper control of the thickness of each layer is afforded by

TABLE II. DEPOSITION PARAMETERS

MATERIAL	METHOD OF EVAPORATION	SUBSTRATE TEMPERATURE	DEPOSITION PRESSURE (TORR)	DEPOSITION RATE
Al_2O_3	E-Beam	200°C	5×10^{-5}	~600 Å/Min
LaF_3	Mo Boat	200°C	8×10^{-6}	~1800 Å/Min
MgF_2	E-Beam	200°C	2×10^{-6}	~1800 Å/Min
MgO	E-Beam	200°C	6×10^{-5}	~1200 Å/Min
PbF_2	E-Beam	200°C	7×10^{-6}	~1800 Å/Min
SiO	Ta Boat	200°C	$<1 \times 10^{-6}$	~3000 Å/Min
SrF_2	Mo Boat	200°C	8×10^{-6}	~1800 Å/Min
ThF_4	E-Beam	200°C	4×10^{-6}	~1800 Å/Min
ZnS	Ta Boat	150°C	8×10^{-6}	~1800 Å/Min
ZnSe	Ta Boat	150°C	4×10^{-6}	~1800 Å/Min

observing the reflectance at the control wavelength of a suitably positioned monitor plate in the coating chamber and stopping deposition when the reflectance reaches a predetermined level. In all cases, care is taken to ensure the uniformity of the thickness of the layers. In order to obtain uniform layers, the window substrates are rotated above the evaporation source during the deposition process.

Deposition parameters utilized in this program are summarized for each material in Table II. Electron beam heating was employed in the evaporation of slightly more than half of the materials, while thermal evaporation from a boat was utilized in the balance of the cases.

2.5 Thin Film Growth Rate Determination

Spectrophotometer scans from 600 to 800 nm of halfwave optical thickness films at 3.8 or 5.3 μm on CaF_2 and SrF_2 substrates were utilized to determine relative growth rates of thin films on three substrate orientations. The position (wavelength) of maxima and minima in the transmission of these materials is related to the higher order interference of the coating on a given substrate orientation. Shifts in transmission maxima (or minima) towards longer wavelengths are indicative of greater optical thickness on a particular substrate orientation; shifts toward shorter wavelengths indicate lesser optical thickness. Since the refractive index of all the coating materials (except MgO) were found independent of substrate orientation and all films were deposited simultaneously on three different orientations of a given substrate material, differences in optical thickness are proportional to differences in physical thickness and hence in growth rate of the coating material. Amplitudes of the maxima and minima in the transmission curves have no particular significance for this interpretation.

Examples of the use of this technique are provided in figures 1-3, which are actual data traces for ThF_4, ZnS, and ZnSe on CaF_2 substrates. In figure 1 for ThF_4 (a low index material) we see that the transmission maxima and minima are shallow and their positions are indistinguishable for the three substrate orientations. We conclude from these traces that the film growth rates are essentially equal on all three substrates. In figure 2 for ZnS (a high index material), the maxima and minima are very pronounced and exhibit large shifts in position for different substrate orientations. We conclude from figure 2 that the growth rate of ZnS on (110) CaF_2 is fastest and on (111) CaF_2 is slowest, with the rate on (100) CaF_2 being intermediate. Finally, for ZnSe on CaF_2, it is clear that growth rates on (100) and (110) CaF_2 are essentially equal, while that on (111) CaF_2 is significantly slower. All ten of the thin film materials were subjected to similar analyses. Results are presented in section 3.3 on film properties.

2.6 Index of Refraction Determination.

The index of refraction of dielectric thin films depends on several factors, such as type of material and composition, crystalline structure, grain size, packing density, and water vapor absorption effects. For elements, the index of refraction increases in general with increasing atomic weights. Compounds with a high degree of ionic bonding show lower indices of refraction than compounds with a high degree of covalent bonding. With the same material different indices of refraction may be obtained due to different crystalline structures. Even films of the same material and the same crystalline structure can show varying indices of refraction due to different grain size and packing density. Oxide films like CeO_2, Al_2O_3, and MgO are typical examples of the increase of the index of refraction with the increasing grain size.[20, 21, 22] Fluorides tend to form films with lower packing density if not deposited on heated substrates, and on exposure to air, water vapor is absorbed in the films, filling the holes with water.

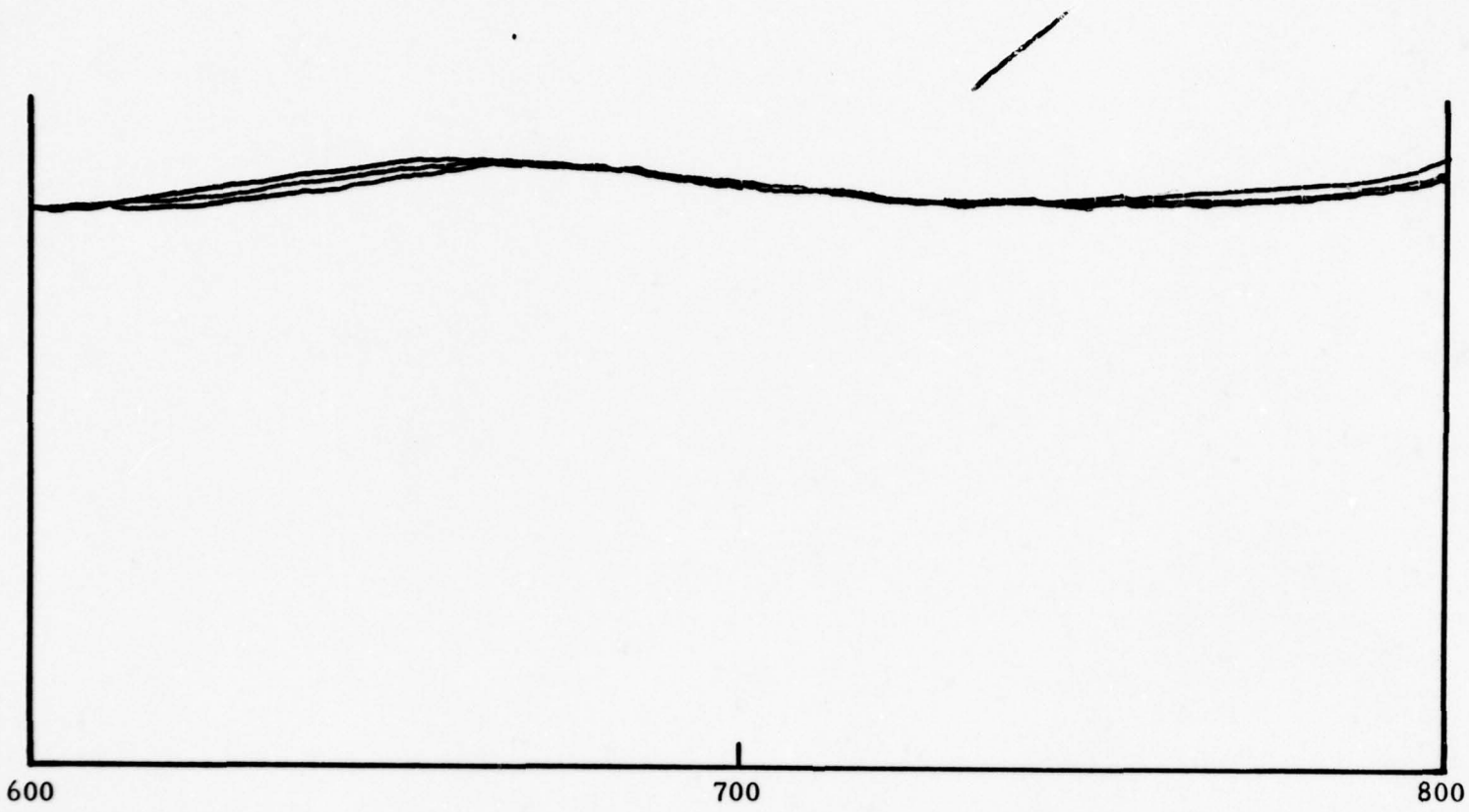

Figure 1 Spectrophotometer Scan of ThF_4 on CaF_2 from 600 to 800 nm.

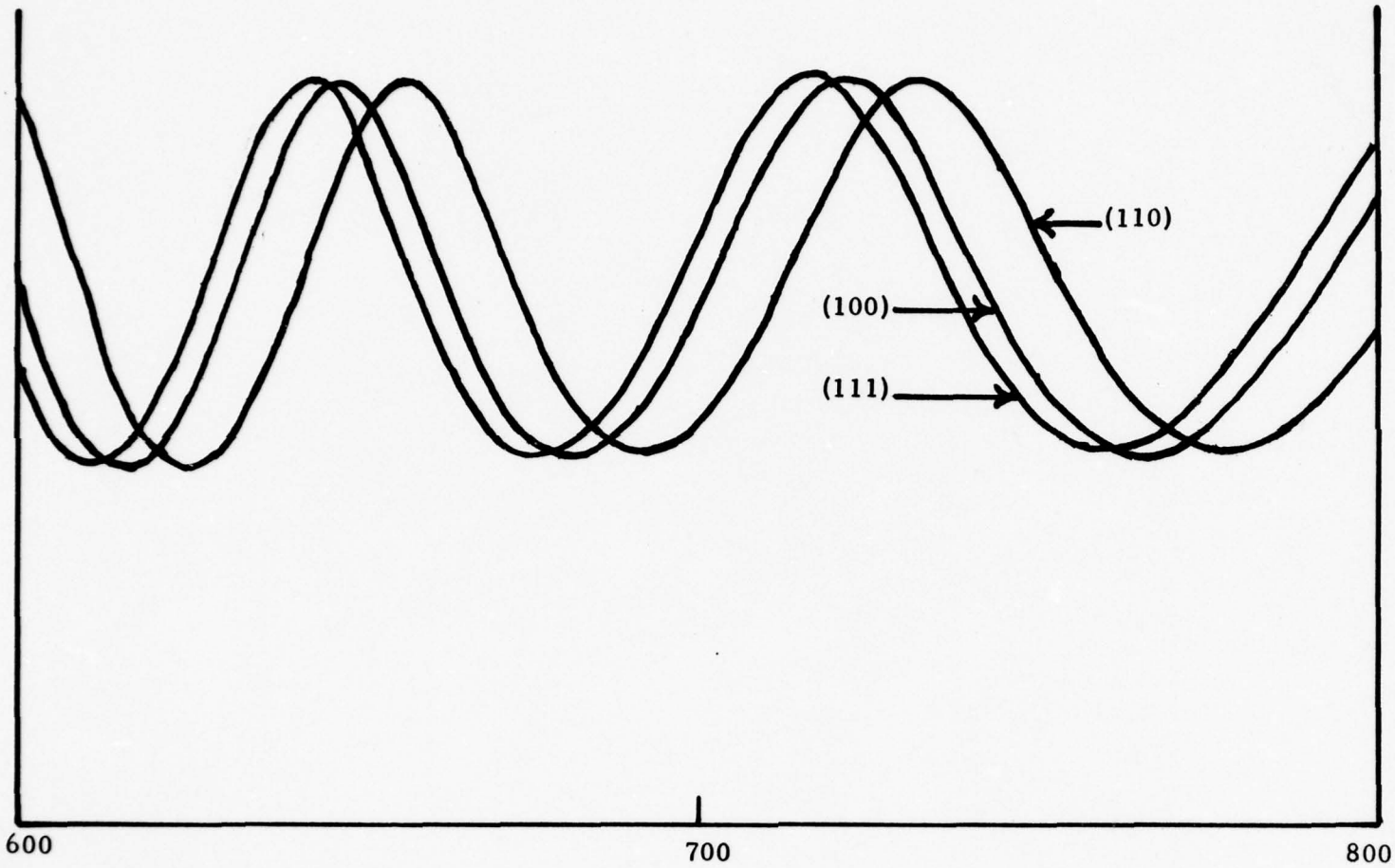

Figure 2 Spectrophotometer Scan of Zn S on CaF_2 from 600 to 800 nm.

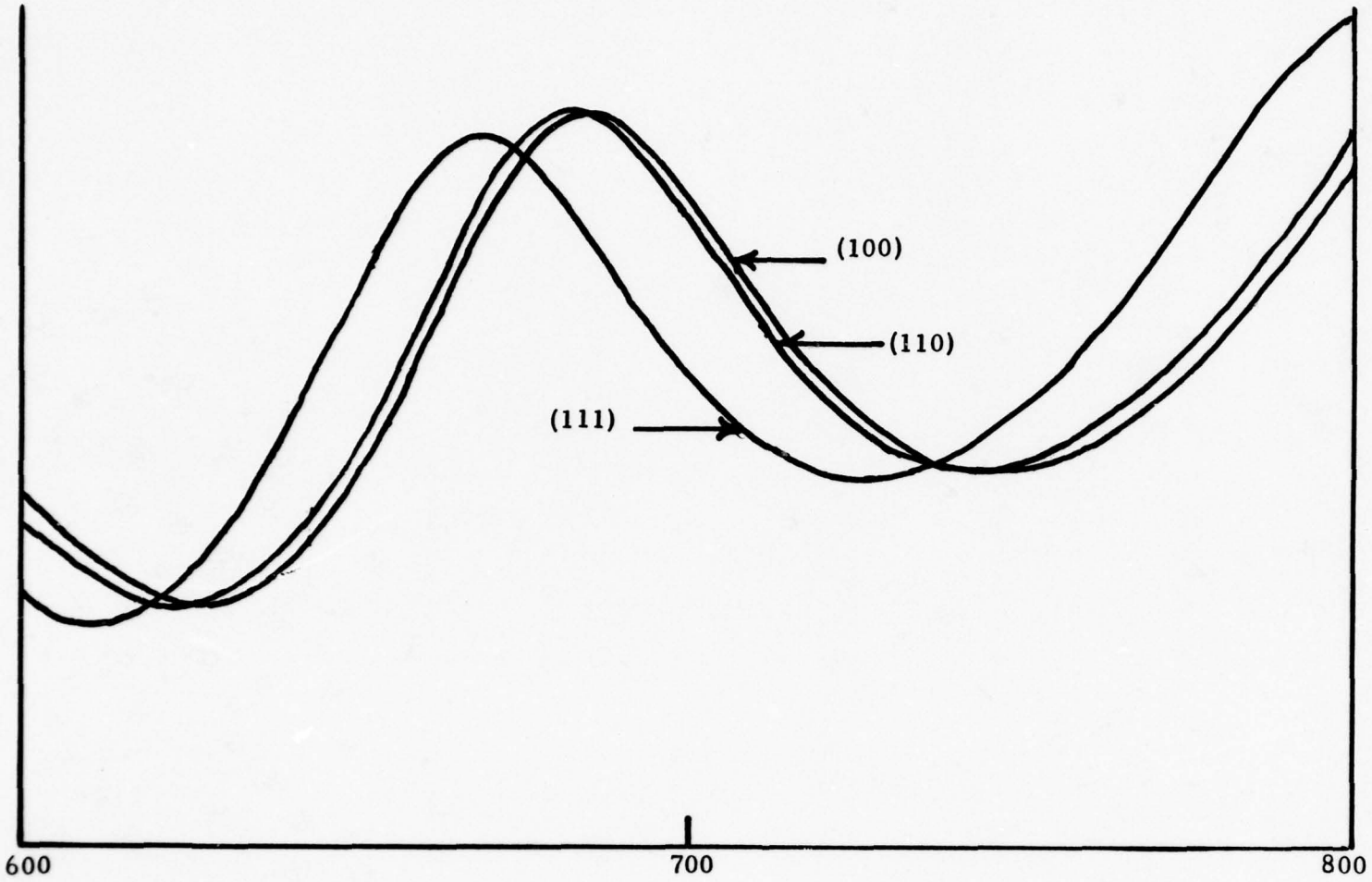

Figure 3 Spectrophotometer Scan of Zn Se on CaF_2 from 600 to 800 nm.

The packing density p is defined as the ratio of the density of the film material ρ_f to the density of the bulk material ρ_m. In a similar sense, the terms packing factor and filling factor are used. Packing density and index of refraction are related by[23]

$$p = \frac{\rho_f}{\rho_m} = \left(\frac{n_f^2 - 1}{n_f^2 + 1}\right)\left(\frac{n_m^2 + 2}{n_m^2 - 1}\right) \qquad (1)$$

where n_f and n_m are the indices of refraction of the film and bulk material, respectively. The cause of a reduced packing density appears as a structural effect or a gas incorporation in the film. Increased substrate temperature normally increases the packing density. For the investigation of the packing density, one of the following methods can be used: (1) observation of the shift in optical thickness on exposure to air,[24] and (2) comparison of index of refraction measured in vacuum and in air.[25]

The method of determining the refractive indices of the films takes advantage of the fact that the transmittance of a substrate coated with a low-loss dielectric film undergoes periodic variations as the optical thickness of the film increases. This is due to the interference between the reflections arising at the two boundaries of the film. If a dielectric film of refractive index n_f is deposited onto a substrate of refractive index n_s, the transmittance of the substrate illuminated by monochromatic light of wavelength λ will be a maximum where n_f is less than n_s and the optical thickness of the film is a quarterwave. The transmittance will be a minimum if n_f is greater than n_s and the optical thickness of the film is a quarterwave.

The measured transmittance will include the effect of the light reflected from the uncoated surface of the substrate. To determine the transmittance of the coated surface, the equations given by Heavens[26] can be used.

According to Heavens,[26] the external transmittance T of an uncoated substrate is given by:

$$T = (1 - R) / (1 + R) \tag{2}$$

where R is the reflectance of one substrate surface. The reflectance R can be calculated from the refractive index n_s of the substrate. If one surface of the substrate is then coated with a thin film of reflectance R_f, the external transmittance T_f of the coated substrate is given by:

$$T_f = (1 - R)(1 - R_f) / (1 - RR_f) \tag{3}$$

Solving equation (3) leads to

$$R_f = (1 - R - T_f) / (1 - R - RT_f) \tag{4}$$

The refractive index n_f of the film is then calculated from the following equation:[27]

$$n_f^2 = n_s (1 + \sqrt{R_f}) / (1 - \sqrt{R_f}) \tag{5}$$

2.7 Absorptance Measurement.

In order to obtain absorptance values (β and k) for halfwave thicknesses of coating materials, absorptances for the uncoated substrates must be known. The determination of the absorption coefficient of a coating material on a substrate which is transparent in the wavelength region of the irradiating laser is in principle quite straightforward. The total absorption due to a coating of specified thickness is obtained as a difference in total absorption between coated and uncoated substrates. Sequential measurements on the same substrate are utilized to obtain either a difference in absorption

between coated areas or a difference in absorption in a single location before and after coating. The former method has the advantages of speed and ease of verification, but substrate inhomogeneity can cause difficulties. In the latter method, substrate inhomogeneity is eliminated, but verification of the absorption measurement on the uncoated substrate is problematic.

For an uncoated transparent substrate irradiated by a laser beam in a standard adiabatic calorimeter configuration, the total absorption A_o is given by[28]

$$A_o = \frac{2n_s}{1 + n_s^2} \quad P_A / P_T \tag{6}$$

where n_s is refractive index of the sample, P_A is power absorbed by the sample, and P_T is the power transmitted through the sample. If the masses and heat capacities of the sample and calorimeter cone are known and irradiation times are held constant for a given series of measurements, the absorption is proportional to the ratio of output voltages from the sample and power cone thermocouples.

The total absorptance calculated from (6) includes both surface and bulk contributions. The absorption coefficient for this substrate is

$$\beta = A_o / L \tag{7}$$

where L is the sample thickness; again, both surface and bulk contributions are included. If a coating is subsequently deposited upon such a substrate and a new absorption measurement made, the total absorption takes on a value

$$A_t = A_o + A_1 \tag{8}$$

where A_1 is the increase in total absorptance due to the coating alone. For the case of a coating of halfwave optical thickness, A_1 can be evaluated using (6) and (8) since the surface reflectivity of the coated sample is identical to that of the uncoated substrate and the parenthetical factor involving n_s in (6) remains unchanged.

To obtain an absorption coefficient for a coating of physical thickness t_1 from a measured value of A_1, we employ a formula of Loomis,[29] with minor rearrangement,

$$\beta_1 = \frac{A_1 n_1}{2t_1 n_o} \quad \frac{(n_o + n_s)^2 \cos^2 \varphi_1 + [n_1 + (n_o n_s / n_1)]^2 \sin^2 \varphi_1}{n_1^2 + n_s^2}, \qquad (9)$$

where

n_1 = film refractive index

n_s = substrate refractive index

n_o = incident medium refractive index

$\varphi_1 = 2 n_1 t_1 / \lambda_o$

λ_o = laser wavelength (vacuum).

For a single coating of thickness $\lambda_o/2$, (9) reduces to

$$\beta_1 = \frac{A_1 n_1}{2t_1 n_o} \quad \frac{(n_o + n_s)^2}{n_1^2 + n_s^2} \qquad (10)$$

The absorption index of the thin film is then

$$k_1 = \frac{\lambda_o \beta_1}{4\pi} \qquad (11)$$

Hence, in order to obtain the absorption coefficient and absorption index of a single layer coating on a transparent substrate, we require only the refractive index of film and substrate, the physical thickness of the film, and two absorption measurements. The method of measuring the absorption has been discussed in the literature.[30, 31]

A convenient program for calculating absorption coefficients of single layer films on either entrant or exit surfaces has been published by Loomis[37] and was used in preference to (10).

The spectral composition of the irradiating laser has been shown to be a significant variable in absorptance measurements at CO laser wavelengths.[30, 31] In order to verify the spectral output of both the CO and DF lasers employed in the present measurements, spectra were analyzed using a Jarrell-Ash Model 78-466 scanning spectrometer with a 50 groove/mm grating blazed at 10.0 μm and a Ge:Au detector. Spectra for the CO laser have been reported previously.[4, 30] with centroids varying from 5.25 μm to 5.45 μm, depending upon CO partial pressure. In the present study, with operating parameters typical of those employed in the calorimetric measurements (i.e. 6 mm intracavity iris, total output power ~ 2.8 W), the mean centroid of two spectra run with identical parameters was 5.29 ± 9.4 μm, with a bandwidth of 0.57 ± 0.1 μm.

A typical output spectrum for the CO laser is illustrated in Figure 4. Table III is an attempt at quantitative characterization of the spectrum. In this table, the first column gives the wavelength of individual lines as measured with the spectrometer (in air). "Line Identification" (column 2) is obtained by comparison with published data. In the third column, the mean intensity of each line is divided by that of the strongest line (7-6, P(16)), to obtain a relative intensity scale for plotting in Figure 4. The fourth column gives the mean intensity of each line divided by the summed

TABLE III. Mean CO Laser Spectrum for 2 Runs with identical Operating Parameters. Mean centroid $< \lambda >$ is at $5.286 \pm 0.04\ \mu m$. Mean Bandwidth is $0.57\ \mu m$. Output power is ~ 3 w, with a 6 mm diameter intracavity iris.

$\bar{\lambda}$ (μm)	Line Ident.	$\bar{I}/\bar{I}_1$	$\bar{I}/\Sigma\bar{I}$	$\lvert\Delta\bar{I}\rvert$	$\lvert\Delta\bar{I}\rvert/\Sigma\bar{I}$
5.1220	6-5, P(15)	0.037	0.009	0.052	0.012
5.1329	6-5, P(16)	0.211	0.051	0.030	0.007
5.1431	6-5, P(17)	0.292	0.070	0.071	0.017
5.1895	7-6, P(15)	0.038	0.009	0.054	0.013
5.1999	7-6, P(16)	1.000	0.240	0.000	0
5.2110	7-6, P(17)	0.420	0.101	0.303	0.073
5.2580	8-7, P(15)	0.054	0.013	0.076	0.018
5.2806	8-7, P(17)	0.412	0.099	0.112	0.027
5.3183	9-8, P(14)	0.854	0.205	0.130	0.031
5.3907	10-9, P(14)	0.050	0.012	0.071	0.017
5.40125	10-9, P(15)	0.169	0.041	0.115	0.028
5.4130	10-9, P(16)	0.031	0.007	0.044	0.011
5.4644	11-10, P(14)	0.223	0.054	0.315	0.076
5.4888	11-10, P(16)	0.043	0 010	0.061	0.015
5.5173	12-11, P(12)	0.020	0.005	0.028	0.007
5.5287	12-11, P(13)	0.044	0.011	0.063	0.015
5.5408	12-11, P(14)	0.062	0.015	0.088	0.021
5.5948	13-12, P(12)	0.090	0.022	0.127	0.030
5.6304	13-12, P(15)	0.022	0.005	0.031	0.007
5.6868	14-13, P(13)	0.012	0.003	0.0017	0.004
5.6976	14-13, P(14)	0.064	0.015	0.023	0.006
5.8394	16-15, P(12)	0.014	0.003	0.020	0.005

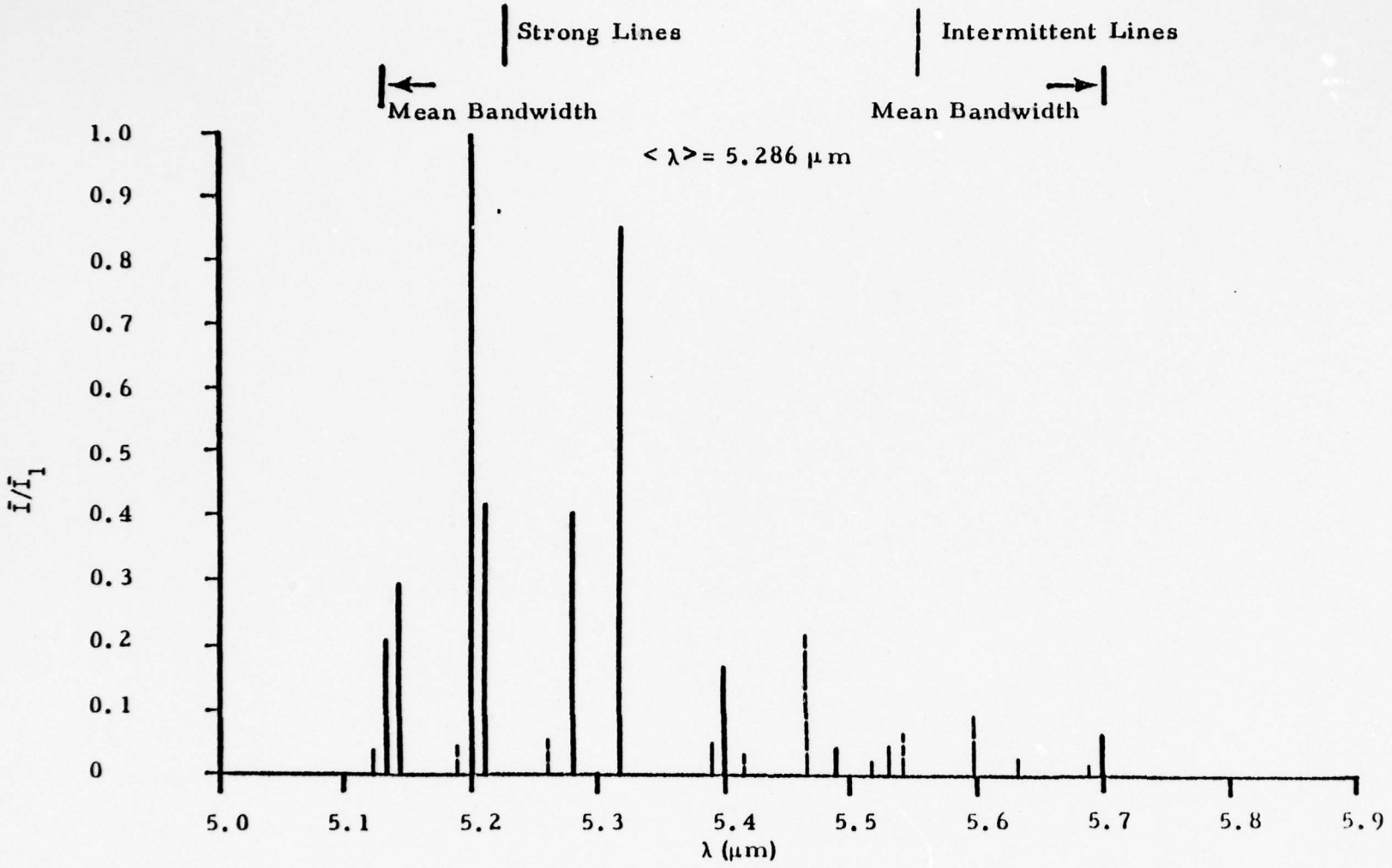

Fig. 4. Mean CO Laser Spectrum For 2 Runs With Identical Operating Parameters.

intensity of all measured lines. The tabulated number is the fraction of laser power in any line. The fifth column, headed $|\Delta \bar{I}|$ is the standard deviation of the relative intensities from which column 3 was prepared. This is divided by the sum of intensities and tabulated in the sixth column to indicate the variability of a given line as a fraction of the laser output.

The DF laser spectrum was also analyzed in some detail since the actual output of the laser in use in the calorimetry laboratory had not been characterized previously. The same spectrometer, grating, and detector employed with the CO laser were used to analyze the DF. Typical operating parameters for calorimetric measurements were used. These include a helium partial pressure of ~ 4 Torr, with about 1.2 Torr each of SF_6 and D_2, and ~0.1 Torr of O_2 for a total of 6-8 Torr. The discharge tube is operated at a voltage of ~ 13 kV and current of ~ 450 mA to produce 2-4 W total power. Cavity temperature is ~65° C. Seven spectra were run over a three-day period and the results averaged to obtain a composite spectrum, presented in Figure 5 and Table IV.

In general, it appears that the overall spectrum is very stable with respect to centroid (~3.9 μm) and bandwidth (~0.3 μm), but individual lines are highly variable. Table IV is an attempt at quantitative characterization of this aspect of the spectrum. In this table, the first column gives the wavelength of individual lines as measured with the spectrometer (in air). "Line Identification" (column 2) is obtained by comparison with published data.[33, 34] Column 3 ($\bar{I}$) gives the mean relative intensity of each line. The tabulated number was obtained by first determining the intensity of the line in question in each of the seven spectra, relative to the strongest line in that spectrum taken as 1.0, and then averaging the results over all seven spectra. (If a line was absent from a particular spectrum, its intensity was counted as 0.)

The mean relative intensities in column 3 of the table were divided by the sum of all of the mean intensities to obtain the fraction of the total laser energy in any given line, listed in the fourth column. The fifth column, headed "Δ I" gives the standard deviation of the mean relative intensities in column 3. This is divided by the sum of the intensities to determine the variability of a given line as a fraction of the total laser output and tabulated in the sixth column. In the seventh column, the mean relative intensity of each line is divided by that of the strongest line (2-1, P(10), to obtain a relative intensity scale for plotting in Figure 5. Note that this number is also the fraction of total laser energy appearing in an individual line, relative to the strongest line in the composite spectrum. Finally, the last column of the table designates the number of spectra, (out of a total of 7) in which an individual line had non-zero intensity.

Fig. 5. DF LASER SPECTRUM COMPILED FROM 7 RUNS OVER A 3-DAY PERIOD, OUTPUT POWER: 2-4 WATTS.

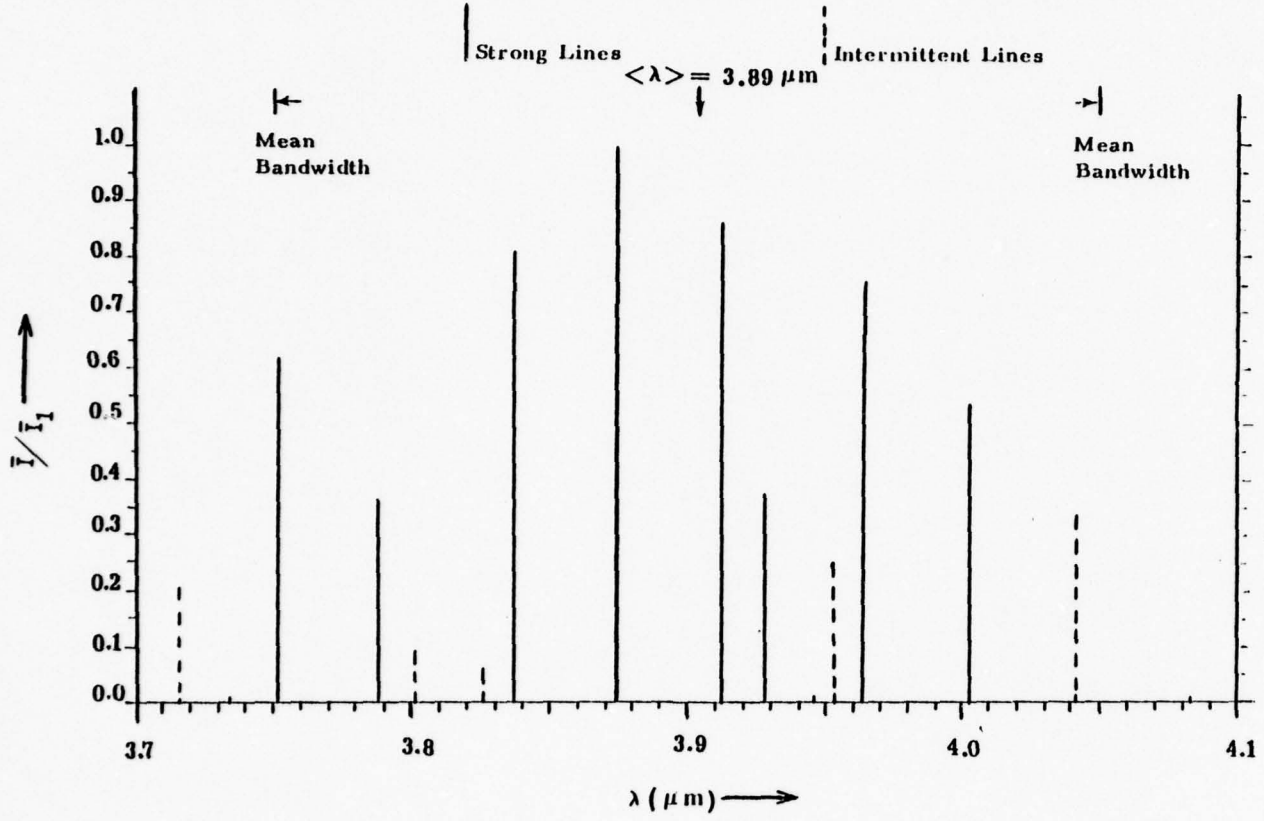

Table IV. DF Laser Spectrum Compiled from 7 Runs on 3 Days. Mean Centroid $>\lambda<$ of All Spectra is 3.89 ± .025 μm. Mean Bandwidth of All Spectra is 0.297 μm ± 0.028 μm. For Individual Lines, Tabulated $\bar{\lambda}$ May Vary by ± 0.007 μm from Run to Run.

$\bar{\lambda}$ (μm)	Line Ident.	$\bar{I}$	$\bar{I}/\Sigma\bar{I}$	$\lvert\Delta\bar{I}\rvert$	$\lvert\Delta\bar{I}\rvert/\Sigma\bar{I}$	$\bar{I}/\bar{I}_1$	No Runs Present
3.1760	1-0, P(9)	0.14	0.032	0.16	0.036	0.21	4
3.7514	1-0, P(10)	0.42	0.096	0.31	0.071	0.62	7
3.7880	1-0, P(11)	0.25	0.057	0.22	0.050	0.37	6
3.8262	1-0, P(12)	0.04	0.009	0.06	0.014	0.06	2
3.7337	2-1, P(6)	<0.01	<0.002	0.02	0.005	<0.01	1
3.8015	2-1, P(8)	0.07	0.016	0.12	0.027	0.10	2
3.8372	2-1, P(9)	0.55	0.125	0.42	0.096	0.81	7
3.8737	2-1, P(10)	0.68	0.155	0.27	0.062	1.00	7
3.9123	2-1, P(11)	0.59	0.134	0.38	0.087	0.86	7
3.9526	2-1, P(12)	0.18	0.041	0.19	0.043	0.26	4
3.9270	3-2, P(8)	0.26	0.059	0.25	0.057	0.38	5
3.9639	3-2, P(9)	0.52	0.118	0.33	0.075	0.76	7
4.0021	3-2, P(10)	0.36	0.082	0.28	0.064	0.53	6
4.0414	3-2, P(11)	0.30	0.068	0.40	0.091	0.44	4
4.0832	3-2, P(12)	<0.01	<0.002	0.02	0.005	<0.01	1
3.9457	4-3, P(5)	0.01	0.002	0.03	0.007	0.01	1

3.0 EXPERIMENTAL RESULTS

All results of experiments performed under the program are presented and discussed in this section, which is divided into five major subsections. The first two of these cover substrate structure and material properties. The third subsection is a tabulation of coating material composition, structure, preferred orientation, growth rates, refractive indices, and absorptance, organized by material such that it provides a materials reference file. The results contained within this subsection comprise the major findings of the contract. The fourth subsection details results of some intensive studies of selected coating materials, including optimization of deposition techniques, absorptance vs. film thickness (βL vs. L), effects of polycrystalline substrates upon single layer film structure and properties, and resistance to an HF vapor environment. Finally, some results obtained from multilayer coating designs incorporating the most promising materials are presented in the fifth subsection.

3.1 Substrate Structure, Orientation, and Surface Quality

Recent interest in molecular gas lasers (HF, DF, and CO) operating in the 2-6 μm region has created a demand for window materials having optimum thermal and mechanical properties as well as low optical absorption in this wavelength range. Substantial progress has been made with the use of CaF_2 in single pulse CO systems, due to the low absorptance, relatively high strength, and ready availability of this material. As interest turns to DF and CO lasers operating in repetitively pulsed or CW modes, material properties requirements become more stringent.

Requirements for very low absorptance in the 2-6 μm region combined with high mechanical strength, hardness, and low solubility have led to consideration of SrF_2 and BaF_2 as alternatives to CaF_2 for window substrates.

Theoretical investigations[1] have indicated that BaF_2 is most favorable with respect to absorptance and thermomechanical properties. However, recent experimental data[2, 3, 4] suggest that absorptance in SrF_2 can be reduced to levels comparable to that in BaF_2, while maintaining mechanical strength comparable to that of CaF_2. In addition, a figure of merit analysis[5], based upon thermal distortion only, indicates that SrF_2 will distort less than either CaF_2 or BaF_2; the difference amounts to a factor of 3.5 relative to CaF_2 and 1.8 relative to BaF_2. An investigation of coating materials for the 2-6 μm region[6] indicates that SrF_2 is compatible with many coating materials due to low lattice mismatch and structural similarities, particularly with other alkaline earth fluorides (BaF_2 and CaF_2) as well as with PbF_2.

Although the information is spotty, it is clear that minimum strengths in the range of 12,000 to 18,000 psi are achievable with polycrystalline CaF_2 and SrF_2 which is properly polished and annealed.[2] From the limited information available, it appears that cast polycrystalline material is superior in terms of mechanical strength and absorptance. Clearly some reliable strength and grain size data on Harshaw polycrystalline material are required to make a firm judgment in this direction. In addition, information on the direction and degree of preferred crystallographic orientation in polycrystalline substrates will be required for coating optimization, as indicated by results of a recent study.[6]

In this respect, it is instructive to examine the crystal structure of the substrates empolyed in the investigation. For the predominantly ionic AX_2 halides (A being a divalent cation and X a monovalent halogen ion), the crystal structure is determined by the relative sizes of the ions, as in the alkali halides, where both A and X are monovalent. The coordination of anions around the cations determines the structural arrangement, since the anions

are usually the larger ions. Thus the possible coordinations are 8:4 (fluorite structure), 6:3 (rutile structure) and 4:2 (cristobalite structure), with the respective (Pauling) radius ratios (r_+/r_-), >0.7, 0.7-0.3, and < 0.3[35] These structures occur in those halides in which the A and X atoms differ widely in electronegativity. They are thus common in fluorides, rare in chlorides and bromides, and unknown in iodides. Typical of the ionic halides crystallizing in the fluorite (CaF_2) structure are the alkaline earth fluorides, CaF_2, SrF_2, and BaF_2, for which the (Pauling) radius ratios (r_+/r_-) are 0.73, 0.83, and 0.99, respectively.

The fluorite and some related structures are illustrated in Figure 6 (redrawn from Wells[36] and Barrett and Massalski[37]. In this structure (Figure 6a) each cation (e.g. Ca^{2+}) is at the center of eight anions (F^-) situated at the corners of a surrounding cube (outlined by dashed lines in Figure 6a). Each anion, in turn, is surrounded by four cations at the corners of a regular tetrahedron (also outlined by dashed lines in Figure 6a).

The symmetry of the structure is cubic with space group $F\,4/m\,\bar{3}2/m$ (or O_h^5)[38] The cubic unit cell contains four molecules ($OHCaF_2$, for example) or four divalent cations and eight monovalent anions.[38] The cations are located at the corners and face-centers of the cubic cell and the anions are centered at 1/4 of the body diagonal from each of the eight corners. An alternative description of the fluorite structure depicts it as a cubic-close-packed (or fcc) array of cations, with anions occupying all tetrahedral interstices[35] (compare Figure 6b).

The fluorite structure is related to the cesium chloride structure through the coordination polydedron of its cation (geometrically a body-centered cube, Figure 6c) and to the tetrahedrally coordinated materials, through the coordination polyhedron of its anion (Figure 6d). Other structures,

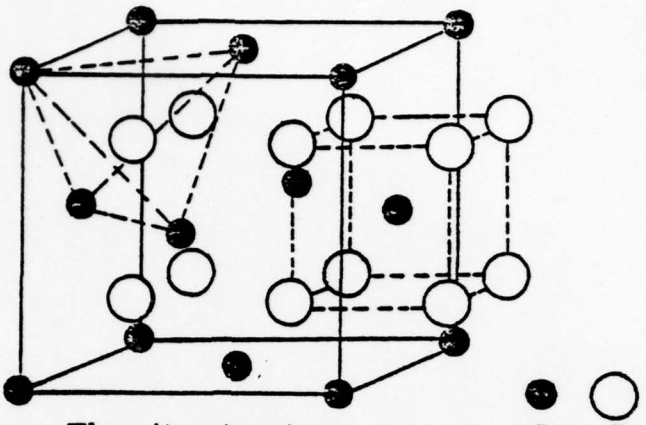

a. Fluorite structure

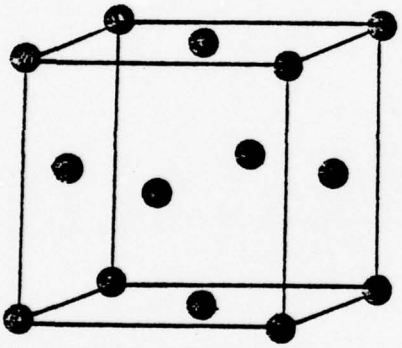

b. Cubic close packed (or fcc) structure

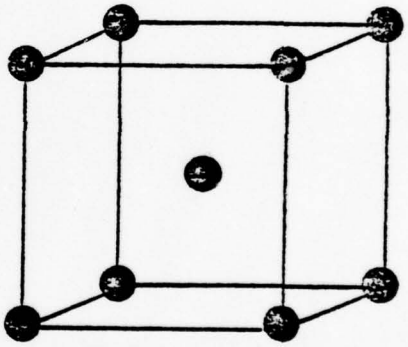

c. Body-centered cubic (bcc) structure

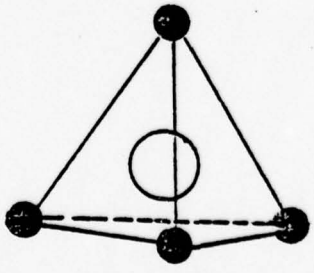

d. Tetrahedral coordination

Figure 6. The Fluorite and Some Related Structures.

called "derivative structures" by Wells,[36] are obtained by imagining the systematic removal of 1/4, 1/2, or 3/4 of the anion positions. For example, the sphalerite (ZnS) structure is obtained by removing 1/2 of the anion positions from the fluorite structure, while the cuprite (Cu_2O) structure is obtained by removing 3/4 of the anion positions.

Over one hundred substances, ranging from halides and oxides to intermetallic compounds and alloys, crystallize in the fluorite or antifluorite structure. These are tabulated by Wyckoff[38] and need not be repeated here. They include: (1) halides of the larger divalent cations; (2) oxides, sulfides, etc. of univalent ions, mostly alkalis; (3) oxides of large quadrivalent cations; (4) intermetallic compounds.[38] Thus the possible choice of coating materials having crystal structures which are identical or at least similar to the substrate is quite broad.

Several coating materials chosen for the program belong to the fluorite family of structures (e.g. SrF_2 and PbF_2). Hence some phase relations among the fluorides are worth noting. For the two component systems comprising CaF_2 - SrF_2, SrF_2 - BaF_2, and CaF_2 - BaF_2, it has been found that CaF_2 - SrF_2 and SrF_2 - BaF_2 form continuous solid solutions for any ratio of components.[39] The solid solutions CaF_2 - BaF_2 are formed only for a BaF_2 content up to 2% and a CaF_2 content up to 6-8%. Other proportions of the end members of this series yield two-phase mixtures of CaF_2 and BaF_2. The materials used in the referenced study were single crystals grown in a vacuum apparatus. The method of determination involved primarily the use of Debye-Scherrer x-ray diffraction patterns.[39] No similar work on PbF_2 equilibria with CaF_2, SrF_2 or BaF_2 has been reported. It is expected (and found)[6] that the compatibility of coating and substrate materials is generally improved if solid solutions are observed between the components.

All three alkaline earth fluorides have cubic symmetry and hence are optically isotropic but elastically anisotropic.[40] The elastic anisotropy affects the state of residual stress in coatings deposited upon fluoride substrates through the thermal expansion coefficients which vary with the crystallographic orientation of the planes exposed at the substrate surface.[16] Young's modulus, which reflects the elastic symmetry of various planes in a crystal, thus exhibits a four-fold symmetry in (100), twofold in (110) and complete radial symmetry in the (111) cleavage plane; (thus thermal expansion parallel to the (111) planes of CaF_2, SrF_2, and BaF_2 is the same in all directions, resulting in uniform stresses in films deposited on these planes).

The most widely spaced and most densely packed planes in the fluorite structure are the (100) planes and the shortest translation vector is in the (110) direction, as may easily be verified from Figures 6 and 7.[41] It is found experimentally that the primary slip system in CaF_2[42] (and also BaF_2[43] and SrF_2) is (100) [110] and that the natural cleavage plane is (111).[44, 45] Recent experimental work[6] indicates that these structural characteristics influence polishing behavior in single crystal CaF_2 as well as the structure and growth of thin film coatings deposited upon it; similar effects are observed with SrF_2.

Single crystal CaF_2 and SrF_2 substrates were purchased from the Harshaw Chemical Co., Solon, Ohio. Nominal orientations parallel to the major low index crystallographic planes, (100), (110), and (111) were chosen to cover the rotational symmetry elements of the space group. A small number of samples oriented parallel to (112) were purchased to test polishing behavior and preferred growth directions of a few coating materials.

Crystallographic orientation of all of these was verified using the back reflection Laue method (x-ray). Of the CaF_2 substrates having a nominal

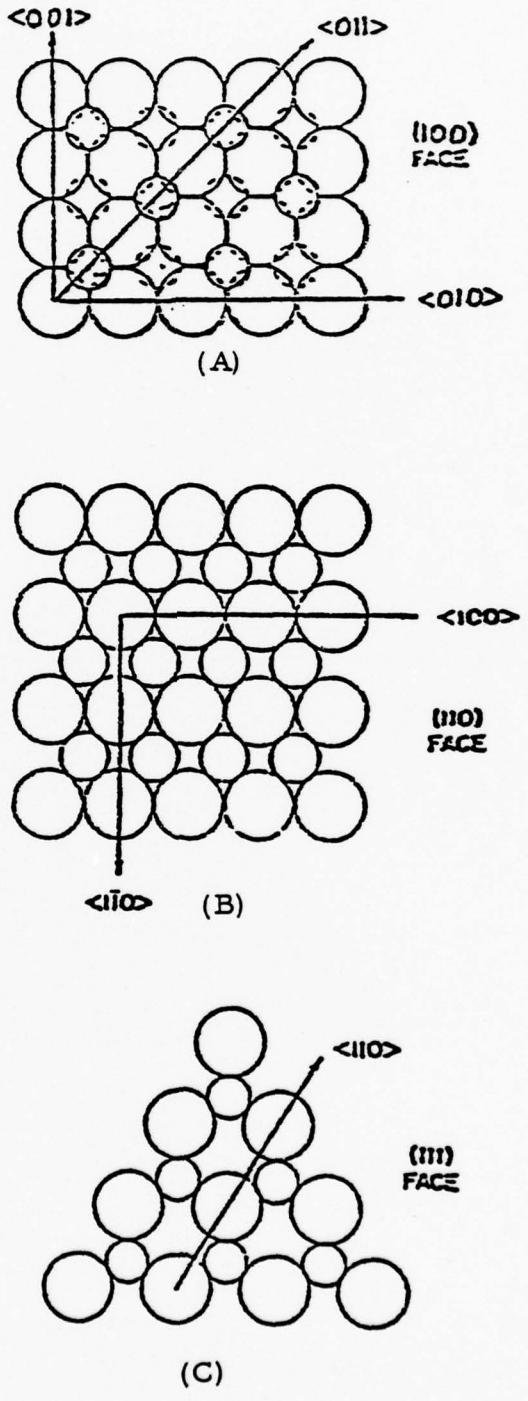

Figure 7. Atomic configuration of three crystallographic planes of calcium fluoride.[41] (A) (100), (B) (110), (C) (111).

(110) orientation, all but one fell within 2° of that orientation. Of the nominal (110) CaF_2 substrates, 99% fell within 2° to 5° of (110) and none was more than 8° from the nominal. Of the nominal (111) CaF_2 substrates, 90% fell within 1.5° of that orientation and none was more than 3° from (111). Of the (112) CaF_2 substrates, all fell within 2.5° to 5.0° of nominal. All SrF_2 samples of the four orientations, (100), (110), (111) and (112) fell within 3° of the nominal orientations.

Ten press-forged polycrystalline CaF_2 samples were also purchased from Harshaw. Preferred orientation in a central area of each sample, approximately 0.6 in. x 0.2 in., was determined by x-ray diffraction. Of these, seven samples showed a predominant (110) preferred orientation with smaller numbers of crystallites oriented parallel to (311) or (111). Two other samples showed essentially equal preferrential orientation parallel to (111) and (110). One sample had a preferred orientation near a high index plane (Laue pattern) and exhibits no diffraction peaks.

The majority of the purchased samples were 1 inch in diameter and approximately 1/4 inch thick to facilitate optical (e.g. laser calorimetry) and x-ray diffraction measurements on the same sample, thus eliminating run-to-run differences (if any) in coating structure and properties as experimental variables. A very small number of 1.5 inch diameter samples was purchased for quantitative evaluation of surface finish by optical scattering technique at the Naval Weapons Center, China Lake, California.

The quality of the surface finish of a high-power laser window is vital to its performance in a practical system. There are three primary aspects which must be considered when preparing such a surface: (1) the surface must be compatible with later coating requirements, (2) the desired optical figure must be maintained, and (3) the optical finishing techniques must be repeatable.

As summarized by Soileau[46] there are numerous reasons for minimizing the surface roughness: (1) increase of the laser damage threshold, (2) minimizing the laser scatter, (3) improved thin film coating adherence, (4) elimination of surface polarization waves and laser induced acoustic waves, (5) decreased surface migration of material into the thin film coating.

Although the surface of the window may be polished to a superquality finish, unless it meets the desired optical figure specifications it cannot perform the function for which it was designed. Thus the surface figure and smoothness must both be addressed during fabrication. A technique which achieves one without the other is of little value for practical high power windows.

A fabrication technique which achieves a superquality finish as well as the desired optical figure, on a particular component is not sufficient. The technique must be one that will provide similar results on any window of the same substrate material.

Examples of the quality of polished surfaces achieved on CaF_2 and SrF_2 are illustrated in Figures 8 through 10. Note that all surfaces are relatively free of defects, indicating that polishing behavior does not vary significantly with crystallographic orientation, as long as samples of a single orientation are polished on one block. In order to investigate this further, samples were submitted to the Michelson Laboratory, NWC, for surface roughness evaluation and quantitative documentation. Results of that investigation are presented here, as provided by Dr. James L. Stanford of NWC.

First measurements were made at 6471Å, in an attempt to deduce the average roughness of each surface by assuming that the bulk scattering was negligible. The intensity of backscattered light divided by the incident light intensity was obtained on four samples as detailed in Table V.

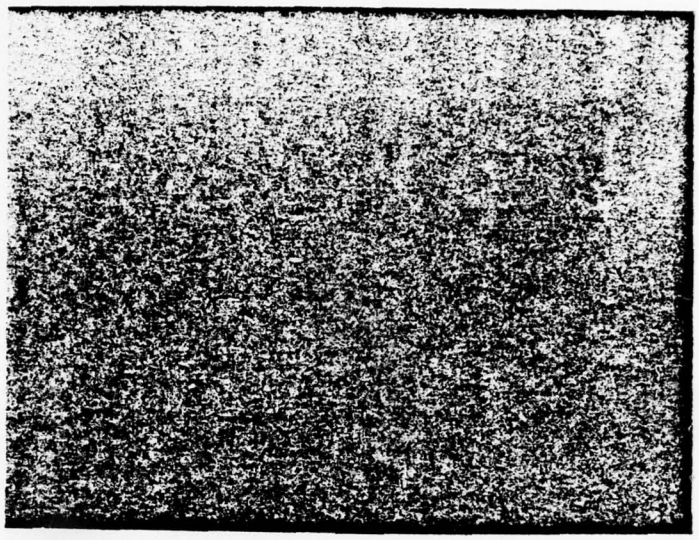

Figure 8 Polished-surface of CaF_2 oeiented parallel to the (111) crystallographic plane. Nomarski photomicrograph, 305X, Sample No. (111)-20.

Figure 9 Polished surface of CaF_2 oriented 2.5° from the (110) crystallographic plane. Nomarski photomicrograph, 305X, Sample No. (110)-27.

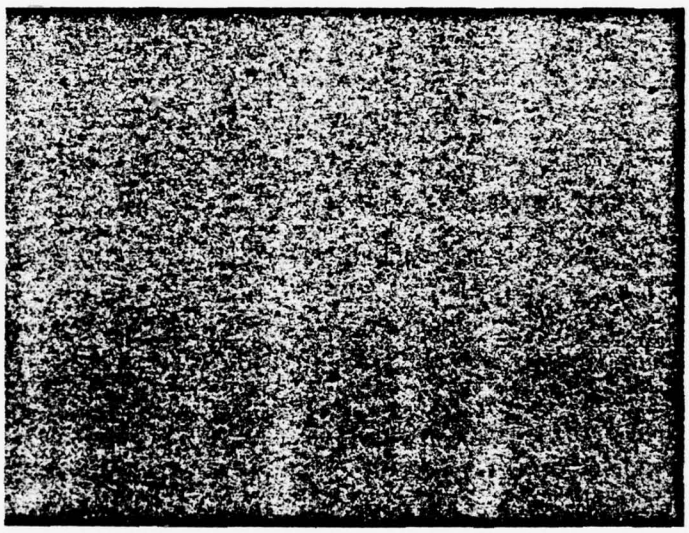

Figure 10. Polished surface of CaF_2 oriented 1° from the (100) crystallographic plane. Nomarski photomicrograph, 3-5X, Sample No. (100)-28.

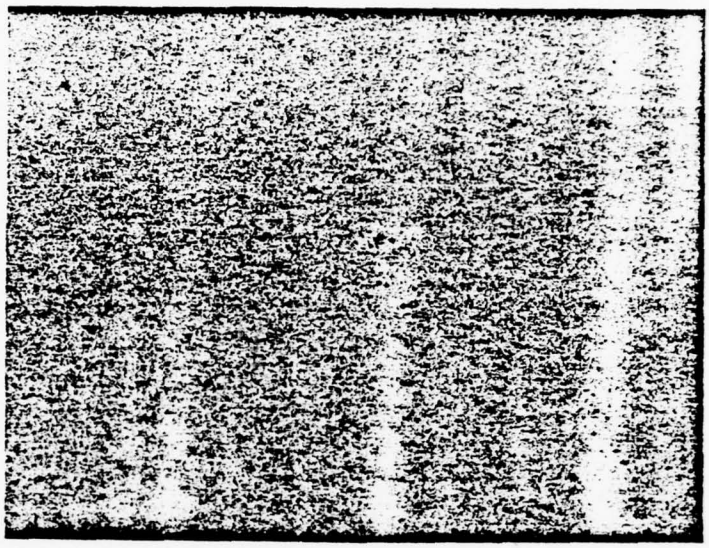

(A)

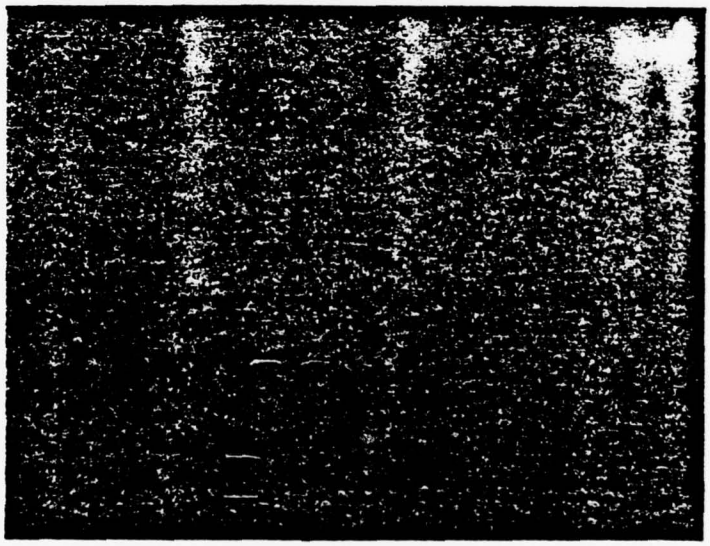

(B)

Figure 11. Polished surfaces of SrF_2 Nomarski photomicrographs (305X). (A) Sample No. (100)-28, oriented 2.5° from (100). (B) Sample No. (110)-28, oriented 0.8° from (110).

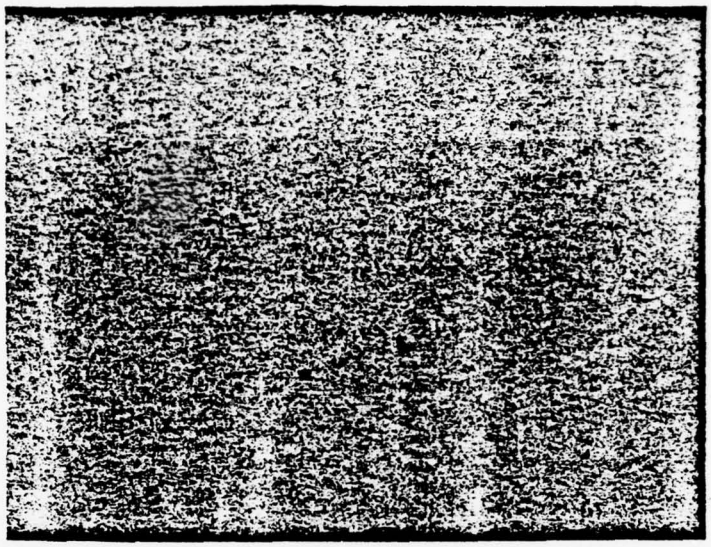

(A)

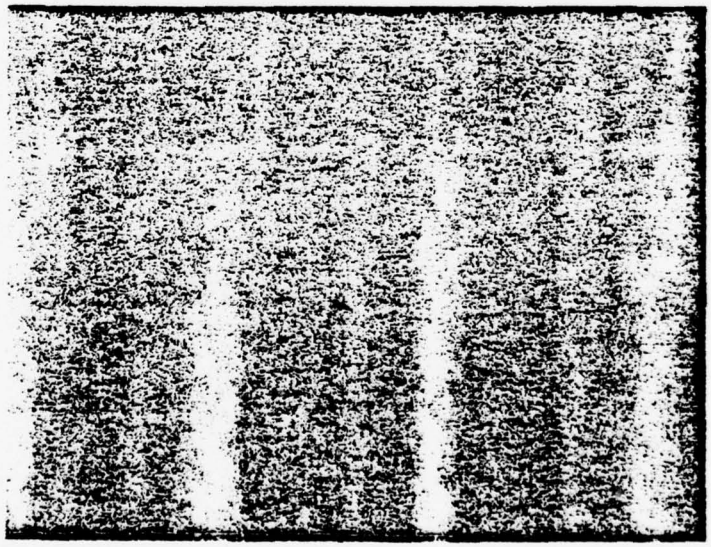

(B)

Figure 12. Polished surfaces of SrF_2. Nomarski photomicrographs (305X). (A) Sample No. (111)-28, oriented 0.8° from (111). (B) Sample No. (112)-10 oriented parallel to (112).

TABLE V. Intensity of Backscattered Light and rms Roughness of Uncoated CaF_2 and SrF_2 Samples.

Sample	I_s/I_o	$\left(I_s/I_R\right)$	δ(Å, rms)
SrF_2 (110)-30	6.78×10^{-4}	1.32×10^{-2}	59
SrF_2 (112)-10	1.06×10^{-4}	2.06×10^{-3}	23
CaF_2 (110)-28	4.16×10^{-4}	8.30×10^{-3}	47
CaF_2 (112)-11	2.38×10^{-4}	4.74×10^{-3}	36

To obtain the roughness the quantity I_s/I_o was divided by the reflectance (.032) and by 1.59, the combined fractional contribution to the measured scattering of the front and back surface. The resulting quantity is I_s/I_R from which the roughness δ is computed from the approximate relation $I_s/I_R = (4\pi\delta/\lambda)^2$.

One side of both SrF_2 (110)-30 and CaF_2 (112)-11 were then coated with silver and the backscatter from this single surface was measured (shifting to 5682Å because of laser problems). The resulting values of I_s/I_o ($\simeq I_s/I_R$, since $R \simeq .98$ for Ag at 5682) were 4.65×10^{-3} and 2.64×10^{-3}, respectively, giving corresponding values of δ of 31Å and 23Å. We thus conclude that there is significant <u>volume</u> scattering from these samples. An estimate of the relative magnitudes of surface and volume scattering can be obtained by multiplying each of the latter values of I_s/I_o by 1.59 and .032 to get the appropriate $\left(I_s/I_o\right)$ associated with the bare surface of each material surface. Also the bulk scattering is underestimated by the measurement, for the bulk scattered light from the vicinity of the back surface is collected with only 60% efficiency, hence only 80% of the total bulk scattered light is

collected. Thus we subtract $\left(I_s/I_o\right)$ surface from the original I_s/I_o, measured on the uncoated sample, and divide the result by 0.8 to get the bulk scattering. The end product is presented in Table VI.

TABLE VI. Surface and bulk scatter from uncoated and silver coated CaF_2 and SrF_2 samples measured at 5682Å.

Sample	$\left(I_s/I_o \text{ uncoated}\right)$	$\left(I_s/I_o \text{ coated}\right)$	$\left(I_s/I_o \text{ surface}\right)$	$\left(I_s/I_o \text{ bulk}\right)$
SrF_2 (110)-30	6.78×10^{-4}	4.65×10^{-3}	2.37×10^{-4}	5.52×10^{-4}
CaF_2 (112)-11	2.38×10^{-4}	2.64×10^{-3}	1.34×10^{-4}	1.30×10^{-4}

To complete the measurements, the backscattered light was then measured from the six uncoated samples at 3.39 μm. The results are shown in Table VII.

TABLE VII. Backscattered Light from six uncoated CaF_2 and SrF_2 samples measured at 3.39 μm.

Sample	I_s/I_o uncoated
SrF_2 x (112)-10	1.6×10^{-5}
CaF_2 (110)-28	5.5×10^{-5}
CaF_2 (111)-29	8.1×10^{-5}
SrF_2 (111)-30	1.5×10^{-5}
SrF_2 (100)-28	5.0×10^{-5}
CaF_2 (100)-29	6.9×10^{-5}

The variation of backscattered intensity over each sample is of the same magnitude as the scattering itself.

Two obvious conclusions to be drawn from the scatter measurements are: (1) bulk scatter contributes appreciably to overall backscattered light which varies appreciably (but not necessarily systematically) from sample to sample; (2) surface roughness of all samples examined lies in the low 20Å to mid 30Å region with no systematic variation with crystallographic orientation being discernible within experimental accuracy. It is also interesting to note that the total backscattered light intensity at 3.39 μm (Table VII) is of the order of 10^{-5} or greater, so that it is likely to perturb sensitive optical measurements, such as laser calorimetry.

3.2 Substrate Absorptance

As noted in section 2.7, in order to obtain the absorptance of a coating by measurement of differences in absorptance between coated and uncoated samples, it is necessary to measure the absorptance of a large number of uncoated substrates. This was done repeatedly throughout the program, as fresh substrates were required for coating operations. While the individual measurements in themselves simply provide necessary background information applicable to determination of coating properties, their overall mean values and variance are of some intrinsic interest. These mean values for substrates measured under the current program are presented in Table VIII.

Looking first at the single crystal mean values for CaF_2 and SrF_2, we see practically no difference at 3.9 μm (DF wavelength) but a difference of a factor of four at 5.3 μm (CO), with CaF_2 being much more higly absorbing. The latter is in accord with expectations, since the values for CaF_2 are within range of the intrinsic values plotted by Deutsch,[31] and the values for SrF_2 are definitely extrinsically limited. The case for extrinsic limitationsof absorptance in SrF_2 is also supported by comparison of the mean values for SrF_2 at 3.9 μm and 5.3 μm, with the 3.9 μm value being approximately double the 5.3 μm value, when it should theoretically be two orders

TABLE VIII. Mean Total Absorption Coefficients of Uncoated CaF_2 and SrF_2 Substrates Measured at 3.9 μm (DF) and 5.3 μm (CO) Wavelengths.

Substrate Material	Orientation	Mean Total Absorption Coefficient x 10^4 CM^{-1}	
		3.9 μm (DF)	5.3 μm (CO)
CaF_2	(100)	1.19 ± 0.39	4.08 ± 0.55
	(110)	1.66 ± 0.26	4.83 ± 0.69
	(111)	1.45 ± 0.30	4.15 ± 0.58
CaF_2 (Sngl. Xtl.)	Mean	1.43	4.35
CaF_2 (Poly. Xtl.)	(110)/(111)	15.88 ± 5.54	———
SrF_2	(100)	1.57 ± 0.29	0.68 ± 0.17
	(110)	1.26 ± 0.14	0.86 ± 0.29
	(111)	1.39 ± 0.20	0.96 ± 0.22
SrF_2 (Sngl. Xtl.)	Mean	1.41	0.83

of magnitude lower. A practical consequence of these observed systematic differences and similarities in absorptance is that SrF_2 has a definite advantage in yielding lower total absorptance at 5.3 μm, but no discernible advantage or disadvantage in terms of absorptance in the DF laser wavelength band.

Considering possible systematic differences in absorptance with crystallographic orientation of substrates shows that all differences are within the overlapping variance of measured values. This again is in accord with expectations. Hence, the mean values for each substrate material and wavelength have practical significance.

On the other hand, the high values for polycrystalline CaF_2 (press forged material from Harshaw) are disappointing, since they indicate definite limitation by extrinsic absorption mechanisms. Apparently, the mechanical properties advantages of polycrystalline substrates are somewhat offset by greater total absorptance.

3.3 Coating Material Structure and Properties

This subsection is a systematic compilation of coating material characteristics determined under the program, arranged by material composition, beginning with the fluorides (LaF_3, MgF_2, PbF_2, SrF_2 and ThF_4) continuing with the oxides (Al_2O_3, MgO, SiO) and concluding with ZnSe and ZnS. The order of presentation for each material begins with general crystallographic information such as usual crystal structure and space group (bulk) and x-ray diffraction data on the raw material, followed by structure and preferred orientation of the material in thin film form. Refractive index and absorptance data for thin films of the material on CaF_2 and SrF_2 substrates at 3.9 μm and 5.3 μm and relative growth rate data are tabulated.

The treatment of each material concludes with comments concerning deposition techniques, residual stress, general application of the material, and resistance to an HF environment, when applicable.

The format of presentation of the material properties data is quite straightforward and should require no explanation, but the format utilized for the x-ray diffraction data may be unfamiliar to some members of the optics community. All tables of x-ray diffraction data presented in this report have a common format, whether for raw materials or for thin films on various substrates. In this format, the first column identifies the material and phase determinable from the diffraction line. The second column, headed "Card Ref." refers to the ASTM Powder Diffraction File Card on which the data for the material or phase in question are tabulated. The columns headed "OBs. d (Å)" and "Obs. I/I_{100}" give the interplanar spacing in Å and relative intensity of diffraction peaks observed in the present study. To facilitate comparison and emphasize peculiarities of the evaporant material, the Powder Diffraction File data are also tabulated in columns headed "ASTM d (Å)" and "ASTM I/I_{100}". Miller indices (hkl) of the respective diffracting planes are also tabulated when given on the cards.

3.3.1 Lanthanum Fluoride, LaF_3

LaF_3 crystallizes in the hexagonal system with space group $P6_3/mmc$; the unit cell dimensions are given as $a_o = 7.184$Å, $c_o = 7.351$ on the ASTM card (#8-461), while Wyckoff[47] gives $a_o = 3.148$Å. Results of an x-ray diffraction study of the LaF_3 raw coating material are presented in Table IX. The main feature worth noting is that diffraction lines for LaOF (which should be present only in trace amounts as an impurity) are as intense or more intense than those for LaF_3, the nominal coating material.

TABLE IX. Results of X-Ray Diffraction Study of LaF_3 Coating Material.

Material Source, Condition, Purity : Balzers Ch72-390/3 (99.9%) As Received, Ground.

Radiation : $Cu K_\alpha$ 35 kV. 18 mA. Ni Filter

Material	Card Ref.	Obs d (Å)	Obs I/I_{100}	ASTM d (Å)	ASTM I/I_{100}	hkl	Notes
LaF_3	8-461	3.667	32	3.67	40	002	
		3.580	19	3.59	32	110	
		3.218	59	3.229	100	111	
		2.5615	07	2.569	11	112	
		2.0213	43	2.025	54	113	
		1.8024	27	1.8064	33	302	
		1.7477	27	1.7451	20	221	
		1.4455	08	1.4487	14	223	
		1.3346	19	1.3354	15	411	
		1.1872	14	1.1877	14	413	
LaOF	5-0470	3.348	100	3.35	100	101	
		2.905	22	2.90	25	110	
		2.0606	46	2.06	60	112	
		1.7634	22	1.76	22	103	

Although the intensity of diffracted x-rays is not simply proportional to the amount of a given phase present in a sample (due to losses from absorption, preferred orientation, etc.), such high relative intensities indicate that LaOF is a major constituent of the coating material. If this material is redeposited on substrates during evaporation, coating inhomogeneities and high absorptance in the mid-infrared would be expected. The redeposition of this material in addition to oxides and hydroxides of Lanthanum is in fact found in conjunction with a very high absorption coefficient at 3.8μm, as demonstrated by the thin film data.

Experimental results of x-ray diffraction scans of LaF_3 films (halfwave at 3.8 μm) on three different orientations of CaF_2 substrates are presented in Tables X, XI, and XII. Two salient features of these results are the moderate to strong preferred orientation in the films with some evidence of correlation with the substrate orientation and the strong peaks attributable to LaOF, La_2O_3, and LaO OH occurring on (100) and (111) substrate orientations.

If LaF_3 exhibits a preferred orientation on (100) CaF_2, it would appear to be (111). However, the other peaks of near half the (111) intensity indicate a high degree of randomness in the thin film orientation. On the other hand the single strong peak arising from LaOF indicates a very strong preferred orientation in that phase. The source of the latter material is undoubtedly the coating raw material itself, which contains an abundance of it (Table IX).

On (110) CaF_2, LaF_3 shows a strong (100) preferred orientation as indicated by the intensity of the (300) peak in Table V. It appears that an appreciable fraction of crystallites in the coating material have taken a (302) orientation. The interplanar spacing of LaF_3 in these two orientations is within approximately 7% of the CaF_2 (220) spacing in the (110) direction

TABLE X. Results of X-Ray Diffraction study of LaF_3 on CaF_2 Substrate.

Substrate Orientation: 1° Λ (100)

Film Thickness: 12,500 Å ($\lambda/2$ at 3.8 μm)

Radiation: CuK_α 35 kV. 18 mA. Ni Filter

Material	Card Ref.	Obs d (Å)	Obs I/I_{100}	ASTM d (Å)	ASTM I/I_{100}	hkl	Notes
LaF_3	8-461	3.587	03	3.59	32	110	
		3.223	08	3.229	100	111	
		2.070	03	2.075	51	300	
		1.8024	04	1.8064	33	302	
		1.0066	04	1.0078	03	117	
La OF	6-0281	1.5087	100	1.503	05	432	
LaO OH	19-656	3.015	02	3.04	60	$10\bar{2}$, 002	
CaF_2	4-0864	2.724	63	2.732	--	200	
		1.3633	>100	1.366	12	400	

TABLE XI. Results of X-Ray Diffraction Study of LaF_3 on CaF_2 Substrate.

Substrate Orientation: 3° Λ (110)

Film Thickness: 12,500 Å (λ/2 at 3.8 μm)

Radiation: Cu K_α 35 kV. 18 mA. Ni Filter

Material	Card Ref.	Obs d (Å)	Obs I/I 100	ASTM d (Å)	ASTM I/I 100	hkl	Notes
LaF_3	8-461	3.587	02	3.59	32	110	
		2.067	100	2.075	51	300	
		1.8057	26	1.8064	33	302	
		1.3329	03	1.3354	15	411	
		1.1872	02	1.1877	14	413	
		1.0357	03	1 0370	03	600	
La_2O_3	22-641	2.293	04	2.298	04	$20\bar{4}, \bar{5}03$	

TABLE XII. Results of X-Ray Diffraction Study of LaF_3 on CaF_2 Substrate.

Substrate Orientation: 1° Λ (111)

Film Thickness: 12,500 Å (λ/2 at 3.8 μm)

Radiation: CuK_α 35 kV. 18 mA. Ni Filter

Material	Card Ref.	Obs d (Å)	Obs I/I 100	ASTM d (Å)	ASTM I/I 100	hkl	Notes
LaF_3	8-461	3.672	76	3.67	40	002	
		3.580	18	3.59	32	110	
		2.070	04	2.075	51	300	
		1.8364	10	1.8377	05	004	
		1.8024	03	1.8064	33	302	
		1.7400	06	1.7451	20	221	
		1.2239	03	1.2254	02	006	
		1.619	01	1.1601	02	116	
La_2O_3	5-0602	3.477	100	3.41	34	100	1
	24-554			3.51	30	100	
CaF_2	4-0864	3.1399	>100	3.153	94	111	
		1.5751	28	1.5765	--	222	

1. The spacing of 3.41Å corresponds to a hexagonal form of La_2O_3 at room temperature, while 3.51Å was obtained on the material at 2100°C. Hence, it appears that a high temperature form of the oxide is quenched in the thin film at room temperature.

i. e. normal to the [110] substrate surface). This indicates influence of the coating orientation by the substrate structure.

The La_2O_3 peak on (110) CaF_2 is not particularly strong. Although substantially equal quantities of contaminants should deposit on all substrate orientations in films of this thickness, it is possible that the crystallite size of this material is very small and orientation near random, so that diffraction peaks are very weak.

On (111) CaF_2, LaF_3 exhibits a strong (001) preferred orientation, with a minority of crystallites oriented near (100) and (110). This orientation of (hexagonal) LaF_3 corresponds to the 3-fold symmetry of the (111) CaF_2 surface. The single La_2O_3 peak is again very strong, showing marked preferred orientation and an appreciable quantity of material. The large spacing may indicate that a high temperature form of the oxide is quenched in the thin film at room temperature.

On SrF_2, LaF_3 films show preferred orientation similar to that on CaF_2. On (100) SrF_2, LaF_3 has a predominantly (111) orientation with strong (100) and (110) type peaks, again indicating a high degree of randomness as on CaF_2 (100). On SrF_2 (110), LaF_3 shows a strong (110) orientation, unlike its behavior on (110) CaF_2. $La(OH)_3$ shows one strong peak (201), indicating strong preferred orientation of this impurity on (110). In addition, the patterns for both (110) and (111) SrF_2 substrates indicate significant microcrystalline or amorphous material with spacings in the 4 to 6Å region. The orientation of LaF_3 on (111) SrF_2 is again the basal (001) orientation shown on CaF_2.

Properties of LaF_3 coatings determined under the program are listed in Table XIII.

TABLE XIII. Optical Properties of LaF_3 Films.

Substrate Material	Orientation	n (3.8 μm)	β (cm^{-1}) (3.9 μm)	Relative Growth Rates
CaF_2	(100)		41.49	
	(110)		28.43	
	(111)		24.88	
	Mean	1.52	31.60	(100) = (110) = (111)
SrF_2	(100		36.61	
	(110)		24.53	
	(111)		29.49	
	Mean	1.52	30.21	(100) = (110) = (111)

3.3.2 Magnesium Fluoride, MgF_2

Magnesium Fluoride crystallizes in the tetragonal cassiterite (SnO_2) structure[38,48] with space group P4/mnm, a_o = 4.623Å, c_o = 3.052Å, Z = 2. Another form designated α - MgF_2, also tetragonal, with cell dimensions a_o = 9.927Å c_o = 6.172Å has been reported[49].

The results of an x-ray diffractometer scan of raw MgF_2 coating material from the electron gun boat are presented in Table XIV. These results indicate that the material consists predominantly of the phase having the smaller unit cell dimensions,[48] with no evidence for the α form[49]. The impurity lines, tentatively identified with ThF_4, could also arise from traces of elemental magnesium.

In thin film form, lines arising from both MgF_2 phases are evident on CaF_2 (100), it takes a strong (001) orientation, with slightly smaller (002) spacing

TABLE XIV. Results of X-Ray Diffraction Study of MgF_2 Coating Material.

Material Source and Condition: Residual from E-Gun boat. Balzers >99.9%.

Material	Card Ref.	Obs. d(Å)	Obs. I/I_{100}	ASTM d(Å)	ASTM I/I_{100}	hkl	Notes
MgF_2	6-0290	3.264	100	3.265	100	100	
		2.547	11	2.545	22	101	
		2.231	59	2.231	96	111	
		2.067	22	2.067	34	210	
		1.710	90	1.711	73	211	
		1.633	42	1.635	31	220	
		1.527	35	1.526	19	002	
		1.461	06	1.462	06	310	
		1.375	34	1.375	35	301	
		1.317	04	1.318	07	311	
		1.281	01	1.282	01	320	
		1.227	02	1.228	06	212	
		1.114	08	1.115	10	222	
		1.0888	47	1.0893	06	330	
		1.0523	06	1.0524	06	411	
		1.0324	02	1.0333	02	420	
ThF_4	23-1426	3.6085	04	3.63	50	312	
		2.4694	03	2.495	10	231	1
		1.8940	03	1.881	10	350	

1. Elemental Mg (101) and (102) lines are also possible sources of the last 2 peaks. For Mg (101) d = 2.453Å, I = 100; for Mg (102) d = 1.901Å, I = 20.

(1.511Å) than the tabulated value of 1.526 Å. Very weak α - MgF_2 (440) and (216) lines are also observed with the tabulated spacings.

On CaF_2 (110), MgF_2 (211) and (112) have equal intensity, while (110) has 70% of this maximum intensity. Hence, this is a more or less randomly oriented film. On CaF_2 (111), a very weak α - MgF_2 (800) line is observed at 1.161Å. The only other diffraction line in the pattern not arising from the substrate has a spacing of 3.477Å, or three times the α - MgF_2 (800) spacing. This may indicate a distorted α - MgF_2 structure with strong preferred orientation. On SrF_2, MgF_2 coatings are highly stressed and exhibit crazing and other defects. They show no X-ray diffraction peaks, indicating either that no long range order is developed or that crystallites are too small to diffract X-rays to yield significant peaks.

Properties of MgF_2 coatings determined under the program are listed in Table XV.

TABLE XV. Optical Properties of MgF_2 Films.

Substrate Material	Orientation	n (3.8 μm)	β(cm^{-1}) (3.9 μm)	Relative Growth Rates
CaF_2	(100)		19.06	
	(110)		21.70	
	(111)		21.17	
	Mean	1.36	20.64	(100) = (110) = (111)
SrF_2	(100)		17.56	
	(110)		18.33	
	(111)		19.20	
	Mean	1.36	18.36	(100) = (110) = (111)

Magnesium fluoride is probably the most widely used coating material. It is easily evaporated from resistance heated sources as well as from electron beam sources. The refractive index of magnesium fluoride films is a function of the substrate temperature with the average value being about 1.33 for the 2-6 μm region.[50] Films deposited on substrates heated to 300°C are extremely stable, hard, and adherent. However, due to the large internal stresses in these films (3000 - 5000 kg/cm^2 for 1000Å)[51], their use is usually restricted to the shorter wavelengths. We have deposited quarterwave films of magnesium fluoride on single crystal calcium fluoride substrates for the 2.8 μm, 3.8 μm, and 5.3 μm wavelengths, and in each case, there was the appearance of various patterns of microcrazing.[6] The degree of microcrazing and the type of pattern seem to be dependent on the crystallographic orientation of the substrates.

3.3.3 Lead Fluoride PbF_2

PbF_2 crystallizes in two polymorphs with a transition temperature near 250°C. One of these, α - PbF_2, is orthorhombic with space group Pbnm, and lattice parameters a_o = 7.357Å, b_o = 4269Å, c_o = 3.891Å.[38] The unit cell contains four formula units of PbF_2. This structure is of the $PbCl_2$ type, in essence a distorted cubic close packing of halogen atoms with lead atoms accommodated in the same plane with them[38]; this phase has a higher atomic packing density than the cubic β - phase and hence should be stable at lower temperatures. The cubic β - PbF_2 polymorph has the fluorite structure with space group Fm3m and unit cell dimension a_o = 5.927Å; the unit cell contains four formula units of PbF_2.[38]

Results of an x-ray diffractometer scan of the raw material from the electron gun boat are presented in Table XVI. Both phases are present in this material, the β form predominating. No diffraction peaks attributable to impurities are evident.

TABLE XVI. Results of X-Ray Diffraction Study of PbF_2 Coating Material.

Material Source and Condition: Residual material from boat. Balzers > 99.9%

Material	Card Ref.	Obs. d(Å)	Obs. I/I_{100}	ASTM d(Å)	ASTM I/I_{100}	hkl	Notes
αPbF_2	6-0288	3.76	05	3.824	10	002	
		3.27	07	3.290	100	012	
		1.2000	09	1.2079	04	151	Overlaps w/ βPbF_2 (422)
βPbF_2	6-0251	3.411	100	3.428	100	111	
		2.954	32	2.970	56	200	
		2.092	59	2.100	73	220	
		1.786	42	1.791	64	311	
		1.709	7	1.715	14	222	
		1.481	8	1.485	10	331	
		1.325	8	1.328	21	420	
		1.2000	9	1.212	26	422	
		1.1406	8	1.143	20	511	
		1.0483	5	1.050	8	440	
		1.0026	8	1.0043	20	531	
		0.9890	4	0.9903	13	600	

Both phases are also found in about the same proportions in thin films of this coating material. It was found previously that both phases occurred in quarterwave thicknesses (at 5.3 μm) of PbF_2 deposited on single crystal CaF_2 substrates maintained at 200°C, with the cubic β - phase predominating and taking an orientation parallel to the substrate, with a mismatch of

the order of 8%.[6] The growth rate of these films was found to vary with substrate orientation, being ~ 3% faster on (110) than on (100) and (111).

Results of the present work are presented in tables XVII, XVIII, and XIX. On CaF_2 (100), β - PbF_2 takes a very strong (111) preferred orientation, with minor (331) and (511) lines. This contrasts sharply with the previous X-ray and electron diffraction results, which showed a (100) orientation throughout the bulk of the film and a (110) orientation near the free surface.

The α - PbF_2 in the present study is oriented near (001); in the previous work it showed a (012) orientation.

TABLE XVII. Results of X-Ray Diffraction Study of PbF_2 on CaF_2 Substrate.

Substrate Orientation: 1° Λ (100)

Film Thickness: 10,900 Å (λ /2 at 3.3 μm)

Radiation: CuK_α 35 kV. 18 mA. Ni Filter

Material	Card Ref.	Obs d (Å)	Obs I/I 100	ASTM d (Å)	ASTM I/I 100	hkl	Notes
β - PbF_2	6-0251	3.424	100	3.428	100	111	
		1.714	11	1.715	14	222	
		1.363	05	1.362	27	331	
		1.143	< 01	1.143	20	511	
α - PbF_2	6-0288	3.782	01	3.824	10	002	

TABLE XVIII. Results of X-Ray Diffraction Study of PbF_2 on CaF_2 Substrate.

Substrate Orientation: 5° Λ (110)

Film Thickness: 10,980 Å (λ/2 at 3.8 μm)

Radiation: Cu K_α 35 kV. 18 mA. Ni Filter

Material	Card Ref.	Obs d (Å)	Obs I/I_{100}	ASTM d (Å)	ASTM I/I_{100}	hkl	Notes
β - PbF_2	6-0251	3.424	100	3.428	100	111	
		2.097	98	2.100	73	220	
		1.711	06	1.715	14	222	

TABLE XIX. Results of X-Ray Diffraction Study of PbF_2 on CaF_2 Substrate.

Substrate Orientation: 1.8° Λ (111)

Film Thickness: 10,980 Å (λ/2 at 3.8 μm)

Radiation: Cu K_α 35 kV. 18 mA. Ni Filter

Material	Card Ref.	Obs d (Å)	Obs I/I_{100}	ASTM d (Å)	ASTM I/I_{100}	hkl	Notes
β - PbF_2	6-0251	3.424	100	3.428	100	111	
		1.714	29	1.715	14	222	
		1.306	<01	1.328	21	420	
		1.142	02	1.143	20	511	
α - PbF_2	6-0288	3.798	05	3.824	10	002	
		1.2798	<01	1.2854	05	143	
		1.2470	<01	1.2570	03	224, 311	
CaF_2	4-0814	3.156	09	3.153	94	111	
		1.0515	<01	1.0512	07	511	

On the (110) surface of CaF_2, β - PbF_2 is the only phase present, showing equally strong (110) and (111) orientations (Table VIII). In previous work, a very strong (110) orientation with minor (111) and α - PbF_2 (103) lines was determined.[6] On (111) CaF_2, the (111) orientation of β - PbF_2 predominates (Table XIX), with minor (420) and (511) lines. The α - phase takes a predominant (001) orientation, with minor lines of higher index. The general behavior of PbF_2 on (111) CaF_2 is in accord with previous results[6].

Present results on relative growth rates of PbF_2 on the three substrate orientations show fastest growth on (110) followed by (111) and (100), again in accord with previous results.[6] Hence, it is difficult to reconcile structure and growth rate data in the two sets of experiments. Present results suggest that the preferred growth direction of PbF_2 is [111] on all three substrate orientations. This is mitigated somewhat on (110) CaF_2, where the (110) line of β - PbF_2 has an intensity equal to (111). Reasons for this behavior are not clear. The degree of mismatch between the lattice parameters of coating and substrate materials, defined as

$$\Delta d = \frac{d_{hkl}\ (\text{coating}) - d_{hkl}\ (\text{substrate})}{d_{hkl}\ (\text{substrate})} \times 100\%$$

is about 8.7% for corresponding (100), (110), and (111) CaF_2 and βPbF_2. On (110) CaF_2, the mismatch with (111) PbF_2 is only 8.8%, so the coexistence of (111) and (110) PbF_2 on (110) CaF_2 is not surprising. However on (100) CaF_2, the mismatch with (111) PbF_2 is 37%.

The orientation of β - PbF_2 films on SrF_2 substrates follows substrate orientations nearly perfectly in all three cases as indicated by the data of Tables XX, XXI and XXII. This is not at all surprising, since the mismatch between corresponding planes of PbF_2 and SrF_2 is 2.4% for (100) and (110)

and 2.3% for (111). α - PbF_2 occurs on the (100) substrate orientation with about equal (010) and (012) orientations; mismatch with the substrate is about 13% while that with β - PbF_2 is about 10%. No α - PbF_2 occurs on (110) SrF_2.

TABLE XX. Results of X-Ray Diffraction Study of PbF_2 on SrF_2 Substrate.

Substrate Orientation: 2.5° Λ (100)

Film Thickness: 5,490 Å ($\lambda/4$ at 3.8 μm)

Radiation: CuK_α 35 kV. 18 mA. Ni Filter

Material	Card Ref.	Obs d (Å)	Obs I/I_{100}	ASTM d (Å)	ASTM I/I_{100}	hkl	Notes
β - PbF_2	6-0251	2.957	100	2.970	56	200	
		1.4816	35	1.485	10	400	
α - PbF_2	6-0288	3.276	02	3.290	100	012	
		3.201	01	3.222	40	020	
		1.6407	01	1.6445	13	024	
		1.6040	04	1.6101	04	040	
SrF_2	6-0262	2.891	53	2.900	25	200	
		1.4485	71	1.4499	15	400	

TABLE XXI. Results of X-Ray Diffraction Study of PbF_2 on SrF_2 Substrate.

Substrate Orientation: 2° Λ (110)

Film Thickness: 5490 Å (λ/4 at 3.8 μm)

Radiation: CuK_α 35 kV. 18 mA Ni Filter

Material	Card Ref.	Obs d (Å)	Obs I/I 100	ASTM d (Å)	ASTM I/I 100	hkl	Notes
β - PbF_2	6-0251	3.424	06	3.428	100	111	
		2.095	100	2.100	73	220	
		1.0485	05	1.050	08	440	
Pb_2O_3	23-331	2.319	02	2.317	02	003	

TABLE XXII. Results of X-Ray Diffraction Study of PbF_2 on SrF_2 Substrate.

Substrate Orientation: 0.5° Λ (111)

Film Thickness: 5490 Å (λ/4 at 3.8 μm)

Radiation: CuK_α 35 kV. 18 mA. Ni Filter

Material	Card Ref.	Obs d (Å)	Obs I/I 100	ASTM d (Å)	ASTM I/I 100	hkl	Notes
β - PbF_2	6-0251	3.418	100	3.428	100	111	
		1.7098	07	1.715	14	222	
		1.1406	01	1.143	20	511	
α - PbF_2	6-0288	3.782	03	3.824	10	002	
		1.8937	< 01	1.912	16	004	
PbO	5-0561	2.506	< 01	2.510	18	002	

The presence of lead oxide, Pb_2O_3 on (110) and PbO on (111), comes as no surprise. It tends to increase the refractive index of the films slightly, but probably does not appreciably increase absorptance. The relative growth rates of PbF_2 on (110) and (100) SrF_2 are essentially equal, with the rate on (110) being slightly greater. The slowest growth rate is on (111) SrF_2.

Properties of PbF_2 coatings determined under this program are listed in Table XXIII. Lead fluoride is an excellent starting film between the substrate and the other films. It has low residual stress at the substrate interfaces, making it possible to apply additional films which together resist peeling and cracking.[52]

TABLE XIII. Optical Properties of PbF_2 Films.

Substrate Material	Orient.	n (3.8 μm)	β(cm^{-1}) (3.9 μm)	n (5.3 μm)	β(cm^{-1}) (5.3 μm)	Relative Growth Rates
CaF_2	(100)		4.24		1.69	
	(110)		3.03		2.14	
	(111)		7.16		3.34	
	Mean	1.73	4.81	1.72	2.39	(110) > (111) > (100)
SrF_2	(100)		2.65		—	
			1.63*			
	(110)		5.39		—	
			2.01*			
	(111)		4.98		—	
			1.94*			
	Mean	1.73	4.34		—	(110) ≥ (100) > (111)
			1.86*			

* These values were determined from βL vs. L plots described in detail in section 3.4.2

Resistance of PbF_2 films to a humid HF environment is generally poor to fair; general chemical attack renders the films unuseable in 30 minutes.

3.3.4 Strontium Fluoride (SrF_2)

Strontium fluoride crystallizes in the cubic fluorite structure with space group Fm3m and lattice parameter a_o = 5.800Å; the unit cell contains four formula units of SrF_2.[38] Results of an x-ray diffractometer scan of SrF_2 raw material are presented in Table XXIV.

TABLE XXIV. Results of X-Ray Diffraction Study of SrF_2 Coating Material.

Material Source and Condition: EMCO Lot 76437/1458 (Crystal Fragments, as received, ground).

Material	Card Ref.	Obs. d(Å)	Obs. I/I_{100}	ASTM d(Å)	ASTM I/I_{100}	hkl	Notes
SrF_2	6-0262	3.298	100	3.352	100	111	
		2.891	05	2.900	25	200	
		2.045	74	2.051	80	220	
		1.7446	18	1.7486	52	311	
		1.6703	5	1.6743	5	222	
		1.4455	3	1.4499	15	400	
		1.3273	8	1.3303	21	331	
		1.2949	2	1.2966	10	420	
		1.1818	6	1.1840	24	422	
		1.1146	2	1.1164	16	511	
		1.0245	2	1.0253	7	440	
		0.9799	5	0.9803	14	531	
		0.9657	18	0.9666	7	600	
		0.9163	4	0.9170	10	620	
$Sr(OH)_2$	18-1273 19-1276	3.6896	04	3.85 3.65	80 75	210 n.i.	

The only disturbing feature of the pattern is the weak line attributable to $Sr(OH)_2$. If this compound is present in appreciable quantities in the raw material, it is probable that oxides or hydroxides of strontium will be deposited in thin films of SrF_2, leading to increased absorptance in the mid-infrared. This is in fact observed.

It was found previously that SrF_2 films deposited on single crystal CaF_2 substrates took on very strong preferred orientations following the substrate.[6] However, behavior of the present material is very similar to that of β - PbF_2 deposited on CaF_2 substrates. For halfwave thicknesses of SrF_2 on CaF_2 at design wavelengths of 3.8 and 5.3 μm, the dominant preferred orientation in the thin films is (111). For the 5.3 μm films, (100) and (110) type peaks are of very low intensity on the corresponding substrate orientations, with (111) always strongest. For the 3.8 μm films, the (100) and (110) - type peaks are about twice the intensity of the (111) peaks. Diffraction lines corresponding to elemental strontium and its oxides are found on all substrate orientations, but in greater numbers and greater intensities on (100) and (111).

Thus it appears that the preferred growth direction of SrF_2 films is [111] on CaF_2 substrates, but the substrate orientation has a variable influence upon this, possibly corresponding to substrate temperature or impurity content of the films. Non-stoichiometry and the presence of oxygen or hydroxyl groups are problematic, as observed in previous work.[6]

Properties of SrF_2 coatings measured under the present program are listed in Table XXV.

TABLE XXV. Optical Properties of SrF_2 Films on CaF_2 Substrates.

Substrate Orientation	n (3.8 μm)	β(cm^{-1}) (3.9 μm)	n (5.3 μm)	β(cm^{-1}) (5.3 μm)	Relative Growth Rates
(100)		39.81		17.67	
(110)		44.71		16.16	
(111)		29.24		I3.41	
Mean	1.34	37.92	1.33	15.75	(100)=(110)=(111)

The average value of the refractive index of strontium fluoride is given in the literature as 1.33 for the 2-6 μm region.[53] There is some dependence of the refractive index of the films on the temperature of the substrate. The increase in the refractive index with the increase of substrate temperature is apparently caused by a more perfect film structure, particularly, by a decrease in its porosity. In previous work, we have coated single crystal calcium fluoride substrates with quarterwave optical thicknesses of strontium fluoride films at 5.3 μm; the average refractive index was determined to be 1.32.[6] Some dependence of the refractive index on the crystallographic orientation of the substrate was observed. High purity and careful outgassing of the starting material is required to prevent inhomogeneity in the films.

3.3.5 Thorium Fluoride (ThF_4)

Thorium tetrafluoride crystallizes in the monoclinic system with the zirconium fluoride structure.[47] Two unit cells of slightly different diensions have been reported in recent entries in the ASTM card file.[54] These are a_o = 13Å, b_o = 11.1Å, c_o = 8.6Å, β = 126.0° and a_o = 12.9Å, b_o = 10.93Å, c_o = 8.58Å, β = 126.4°, with space group C 2/c and cell content Z = 12 formula units of ThF_4. In the older literature,[47] a body-centered cell (I 2/c)

was chosen, with dimensions a_o = 10.64Å, b_o = 11.0 Å, c_o = 8.6Å, β = 94°50', Z = 12.

Data from an x-ray diffraction scan of some ThF_4 raw material supplied by Cerac are presented in Table XXVI. X-ray patterns from recently manufactured Balzers raw material are identical. If the single, spurious line arises in fact from a contaminant containing water, oxygen, or hydroxyl groups, excessive absorptance in thin films of the material are expected at 2.8 μm, 3.9 μm, and 5.3 μm.

TABLE XXVI. Results of X-Ray Diffraction Study of ThF_4 Coating Material.

Material Source and Condition: Supply Cerac TS-106 5466

Material	Card Ref.	Obs. d(Å)	Obs. I/I_{100}	ASTM d(Å)	ASTM I/I_{100}	hkl	Notes
ThF_4	23-1426	7.59	14	7.63	10	110	
		5.24	11	5.24	10	200	
		4.297	81	4.29	80	$20\bar{2}$	
		4.019	58	4.02	60	$3\bar{1}\bar{1}$	
		3.806	100	3.80	100	220	
		3.630	51	3.63	50	312	
		3.354	34	3.35	50	310	
		2.855	08	2.848	05	102	
		2.736	15	2.747	15	$13\bar{2}$	
		2.533	07	2.528	10	311	
		2.496	10	2.495	10	231	
		2.162	22	2.156	15	430	
		2.130	83	2.132	35	$13\bar{3}$	
		2.063	17	2.067	05	$50\bar{4}$	
		2.030	22	2.040	20	$20\bar{4}$	
		1.984	22	1.985	35	611	
		1.932	12	1.937	15	312	
		1.770	14	1.771	10	$63\bar{1}$	
		1.576	12	1.585	10	644	
		1.436	46	1.431	10	645	
ThB_{66}	21-1220	6.752	08	6.799			1
ThF_4	15-413	3.167	52	3.15	10	n.i.	

1. Other possibilities include $ThOCl_2 \cdot 14\ H_2O$ (6.706Å), $Th(SO_4)_2 \cdot 9H_2O$ (6.90Å), and KTh_6 (6.928Å).

On (100) CaF_2, ThF_4 films are crystalline with nearly equal (270) and (21$\bar{3}$) preferred orientations. Mismatch of ThF_4 (270) with the (100) spacing of CaF_2 is approximately 11%; mismatch of (21$\bar{3}$) with (200) CaF_2 is less than 1%. On (110) CaF_2, ThF_4 films are microcrystalline (amorphous to X-ray) with subequal diffuse maxima in diffracted X-ray intensity at approximately 3.8 Å and 2.01Å, corresponding respectively to ThF_4 (220) and (103).[54] Mismatch between ThF_4 (220) and CaF_2 (110) is 1.6% while that between ThF_4 (103) and CaF_2 (220) is 4.8%. On (111) CaF_2, ThF_4 is crystalline, taking a very strong (32$\bar{1}$) orientation, with one weak (332) line. Mismatch between CaF_2 (111) and ThF_4 (32$\bar{1}$) is approximately 9%; that between ThF_4 (332) and CaF_2 (222) is approximately 10%.

These results are in general accord with previous work,[6] but details of the preferred orientations differ. This is not surprising since overall behavior remains the same: ThF_4 films tend to adopt a preferred crystallographic orientation leading to minimal mismatch with a CaF_2 substrate. Since the structure of ThF_4 is more complex than that of CaF_2, several interplanar spacings may lie near a given CaF_2 spacing. The particular orientation adopted by the film may then depend upon other considerations than mismatch across the film-substrate interface, e.g. contaminants, stacking faults, and preferential growth directions in the film material itself.

ThF_4 coating material from two different vendors (Cerac and Balzers) was deposited on SrF_2 substrates. Although the number and intensity of diffraction peaks attributable to oxides, oxyfluorides, and hydrated fluorides of thorium differ in thin films deposited using raw material from different vendors, the overall structure and orientation of the films is remarkably consistent.

On (100) SrF_2 the strongest coating diffraction line for Cerac material is attributable to hydrated ThF_4 with an observed spacing of 3.20Å corresponding to a strong (132) preferred orientation. The line of secondary intensity is attributable to ThF_4 (252) with a spacing of 1.61Å. Minor amounts of amorphous or microcrystalline material with spacings in the 5 to 9Å region, corresponding to ThF_4 (200) and (110) are observed.

For Balzers ThF_4, the coating is microcrystalline with primary orientation near (512) with an observed spacing of 1.466Å and subequal secondary orientations near (103) (d = 2.004Å) and (220) (d = 3.80Å). Mismatch between the (512) spacing and (400) SrF_2 is 1%, that between (103) and (220) SrF_2 (exposed on the SrF_2 (100) surface) is 2%, and that between (220) and (111) SrF_2 is 13%.

On (110) SrF_2, ThF_4 comprises predominantly well crystallized material with a strong $(52\bar{1})$ orientation (d = 2.27Å), a mismatch of 10.7% with (220) SrF_2 for films fabricated using material manufactured by either Cerac or Balzers. Both materials show minor amounts of poorly crystallized thin film with spacings corresponding to ThF_4 $(31\bar{1})$, (220), (030), $(31\bar{2})$, $32\bar{1}$) and (310). Evidence for a substantial amount of microcrystalline, hydrated ThF_4 with a spacing of approximately 3.48Å was observed in a pattern from one coating fabricated from Cerac material.

On (111) SrF_2, ThF_4 from either vendor is crystalline, taking a strong (030) orientation, with an observed spacing of 3.697Å, a mismatch of 10.3% with the substrate (111) spacing of 3.35Å. Material with a spacing of 1.85Å, corresponding to (322) ThF_4 is also observed, giving rise to a diffracted X-ray intensity about 25% of the (030) line. Minor amounts of hydrated ThF_4 with a spacing of 2.45Å, corresponding to a (151) orientation are found in films fabricated from Cerac material, but not in those fabricated from Balzers material.

In summary of ThF_4 film structure, it appears that the material may be crystalline, microcrystalline, or amorphous, depending upon substrate type and orientation. When crystalline, it tends to take an orientation which minimizes mismatch with the fluoride substrate spacing. Hydrated material in thin film form is more common when Cerac raw material is used.

Properties of ThF_4 determined under the present program are listed in Table XXVII.

TABLE XXVII. Optical Properties of ThF_4 Films.

Substrate Material	Orient.	n (3.8 μm)	β(cm^{-1}) (3.9 μm)	n (5.3 μm)	β(cm^{-1}) (5.3 μm)	Relative Growth Rates
CaF_2	(100)		2.86		3.24	
	(110)		1.65		3.11	
	(111)		3.58		2.98	
	Mean	1.49	2.70	1.48	3.11	(100) = (110) = (111)
SrF_2	(100)		4.43		1.41*	
	(110)		2.76		0.78*	
	(111)		3.59		0.78*	
	Mean	1.49		1.48	0.99*	(100) = (110) = (111)

* Balzers Raw Material; All other coatings used Cerac.

Thorium fluoride films have been used extensively in the infrared region as a protective coating for highly reflecting metal mirror surfaces and in combination with zinc sulfide films to fabricate multilayer coatings at 10.6 μm.[55] This material deposits as a strongly adherent film and is very nearly insoluble in water. The average refractive index is 1.48 for the 2-6 μm region.[6] The transmission range of thorium fluoride films extends to 15 μm.[56]

ThF_4 films in quarterwave thicknesses on SrF_2 have fair resistance to attack by humid HF. The attack occurs only at isolated defects, doing noticeable damage within 30 minutes (section 3.4.4). In halfwave films on CaF_2, destruction is extensive, comprising a unique spiral crazing pattern (sec. 3.4.4).

3.3.6 Aluminum Oxide (Al_2O_3)

Although Al_2O_3 may crystallize in a multiplicity of forms, we shall be concerned only with the common form known variously as α - Al_2O_3, corundum, or sapphire. The structure is most easily visualized as a hexagonal close-packing of oxygen ions with small metallic ions lying in some interstices.[38] The space group is R 3 c and the structure may be referred to a primitive rhombohedral cell having $a_o = 3.76\text{Å}$, and containing six formula units of Al_2O_3.

Results of an x-ray diffractometer scan of Al_2O_3 raw coating material are presented in Table XXVIII. The presence of minor amounts of the θ-phase is interesting, but has no practical significance. No impurities were detected.

TABLE XXVIII. Results of X-Ray Diffraction Study of Al_2O_3 Coating Material.

Material Source and Conditions: Crystalline fragments from supply. (Crystal products-end cuttings from Boule of UV grade saphire)

Material	Card Ref.	Obs. d(Å)	Obs. I/I_{100}	ASTM d(Å)	ASTM I/I_{100}	hkl	Notes
α-Al_2O_3	10-173	3.483	30	3.479	75	012	
		2.551	38	2.552	90	104	
		2.378	09	2.379	40	110	
		2.085	43	2.085	100	113	
		1.737	60	1.740	45	024	
		1.600	100	1.601	80	116	
		1.404	46	1.404	30	124	
		1.376	11	1.374	50	030	
		1.1921	06	1.1898	07	220	
		1.0780	15	1.0781	07	134	
θ-Al_2O_3	11-517	2.812	17	2.85	80	004	
		1.773	06	1.80	30	015	

On (100) CaF_2, Al_2O_3 films are crystalline with the corundum structure and a very strong (018) preferred orientation. A small amount of material takes a (1 2 10) orientation and a minor amount of microcrystalline material having spacings in the 3 to 5 Å region is observed. On (110) CaF_2, the film is microcrystalline or amorphous with spacings in the 1.8 to 2.1Å region, corresponding to spacings for several different forms of aluminum oxide. On (111) CaF_2, Al_2O_3 films are largely microcrystalline or amorphous with spacings in the 5.9 and 7.4Å regions. A single, sharp peak at a spacing of 3.497Å corresponding to α-Al_2O_3 (012) is of low intensity, indicating that crystallinity is poorly developed on this substrate orientation.

On SrF_2, Al_2O_3 is apparently entirely amorphous to X-rays on two of the three substrate orientations, (100) and (110). On (111) SrF_2, microcrystalline material predominates with a spacing in the 6Å region. In addition, a single weak peak at 3.69Å is observed. This is not attributable to common phases of Al_2O_3, $Al(OH)_3$, AlF_3, or elemental Al, or to the SrF_2 substrate.

Properties of Al_2O_3 coating measured under the present program are presented in Table XXIX.

TABLE XXIX. Optical Properties of Al_2O_3 Films.

Substrate Material	Orientation	n (3.8 μm)	β (cm^{-1}) (3.9 μm)	Relative Growth Rates
CaF_2	(100)		40.75	
	(110)		37.70	
	(111)		29.65	
	Mean	1.57	36.03	(100) ≅ (110) > (111)
SrF_2	(100)		45.13	
	(110)		43.90	
	(111)		32.71	
	Mean	1.57	40.58	(100) ≅ (110) > (111)

The electron beam evaporation of aluminum oxide (synthetic sapphire) produces extremely hard and durable films. Films deposited on heated substrates have a slightly higher refractive index than those deposited on unheated substrates. The films are transparent from 0.2 μm to 7 μm if they are prepared correctly. The water absorption band will have to be considered at the 2.8 μm HF laser wavelength and the long wavelength transmission cut-off of aluminum oxide may produce unacceptable absorption at the 5.3 μm CO laser wavelength. At 5.3 μm, a bulk absorption coefficient of 1.4 cm^{-1} has been reported by Deutsch.[31] The films have been extensively used as protective films for metal mirrors and temperature stabilization coatings on satellites.

Exposure of Al_2O_3 films to a humid HF vapor environment (sec. 3.4.4) reveals that they are the most resistant of the films subjected to that severe test, with their physical integrity surviving for more than one hour. The mode of chemical attack involved both general reaction of the entire coating surface, forming a thin interference film in the visible region and deeper attack at film defects. The latter eventually leads to destruction of the coating.

3.3.7 Magnesium Oxide (MgO)

Magnesium oxide (periclase) crystallizes in the cubic sodium chloride structure with space group Fm3m and lattice parameter $a_o = 4.211$Å.[38] Recently reported experimental work with thin films of MgO on amorphous substrates[57] indicates that the preferred growth direction is < 111 >, independent of substrate temperature and deposition rate. Our results on oriented single crystal CaF_2 substrates tend to confirm this for the (100) and (110) substrate orientations, but not for the (111) orientation.

The results of an x-ray diffractometer scan of the raw MgO coating material are presented in Table XXX. The presence of α-MgF_2 as an impurity is not alarming in terms of optical properties. If present in sufficient quantities (which is not indicated by the x-ray diffraction data) this impurity could reduce the refractive index of coatings utilizing this raw MgO material, but should not increase absorptance.

TABLE XXX. Results of X-Ray Diffraction Study of MgO Coating Material.

Material Source and Condition: Supply - Balzers Ch 73-085/2

Material	Card Ref.	Obs. d(Å)	Obs. I/I_{100}	ASTM d(Å)	ASTM I/I_{100}	hkl	Notes
MgO	4-0289	2.427	11	2.431	10	111	
		2.106	100	2.106	100	200	
		1.488	53	1.489	52	220	
		1.269	06	1.270	04	311	
		1.215	14	1.216	12	222	
		1.0523	05	1.0533	05	400	
α-MgF_2	16-160	2.330	04	2.261	20	222, 410	1
		1.6474	03	1.647	70	440	

1. Best fit of probable Mg compounds; i.e., other oxides, hydroxides, and fluorides.

On (100) CaF_2, MgO films take a strong (111) orientation with a slightly expanded (111) spacing (2.496Å as compared to the expected 2.431Å).[16] A weak MgO (220) peak is also observed, with a 1.506Å (near nominal) spacing. On (110) CaF_2, the strongest MgO peaks again correspond to (111) and (222), with (111) having the expanded spacing observed on (100) CaF_2. The (222) spacing has the nominal value. Peaks corresponding to (100) and (110) MgO are also observed, with intensities 20 to 33% of the (111) intensity, indicatint that appreciable fractions of crystallites in the MgO film are oriented in these directions. Mismatch of (111) MgO on (100) or (110) CaF_2 is about 9%, as is (100) MgO on (110) CaF_2 and (110) MgO on (100) CaF_2, so these observed combinations are not unexpected. However, the mismatch of (110) MgO on (110) CaF_2 is 23%, so this observed orientation is unexpected.

On (111) CaF_2, the only diffraction line not attributable to the substrate corresponds to a spacing of 3.50Å, which is not identifiable with any known spacing of MgO, MgO_2, $Mg(OH)_2$ or elemental Mg. However, this spacing is close to double the $Mg(OH)_2$ (102) spacing of 1.794Å[17] or the MgO_2 spacing of 1.700Å.[18] Thus, the formation of a magnesium oxide or hydroxide superstructure in the thin film form is a possibility on the (111) CaF_2 surface.

On SrF_2, MgO films are apparently largely amorphous to X-ray and exhibit stoichiometry problems. On (100) SrF_2, a weak MgO (111) diffraction peak occurs with the nominal 2.43Å spacing, in addition to a strong peak with a spacing of 3.22Å. This is almost exactly double the (110) spacing of elemental Mg[19] and could imply formation of a Mg superstructure. The Mg (200) line also occurs on this substrate orientation. On (110) SrF_2, the material is microcrystalline with spacings in the 4.5Å and 3.8Å regions. One weak diffraction peak at 2.266Å is attributable to α - MgF_2[12] (222, 410).

On (111) SrF_2, the material is again microcrystalline with spacings in the 5.9Å region. Electron beam evaporation of magnesium oxide produces extremely hard films with an average refractive index of 1.68 for the 2-6 μm region.[58] The transmission range of magnesium oxide extends from 0.23-9 μm.[59] A bulk absorption coefficient of 0.05 cm^{-1} at 5.25 μm has been reported for magnesium oxide.[60] Magnesium oxide films have not yet found wide application since their stability is limited when exposed to atmospheric conditions. Film combinations that utilize magnesium oxide as an inside layer do not deteriorate.[60]

Properties of MgO films determined under the present contract are listed in Table XXXI.

TABLE XXXI. Optical Properties of MgO Films in the DF Laser Wavelength Region.

Substrate Material	Orientation	n (3.8 μm)	β (cm^{-1}) (3.9 μm)	Relative Growth Rates
CaF_2	(100)	1.63	65.91	
	(110)	1.63	86.14	
	(111)	1.63	79.06	
	Mean	1.63	77.04	(100) > (110) ≅ (111)
SrF_2	(100)	1.62	62.55	
	(110)	1.66	100.85	
	(111)	1.65	102.03	
	Mean	1.64	88.48	(110) ≥ (111) > (100)

On CaF_2, MgO films show no variation in refractive index with substrate orientation, but different growth rates are observed. The growth rate on (100) CaF_2 is fastest, corresponding to the strongest (111) preferred orientation in the MgO film. On (110) and (111) CaF_2, growth rates are about equal and slower than on (100), corresponding to the poorer preferred orientation and formation of superstructures. On SrF_2, both growth rates and refractive indices vary with substrate orientation, greatest index and fastest

growth rate occurring on (110), slowest growth and lowest index on (100), intermediate rates and index on (111). Material on (100) CaF_2 is generally crystalline while that on (110) and (111) is amorphous or microcrystalline.

3.3.8 Silicon Monoxide (SiO)

By evaporation of silicon monoxide without oxygen, films are produced which are absorbing in the visible region but are transparent in the infrared region up to approximately 8 μm.[61] The refractive index averages 1.7 for the 2-6 μm region.[61] Silicon Monoxide films are mechanically and chemically very stable and can be used as excellent coatings for the infrared region. The stress in silicon monoxide films is very dependent upon the evaporation conditions and can be either compressive or tensile. An excellent account of the influence of these process variables is given by Behrndt.[62]

Silicon Monoxide raw material was subjected to x-ray diffraction analysis, with the expectation that it would be amorphous to x-ray and show no diffraction peaks. This expectation was very nearly fulfilled. A single, broad, very weak diffraction peak attributable to α quartz (101) with a spacing of approximately 3.348Å was detected. This is not unexpected and should cause no particular concern for the 3.8 μm wavelength region. Although SiO_2 itself is not especially detrimental to coating absorption in the mid infrared, its tendency to act as a getter for water is a problem. Thus, a film consisting of SiO and redeposited SiO_2 could absorb heavily at 5.3 μm or 2.7 μm if it contained trapped water.

On (100) CaF_2, SiO deposits with one strong tridymite (unindexed) peak with a spacing of 1.507Å.[63] No microcrystalline material is evident on this substrate orientation. On (110) CaF_2, it deposits as amorphous or microcrystalline material with spacings of the order of 1.9 Å, also indicative of the tridymite phase of SiO_2[63] and of elemental silicon.[64] On (111)

CaF_2, SiO deposited as amorphous or microcrystalline material with spacings in the 1Å and 6.3Å regions.

On SrF_2 (100), SiO films are amorphous or microcrystalline with spacings in the 1.41 and 1.46Å regions, corresponding to the tridymite phase of SiO_2.[20] On (110) SrF_2, SiO films comprise both microcrystalline and well crystallized material. Microcrystalline material has spacings in the 4Å and 2.28Å regions, corresponding to tridymite. On (111) SrF_2, SiO films show microcrystalline material in the 4 - 9Å region and the 3.7Å region, corresponding again to tridymite.

Properties of SiO thin films determined in this investigation are presented in Table XXXII. The most notable feature of these data is the great difference in absorptance at 3.9 μm and 5.3 μm, which is expected from the oxygen-rich composition of the films.

TABLE XXXII. Optical Properties of SiO Films.

Substrate Material	Orient.	n (3.8 μm)	β(cm^{-1}) (3.9 μm)	n (5.3 μm)	β(cm^{-1}) (5.3 μm)	Relative Growth Rates
CaF_2	(100)		2.05		38.59	
			2.25*			
	(110)		2.40		41.17	
			1.58*			
	(111)		2.11		39.16	
			1.07*			
	Mean	1.73	2.19	1.78	39.64	(100) > (111) > (110)
			1.63*			
SrF_2	(100)		3.67		—	
	(110)		5.74		—	
	(111)		2.22		—	
	Mean	1.73	3.88	—		(110) ≅ (111) > (100)

* Film absorptance determined from βL vs. L data (Section 3.4.2).

In the humid HF environment test (section 3.4.3) SiO films show good durability, their physical integrity surviving for about one hour. Damage to

these films is by general, rather than selective, chemical attack and is more severe than that to Al_2O_3 films in the same test.

3.3.9 Zinc Selenide (ZnSe).

Zinc selenide crystallizes in the cubic β - ZnS structure, with space group $F\bar{4}3m$ and lattice parameter 5.668Å.[38, 65] A hexagonal form with a_o = 3.996Å and c_o = 6.53Å has also been reported, although the space group is not given, the structure is most likely similar to the α - ZnS structure.

Results of an x-ray diffractometer scan of ZnSe raw coating material are presented in Table XXXIII. The source of this particular sample was Balzers; patterns for Raytheon material are essentially identical, showing predominantly cubic material, practically none of the hexagonal phase, and no notable impurities.

TABLE XXXIII. Results of X-Ray Diffraction Study of ZnSe Coating Material.

Material Source and Condition: Balzers 72-190/12 (As Received)

Material	Card Ref.	Obs. d(Å)	Obs. I/I_{100}	ASTM d(Å)	ASTM I/I_{100}	hkl	Notes
β-ZnSe (Cubic)	5-0522	3.276	94	3.273	100	111	
		2.004	100	2.003	70	220	
		1.710	87	1.707	44	311	
		1.414	14	1.416	09	400	
		1.2995	22	1.299	13	331	
		1.1562	14	1.1561	15	422	
		1.0900	07	1.0901	08	511	
		1.0011	07	1.0018	04	440	
		0.9576	08	0.9577	08	531	
α-ZnSE (Hex)	15-105	3.483	03	3.43	100	100	

On both (100) and (110) CaF_2, cubic ZnSe films are deposited with a strong (111) preferred orientation,[66] as indicated in Tables XXXIV and XXXV. Mismatch of (111) ZnSe with (100) and (110) CaF_2 is 20% and 15%, respectively.[65] On (111) CaF_2, ZnSe is deposited in the hexagonal form with very strong (100) preferred orientation,[66] as shown in Table XXXVI. On the latter substrate, several very weak peaks attributable to $ZnSeO_4$ are also evident, as indicated in Table XXXV. Tables XXXIV - XXXVI provide a fair representation of the ZnSe structure on three sets of CaF_2 substrates. Growth rates of ZnSe on CaF_2 are fastest (and essentially equal) on (100) and (110) and slowest on (111).

TABLE XXXIV. Results of X-Ray Diffraction Study of ZnSe on CaF_2 Substrate.

Substrate Orientation: 0° Λ (100)

Film Thickness: 10,950 Å (λ/2 at 5.3 μm)

Radiation: Cu K_α 35 kV. 18 mA. Ni Filter

Material	Card Ref.	Obs d (Å)	Obs I/I 100	ASTM d (Å)	ASTM I/I 100	hkl	Notes
ZnSe	5-0522	3.270	100	3.273	100	111	
		1.0893	<01	1.0901	08	511	
$ZnSeO_4$	19-1476	3.608	03	3.645	100	111	
CaF_2	4-0864	1.3625	08	1.366	12	400	

TABLE XXXV. Results of X-Ray Diffraction Study of ZnSe on CaF_2 Substrate.

Substrate Orientation: 8° Λ (110)

Film Thickness: 10,950 Å (λ/2 at 5.3 μm)

Radiation: Cu K_α 35 kV. 18 mA. Ni Filter

Material	Card Ref.	Obs d (Å)	Obs I/I 100	ASTM d (Å)	ASTM I/I 100	hkl	Notes
ZnSe	5-0522	3.270	100	3.273	100	111	
		1.0893	<01	1.0901	08	511	
$ZnSeO_4$	19-1476	3.616	03	3.645	100	111	

TABLE XXXVI. Results of X-Ray Diffraction Study of ZnSe on CaF_2 Substrate.

Substrate Orientation: 1° Λ (111)

Film Thickness: 10,950 Å (λ/2 at 5.3 μm)

Radiation: CuK_α 35 kV. 18 mA. Ni Filter

Material	Card Ref.	Obs d (Å)	Obs I/I 100	ASTM d (Å)	ASTM I/I 100	hkl	Notes
ZnSe	15-105	6.50	05	----	---	001 ?	1
		3.490	100	3.43	100	100	
ZnSeO4	20-1449	4.84	03	4.94	85	011, 111	
ZnSeO4	19-1476	3.767	02	3.76	35	021	
		3.616	02	3.645	100	111	
		1.745	06	1.756	02	142	
		1.576	05	1.582	02	114	
		1.163	10	1.168	02	172, 314	
CaF_2	4-0864	3.151	>100	3.153	94	111	
		1.0515	21	1.0512	07	511	

1. d(002) = 3.25Å; d(001) Not Listed.

This growth behavior correlates very well with the structural and orientational similarities of the films on (100) and (110) and the dissimilarity on (111).

On SrF_2 substrates, the tendency toward crystallization of ZnSe in the cubic form with the (111) preferred orientation is again seen on the (100) and (110) substrate orientations. However, peaks attributable to zinc oxides, hydroxides, and selenates are also present along with broad humps in the diffractometer traces arising from microcrystalline material with spacings in the 3 to 4Å region on (110). On the (111) orientation of the SrF_2 substrates, hexagonal ZnSe is again evident, but with a weak (103) or (105) orientation (rather than (100)). In addition, large amounts of microcrystalline material with spacings in the 5-7Å region are evident on the (111) substrate orientation.

Growth rates of ZnSe on SrF_2 are fastest and about equal on (110) and (111) and slowest on (100). This behavior does not correlate well with the structural data, except for the presence of microcrystalline material on (110) and (111) and its absence on (100). This may mean that more rapid growth is associated with the formation of films having a lower degree of long range order.

Reasons for the differences in the coatings on SrF_2 and CaF_2 substrates are difficult to ascertain. Apparently, the crystal structure of the coatings on either substrate is not governed by the substrate structure or orientation for the deposition conditions employed to date. The predominant impurities on SrF_2 appear to be $Zn(OH)_2$, while those on CaF_2 appear to be $ZnSeO_4$, which may indicate indicate the presence of small amounts of oxygen during deposition in the latter case. The hydroxide would imply the presence of water vapor in the deposition environment. These differences are not dependent on conditions in a single coating run, but represent results of at least three coating runs on each substrate material, or a total of nine samples.

Properties of ZnSe determined in the present investigation are listed in Table XXXVII. In spite of the large variation in absorptance with substrate orientation (a factor of four), the material clearly can be deposited with low absorptance at both 3.8 μm and 5.3 μm.

TABLE XXXVII. Optical Properties of ZnSe Films.

Substrate Material	Orient.	n (3.8 μm)	β(cm^{-1}) (3.9 μm)	n (5.3 μm)	β(cm^{-1}) (5.3 μm)	Relative Growth Rates
CaF_2	(100)		3.67		3.98	
	(110)		1.59		0.96	
	(111)		1.41		1.69	
	Mean	2.42	2.22	2.41	2.21	(100) ≅ (110) > (111)
SrF_2	(100)		1.08		1.76	
	(110)		3.73		2.10	
	(111)		4.69		2.04	
	Mean	2.42	3.17	2.41	1.97	(110) (111) > (100)

Zinc selenide films have been used in combination with thorium fluoride films to fabricate multilayer high reflectance, low loss coatings for laser mirrors in the visible region.[67] They have also been used in the infrared region as antireflection coatings for high power laser windows of potassium chloride.[55] The average refractive index of zinc selenide is 2.43 and its transmission range extends from 0.5 - 22 μm.[68] Zinc selenide films are insoluble in water and are harder than zinc sulfide films. Care must be taken not to overheat the material during evaporation. The temperature should be just high enough to cause the evaporation to proceed, otherwise some alteration in the composition of the film will take place resulting in an increase in absorption.

Resistance of ZnSe films to humid HF vapor is unfortunately very low (sec. 3.4.4). They survive only about 15 minutes before succumbing to general chemical attack. In this sense they are inferior to ZnS films, which survive the same environment for 30 minutes.

3.3.10 Zinc Sulfide (ZnS).

Zinc sulfide crystallizes in two structures, the hexagonal α - ZnS or Wurtzite type having space group $P6_3mc$, and the cubic β - ZnS or Sphalerite type having space group $F\bar{4}3m$.[38] Both structures are based on tetrahedral coordination. In the cubic phase, zinc atoms are arranged on a face-centered cubic lattice while in the hexagonal form they fall into a distorted hexagonal close-packing. Lattice parameters of the hexagonal phase are $a_o = 3.820$Å, $c = 6.250$Å[69] while the cubic phase has a unit cell dimension $a_o = 5.406$Å.[70] Alternative stacking arrangements in the c-axis direction of the hexagonal phase give rise to several polytypes of ZnS; the best known of these are designated 8H and 10H, with c-axis dimensions of 24.96Å and 31.20Å, respectively.[71, 72]

Results of an x-ray diffraction scan of raw ZnS coating material are presented in Table XXXVIII, showing predominantly hexagonal material with small amounts of the 8H polytype and some cubic material.

TABLE XXXVIII. Results of X-Ray Diffraction Study of ZnS Coating Material

Material Source and Condition: Supply Balzers Ch 73-027/5 as received.

Material	Card Ref.	Obs. d(Å)	Obs. I/I_{100}	ASTM d(Å)	ASTM I/I_{100}	hkl	Notes
d-ZnS (Hex)	5-0492	3.300	34	3.309	100	100	
		3.118	100	3.128	86	002	
		2.924	22	2.925	84	101	
		2.266	06	2.273	29	102	
		1.909	68	1.911	74	110	
		1.763	11	1.764	52	103	
		1.627	44	1.630	45	112	
		1.598	05	1.599	12	201	
		1.350	04	1.351	06	400	
		1.2965	05	1.296	14	203	
		1.1018	09	1.1029	13	300	
		1.0397	07	1.0401	05	302	
α-ZnSe	15-105	3.450	04	3.43	100	100	
α-ZnS (Polytype)	12-688	2.111	04	2.08	02	---	
β-ZnS	5-0566	2.700	05	2.705	10	200	
		1.350	04	1.351	06	400	
		1.239	06	1.240	09	331	

On CaF_2 substrates, ZnS deposits in the hexagonal (Wurzite or α - ZnS) form, yielding diffraction patterns indicative of the 8H polytype.[68] On (100) and (110) substrate orientations the film orientation is predominantly basal with spacings of approximately 3.10Å, or slightly smaller than the

nominal 3.12Å spacing between successive layers of Zn or S atoms.[72] The strongest diffraction peak on (100) CaF_2 corresponds to a spacing of 1.51Å, less than half of the 3.12Å fundamental ZnS spacing. This diffraction line is attributable to a form of α - $Zn(OH)_2$[73] with a spacing of 1.511Å. However, the absorption results to be presented in the next section do not justify large amounts of the hydroxide material. It is thus possible that the 1.51Å spacing corresponds to a basal ZnS spacing, considerably smaller than the nominal 1.56Å.[69,70,71] Minor diffraction lines on the (100) substrate orientation correspond to (110) ZnS(8H), at 1.905Å, (300) ZnS(8H) at 1.102Å, and α - $Zn(OH)_2$ (031) at 3.02Å.

On (110) CaF_2 substrates, the situation is somewhat simpler, the strongest peak arising from the (008) spacing of ZnS (8H) at 3.11Å. Lower intensity lines arise from (10 10), (10 13), and (110) spacings of the same material at 1.979, 1.943, and 1.887Å (observed) and Wurtzite (102) at 2.24Å.[69] No lines attributable to zinc oxides or hydroxides were observed.

On (111) CaF_2, ZnS again deposits in the hexagonal form with a strong preferred orientation. The strongest diffraction line corresponds to a spacing of 3.477Å, which is very nearly three times the α - ZnS (212) spacing of 1.161Å, also observed on these substrates. The 3.477Å spacing does not correspond to diffraction lines for common oxides, hydroxides, sulfites, sulfates, or fluorides of zinc or to elemental zinc or sulfur. In fact, the only (non-substrate) diffraction lines observed with this substrate orientation are at 3.477Å, 1.161Å, and 1.06Å, the latter attributable to α - ZnS (213). Hence we conclude that the material takes a strong preferred orientation parallel to (212), but possibly has developed a superstructure having triple the (212) spacing.

Structural mismatch criteria between the substrate and film do not appear to govern the choice of structure and orientation in these ZnS films. These criteria would predict a cubic (sphalerite or β - ZnS) structure for films on CaF_2, with a strong preferred orientation paralleling the substrate, since the structures and spacings are similar to within 1%.[69, 70, 74] On SrF_2, these same criteria would predict α - ZnS on all three substrate orientations, with (101) ZnS paralleling (100) SrF_2, (102) ZnS on (110) SrF_2 and (100) ZnS on (111) SrF_2.[24, 29] Some of these relationships are in fact observed.

On CaF_2, the growth rate of ZnS is fastest on (110), intermediate on (100) and slowest on (111), exhibiting no obvious correlation with the structural data, except that the structure is simplest and preferred orientation strongest on (110). No extraneous lines attributable to impurities are observed on (110), but they are observed on the other substrate orientations.

Results of X-ray diffraction investigations of ZnS films on SrF_2 substrates are detailed in Tables XXXIX, and XL. On (100) SrF_2 (Table XVI) the predicted very strong (101) orientation of the α - ZnS film is observed. Mismatch between film and substrate spacings in this orientation is 9.9%. On (110) SrF_2 (Table XXVII), the predicted (102) orientation of α - ZnS is observed. Mismatch in this orientation is 11%. Minor lines corresponding to poorly crystalline material of the 10H polytype of ZnS are also observed on this substrate orientation; none of these correspond closely to the substrate spacing.

On (111) SrF_2, the predicted (100) α - ZnS film structure and orientation are not observed (Table XLI). The observed orientation of the ZnS (10H) polytype corresponds to a mismatch of approximately 10% with the substrate.[25, 29] The predicted (100) orientation of α - ZnS on (111) SrF_2 would result in a mismatch of 1.3%.[69, 70, 75]

TABLE XXXIX. Results of X-Ray Diffraction Study of ZnS on SrF_2 Substrate.

Substrate Orientation: 3° Λ(100)

Film Thickness: 5995 Å (λ/4 at 5.3 μm)

Radiation: CuK_α 35 kV. 18 mA. Ni Filter

Material	Card Ref.	Obs d (Å)	Obs I/I 100	ASTM d (Å)	ASTM I/I 100	hkl	Notes
c - ZnS	5-0492	2.919	38	2.925	84	101	
		1.466	100	1.462	05	202	
SrF_2	6-0262	1.4515	80	1.4499	15	400	

TABLE XL. Results of X-Ray Diffraction Study of ZnS on SrF_2 Substrate.

Substrate Orientation: 0.8° Λ(110)

Film Thickness: 5995 Å (λ/4 at 5.3 μm)

Radiation: CuK_α 35 kV. 18 mA. Ni Filter

Material	Card Ref.	Obs d (Å)	Obs I/I 100	ASTM d (Å)	ASTM I/I 100	hkl	Notes
c - ZnS	5-0492	2.271	100	2.273	29	102	
		1.1337	16	1.1364	<01	204	
Zn S(10H)	12-688	3.113	06	3.12	100	0 0 10	
		2.81	02	2.81	02	106	1
		2.469	01	2.49	02	--	2
SrF_2	6-0262	2.052	>100	2.0508	80	220	
		1.0253	>100	1.0253	07	440	

1. Very broad and poorly defined; microcrystalline or amorphous material.

2. The (002) spacing of elemental zinc is 2.473Å, and is thus indistinguishable from this one, within experimental error.

TABLE XLI. Results of X-Ray Diffraction Study of ZnS on SrF_2 Substrate.

Substrate Orientation: 0° Λ (111)

Film Thickness: 5995 Å (λ/4 at 5.3 μm)

Radiation: Cu K_α 35 kV. 18 mA. Ni Filter

Material	Card Ref.	Obs d (Å)	Obs I/I 100	ASTM d (Å)	ASTM I/I 100	hkl	Notes
ZnS(10H)	12-688	3.6972	100	----	---	---	1
		1.8486	16	1.841	02	1 0 14	
		1.2339	13	1.239	04	ni	2
ZnS_2O_4	1-0162	~5.9	~50	5.88	100	ni	3
SrF_2	2-0262	3.336	>100	3.352	100	111	
		1.6710	86	1.6743	05	222	
		1.1149	60	1.1164	16	511	

1. Not Listed; this spacing is exactly 2 times the observed (1 0 14) spacing of ZnS (10H).

2. Other materials having similar spacings include elemental zinc (004), 1.237Å and ZnO (202), 1.238Å.

3. Broad, poorly defined; Microcrystalline or Amorphous phase with spacing corresponding to this material.

The growth rate of ZnS is fastest on (110) SrF_2, slowest on (100), and intermediate on (111), correlating poorly with observed structure and orientation. Slow growth of the strongly oriented, well crystallized material with low mismatch on (100) SrF_2 is quite plausible, but the rapid growth in the (102) orientation on (110) SrF_2 is difficult to reconcile with the slower growth of the 10H polytype on (111), where both have a 10% mismatch with the substrate spacing and somewhat disordered structure.

Properties of ZnS measured under the contract are listed in Table XLII.

TABLE XLII. Optical Properties of ZnS Films.

Substrate Material	Orient.	n (3.8 μm)	$\beta(cm^{-1})$ (3.9 μm)	n (5.3 μm)	$\beta(cm^{-1})$ (5.3 μm)	Relative Growth Rates
CaF_2	(100)		10.10		9.65	
	(110)		8.81		11.49	
	(111)		10.20		10.94	
	Mean	2.23	9.70	2.22	10.69	
SrF_2	(100)		16.73		6.68	
	(110)		13.52		6.85	
	(111)		19.61		8.26	
	Mean	2.23	16.62	2.22	7.26	(110) > (111) > (100)

Although its absorptance is not as low as that of zinc selenide, zinc sulfide is a particularly useful coating material in the infrared region out to about 15 μm.[76] The refractive index varies from 2.26 at 2 μm to 2.15 at 14 μm.[76] Evaporated zinc sulfide films show high compressive stress.[52] Electron beam evaporated films have slightly lower values of compressive stress as compared to films prepared by resistance heating evaporation.[77] This reduction in stress is accompanied by an increase in optical absorption as a result of decomposition into a high percentage of free zinc as a result of electron bombardment. Zinc sulfide films are slightly hygroscopic and show a tendency to craze when exposed to high humidity.[78] For maximum durability, zinc sulfide films should be deposited on substrates freshly cleaned by a glow discharge and held at a temperature of approximately 150°C.[79]

When exposed to a humid HF environment, ZnS is destroyed by general chemical attack within 30 minutes (section 3.4.4). Its survival time is about double that of ZnSe, but is still quite poor; destructive effects are extensive.

3.4 Detailed Studies and Optimization of Selected Single Layer Films:

On the basis of the coating material properties results presented in the previous section, five coating materials were selected for detailed study: PbF_2, ThF_4, SiO, ZnS, and ZnSe. These studies included optimization of deposition techniques for all five materials, correlation of absorptance and film thickness (βL vs. L) for PbF_2, ThF_4, and SiO, determination of effects of polycrystalline substrates upon absorptance and structure in PbF_2, ThF_4, SiO, and ZnSe, and exposure to a humid HF environment for all five materials. Al_2O_3 was also subjected to this last test, due to its attractive characteristics for the 2.7 μm wavelength region.

3.4.1 Deposition Techniques and Optimization:

Any coating optimization effort requires careful control of evaporation techniques and parameters. A complicated interdependence exists among deposition parameters and thin film properties, so that one property may be influenced by several conditions and one parameter may influence several properties.

All of the coating depositions described in this report were done in a commercial coating system (Balzers Model 710) which was pumped by an oil diffusion pump and a liquid nitrogen trap. The system was evacuated to a pressure of less than 10^{-6} Torr and a pressure of less than 5×10^{-6} Torr was maintained during the coating depositions. To ensure the uniformity of the thickness of the layers, the samples were rotated above the evaporation source (approximately 30 inches) during the deposition process. The mode of evaporation was either by resistance heating or electron beam heating. Proper control of the thickness of each layer

was afforded by monitoring the reflectance at the control wavelength of a suitably positioned witness plate in the coating chamber and stopping deposition when the reflectance reached a predetermined value. Before placing the sample into the system for coating, they were cleaned by washing with a detergent and warm water, then rinsed with distilled water and alcohol and blown dry with nitrogen gas.

Parameters used to deposit each of the most promising coating materials are described in detail below. All of the materials were purchased from commercial sources, and no attempt was made to further purify any of these materials.

Thorium Fluoride. The starting material for these films was granular thorium fluoride (99.9% purity) purchased from the Balzers High Vacuum Corporation. The material was evaporated by electron-beam heating, and an evaporation rate of approximately 1800Å/Min was used throughout the deposition. Films deposited at lower substrate temperatures (< 100°C) showed the appearance of hydroxyl absorption bands at 2.8 μm and 6.2 μm, whereas, for films deposited at approximately 200°C, the hydroxyl absorption bands were not observed. Thorium fluoride deposits as a strongly adherent film having an average refractive index of about 1.49 for the 2 -6 μm region. Increasing the residual gas pressure from 5×10^{-6} to 1×10^{-5} Torr had no apparent influence on the refractive index.

Lead Fluoride. The coating material for these films was purchased from Balzers High Vacuum Corporation. The material comes as fused granules (~4 mm) of lead fluoride with a stated purity of 99.99%. Lead fluoride is reduced by hot tantalum, tungsten, or molybdenum evaporation sources. It is best evaporated by using electron-beam heating techniques. To assure a constant rate of evaporation, and to avoid overheating and decomposition of the material, a defocused electron-beam of at least 1.5 - 2 cm in

diameter was used. A vacuum pressure of less than 5×10^{-6} Torr and a deposition rate of approximately 1800 Å/min was used. The substrate temperature was approximately 200°C. The average refractive index of the films was 1.73 for the 2-6 μm region.

Silicon Monoxide. The silicon monoxide was evaporated from a tantalum baffled-box type source, available from R. D. Mathis Company, Long Beach, California. This source produced less spattering of silicon monoxide particles than the electron gun, and resulted in films which were more defect free. The starting material was lumps of Linde select grade of silicon monoxide, also available from the R. D. Mathis Company. True silicon monoxide films can only be prepared by fast evaporation (~ 30 Å/sec) under good vacuum conditions ($< 10^{-6}$ Torr). The films were deposited onto substrates heated to approximately 200°C. The average refractive index was 1.75 for the 2-6 μm region.

Zinc Sulfide. The starting materials for the zinc sulfide films were purchased from the Balzers High Vacuum Corporation. This material came in the form of hot-pressed tablets. The stated purity was 99%. Consistent data for the zinc sulfide films were obtained only after the material was preheated in a vacuum for an hour at approximately 900°C. The material was then evaporated from a tantalum box source having a perforated tantalum cover. The films were evaporated at a rate of approximately 1800 Å/min and at a vacuum pressure less than 5×10^{-6} Torr. For maximum durability, the films were deposited on substrates freshly cleaned by a glow discharge and held at temperatures of around 150°C. The average refractive index of the films was 2.25 for the 2-6 μm region.

Zinc Selenide. The starting material for the zinc selenide films was random lumps of CVD zinc selenide obtained from the Raytheon Research Division. In this form, the starting material is dense and no preheating or

outgassing is required. The material was evaporated from a tantalum box source having a perforated tantalum cover. Care must be taken not to overheat the material. The source temperature should be just high enough to cause evaporation to proceed, otherwise some alteration in the composition of the material will take place resulting in an increase in absorption in the films. The films were evaporated at a rate of approximately 1000 Å/min and at a vacuum pressure of less than 5×10^{-6} Torr. The substrates were maintained at a temperature of approximately 150°C and just prior to deposition they were cleaned by an argon glow discharge. The average refractive index of the films was 2.4 for the 2-6 μm region.

3.4.2 Absorptance and Film Thickness

In a technical report (September, 1977), some advantages of measuring absorptance as a function of coating thickness (βL vs. L) for single layer films of selected materials were discussed briefly in connection with some preliminary results for PbF_2. These measurements were completed under the contract for PbF_2, ThF_4, and SiO films at a design wavelength (λ_o) of 3.8 μm. Results, and particularly, statistical features, are quite encouraging for PbF_2 and SiO, tending to lend credence to the methodology employed. Results for ThF_4 are problematic, pointing out the need for further work.

The experimental procedure employed for all three coating materials and substrate orientations involved choosing a group of single crystal CaF_2 or SrF_2 substrates having absorptance values falling within a very narrow range (typically 10 - 15%) to minimize this potential contribution to experimental dispersion. Coatings of thickness $\lambda_o/2$, λ_o, and $3\lambda_o/2$ were then deposited on three groups of three substrates, each group comprising one each of (100), (110), and (111) substrate orientation.

Identical deposition conditions (deposition rates, substrate temperatures, etc.) were utilized for all three groups of substrates (film thicknesses) within experimental feasibility. Glow discharge cleaning of substrates was not employed in any of these coating runs in order to minimize complications associated with that operation, as detailed in the technical report dated January, 1977.

$\underline{PbF_2}$

Results for PbF_2 on SrF_2 substrates are listed in Table XLIII and plotted in Figure 13.

TABLE XLIII. Absorptance of PbF_2 films of integral halfwave optical thicknesses at 3.8 μm (λ_o) on oriented single crystal SrF_2 substrates.

Substrate Orientation	Total Absorptance for Film Thickness of: (10^{-4})			Intercept	Slope (10^{-4})	Film Absorption Coefficient, β (cm^{-1})
0	$\lambda_o/2$	λ_o	$3\lambda_o/2$			
(100)	3.55	4.91	7.53	1.35 ± 1.80	1.99	1.63 ± 0.17
(110)	1.99	4.92	6.90	-0.30 ± 0.08	2.45	2.01 ± 0.13
1.01 ± 0.15						
(111)	2.55	4.56	7.29	0.06 ± 0.02	2.37	1.94 ± 0.10
Mean	2.70	4.80	7.24	0.37 ± 2.27	2.27	1.86 + 0.20

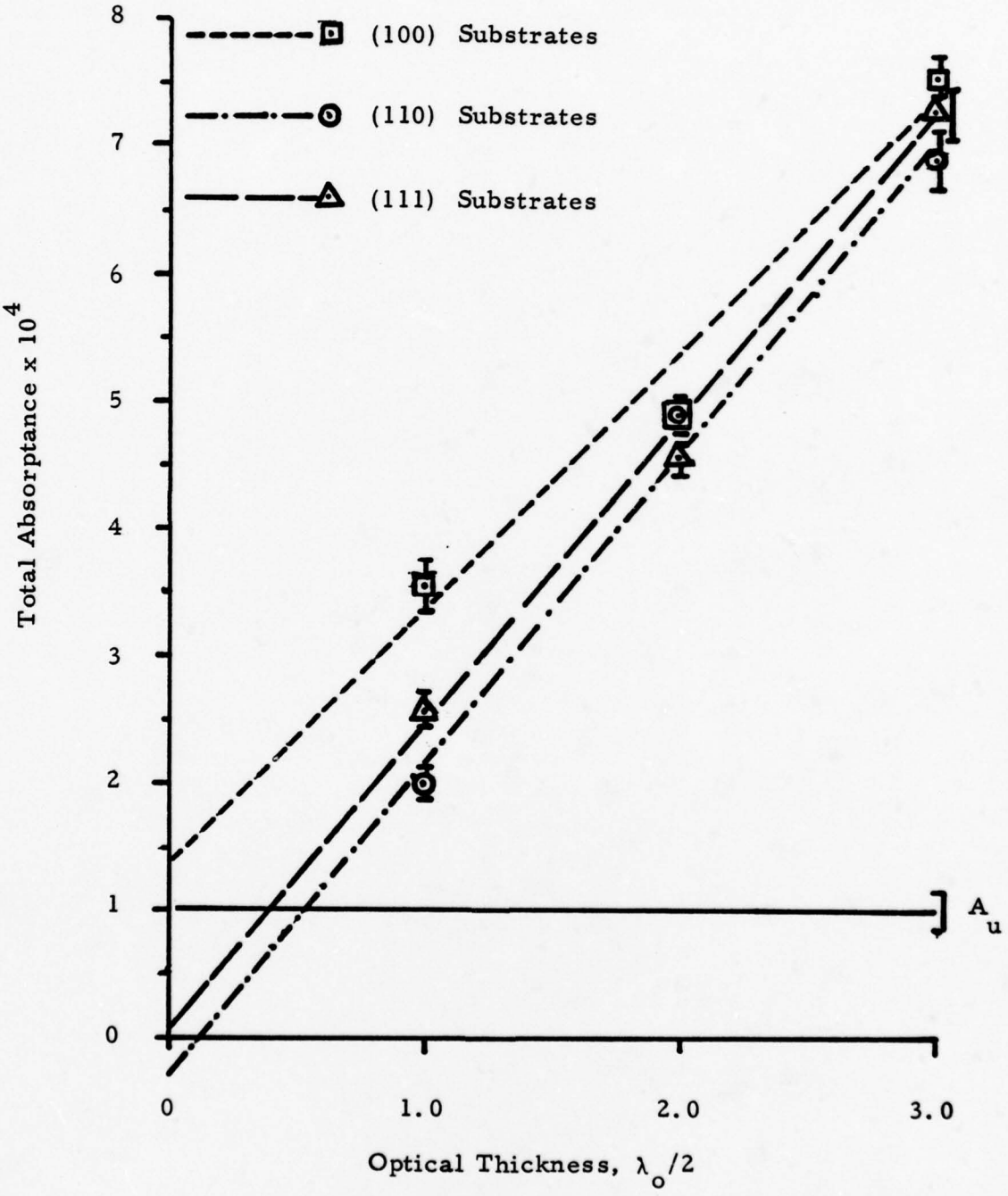

Fig. 13 Total Optical Absorptance at 3.8 μm vs. Film Thickness for PbF_2 on SrF_2 Substrates.

The Miller indices of substrate surfaces are given in the first column of Table XLIII. Total absorptance values for the samples are listed in the next four columns in units of 10^{-4}; The mean values for the uncoated substrates appears in the column headed "O" and values for substrates with halfwave, full wave, and one-and-one-half wave optical thicknesses of PbF_2 at a design wavelength of 3.8 μm appear in appropriately labeled columns. Results of least squares analyses of the absorptance for each substrate orientation appear in the next two columns of the table with the final result, the absorption coefficient of the thin film (cm^{-1}) appearing in the last column. The least squares lines for all three substrate orientations are plotted in Figure 13.

Comparing the absorption coefficients of Table XLIII with our previous data for PbF_2 (Sect. 3.3.3) shows that the mean value for all substrate orientations has been reduced by more than a factor of two, differences among the substrate orientations have been substantially reduced, and precision has been improved. Absorption coefficients (β) for PbF_2 films on (110) and (111) SrF_2 substrates are essentially identical within experimental error, while that on (100) is significantly (~17%) lower. Our previous data showed a similar trend, but β (100) was approximately 1/2 β (110) β (111). Probable reasons for these changes include improved measurement accuracy, based on three uncoated and coated substrate absorptance determinations for each absorption coefficient and better control of deposition conditions over the three coating runs involved.

The intercepts of the least squares plots deserve some comment. Ideally, plots of absorptance vs. coating thickness should intersect the y-axis at the uncoated substrate absorptance value, A_u, within experimental error, provided that the absorptance of the substrate does not change appreciably from the measured value prior to coating. Positive changes would be associated with increases in total absorptance and intercept of the

βL vs. L plot, while negative changes would result in intercepts below A_u. Changes of either sign could result from exposure to ambient atmosphere or vacuum baking at 200°C immediately prior to coating deposition. For two of the three substrate orientations considered here (110) and (111), the intercepts of the β L vs. L line for PbF_2 falls well below A_u, indicating that substrate surface absorptance is markedly reduced prior to coating. (No physical significance is to be attached to the negative intercept for the (110) substrate orientation; it simply indicates that the surface absorptance is substantially reduced by processes preceding coating, so that substrate absorptance approaches intrinsic levels.) For the (100) surface of SrF_2 the surface absorptance apparently increases slightly prior to coating.

ThF_4

Absorptance measurements for this material were carried out using a methodology and procedures identical to those successfully employed for PbF_2 and SiO. Mean absorptance of the uncoated substrates was $(1.50 \pm 0.21) \times 10^{-4}$. Coated substrate absorptance results were erratic, showing a tendency toward higher total absorptance for thinner films, e.g. for the (100) substrate orientation, $A(\lambda_o / 2) = 7.11 \times 10^{-4}$, $A(\lambda_o) = 4.61 \times 10^{-4}$ and $A(3\lambda_o / 2 = 5.27 \times 10^{-4}$, where $\lambda_o = 3.8\ \mu m$. The mean absorption coefficient $(\bar{\beta})$ for the $(\lambda_o/2)$ films on all substrate orientations was $4.00 \pm 0.23\ cm^{-1}$, that for the λ_o films was $1.51 \pm 0.31\ cm^{-1}$, and that for $3\lambda_o/2$ films was $0.93 \pm 0.4\ cm^{-1}$. Mean $\bar{\beta}$ for all the films on all three substrate orientations, irrespective of thickness, was $2.15\ cm^{-1}$.

This last result may be fairly representative of the average behavior of the films on alkaline earth fluoride substrates at 3.8 μm. Comparison with our previous results for the ThF_4 on SrF_2 (Section 3.3.5) shows a reduction in the average absorptance by a factor of 1.7 or approximately 40%. However, the uncertainty in the results is much greater, due to the large differences with film thickness.

Detailed x-ray diffraction analyses of the ThF_4 films for all substrate orientations and film thicknesses showed sharp and consistent differences correlating with substrate orientation, but no systematic changes with film thickness on any single substrate orientation. On (100) SrF_2, ThF_4 is microcrystalline with spacings of 2.02Å and 3.80Å, corresponding to (103) and (220), respectively.[80] An additional sharp peak at 3.21Å is attributable to $ThF_4 \cdot nH_2O$[81] or $ThOF_2$[82]. On (110) SrF_2, the ThF_4 is entirely amorphous with no diffraction maxima except those arising from the uncoated substrate. On (111) SrF_2, ThF_4 is well crystallized with very strong strong preferred orientation, showing a single diffraction peak corresponding to (322) with a spacing of 1.85Å[80]. A second sharp diffraction peak corresponding to a spacing of 1.235Å could be attributed to an uncataloged ThF_4 line, but is more probably associated with a hydrated phase (the (640) line of $ThF_4 \cdot 0.88H_2O$)[83].

The possible presence of hydrated ThF_4 or Thorium oxides would account for the higher absorptance values at 3.8μm. The evaporant starting material is the most probable source of these impurities. However, the apparent decrease in absorptance with increased film thickness is not so easily explained. A possible mechanism which could account for these observations would involve film defects (pinholes, stacking faults, dislocation pile-ups, vacancies, etc.) as primary contributors to absorptance. If the concentration of these decreases with increasing film

thickness (this is unlikely for the thicknesses involved here), then the absorptance would decrease, as is observed.

SiO

Results of βL vs. L experiments involving silicon monoxide films on oriented single crystal CaF_2 substrates are presented in Table XLIV and figure 14 (the format is exactly analogous to that employed with PbF_2, Table XLIII figure 13). It is immediately clear that the slopes of the plots, and hence the thin film absorption coefficients, are significantly different for the three substrate orientations. This deviates from previous results reported in September, 1977, wherein little influence of substrate orientation upon absorption coefficient was noted. However, the precision of the present results is undoubtedly higher and the statistical parameters are excellent, with the exception of the intercept of the plot for the (110) substrate orientation.

Again, the intercepts for all three substrate orientations are worth noting. On the (100) substrates, surface absorptance apparently decreases to about half the previously measured uncoated value prior to coating deposition. On (110) it increases moderately (but with a very large uncertainty), and on (111) it increases by more than a factor of two. These results are in startling contrast to those for SrF_2 (Figure 13 and Table XLIII) wherein (100) substrates were unique in showing an increase in absorptance prior to coating. This indicates that surface chemistry and absorptance changes prior to and during coating are poorly understood and further work is needed.

The absorptance results themselves are quite encouraging, both in terms of their absolute magnitude, and their relatively high precision, again

TABLE XLIV. Absorptance of SiO films of integral halfwave optical thicknesses at 3.8 μm (λ_o) on oriented single crystal CaF_2 substrates.

Substrate Orientation	Total Absorptance for Film Thickness of: (10^{-4})			Intercept (10^{-4})	Slope (10^{-4})	Film Absorption Coefficient, β (cm^{-1})
	0	λ_o	λ_o	$3\lambda_o/2$			
(100)		3.41	6.09	8.87	0.67 ± 0.05	2.73	2.25 ± 0.014
(110)		3.86	4.89	7.69	1.65 ± 2.01	1.91	1.58 ± 0.24
(111)	1.13 ±0.11	3.92	5.31	6.51	2.65 ± 0.12	1.30	1.07 ± 0.03
Mean		3.73	5.43	7.69	1.66 ± 0.99	1.98	1.63 ± 0.60

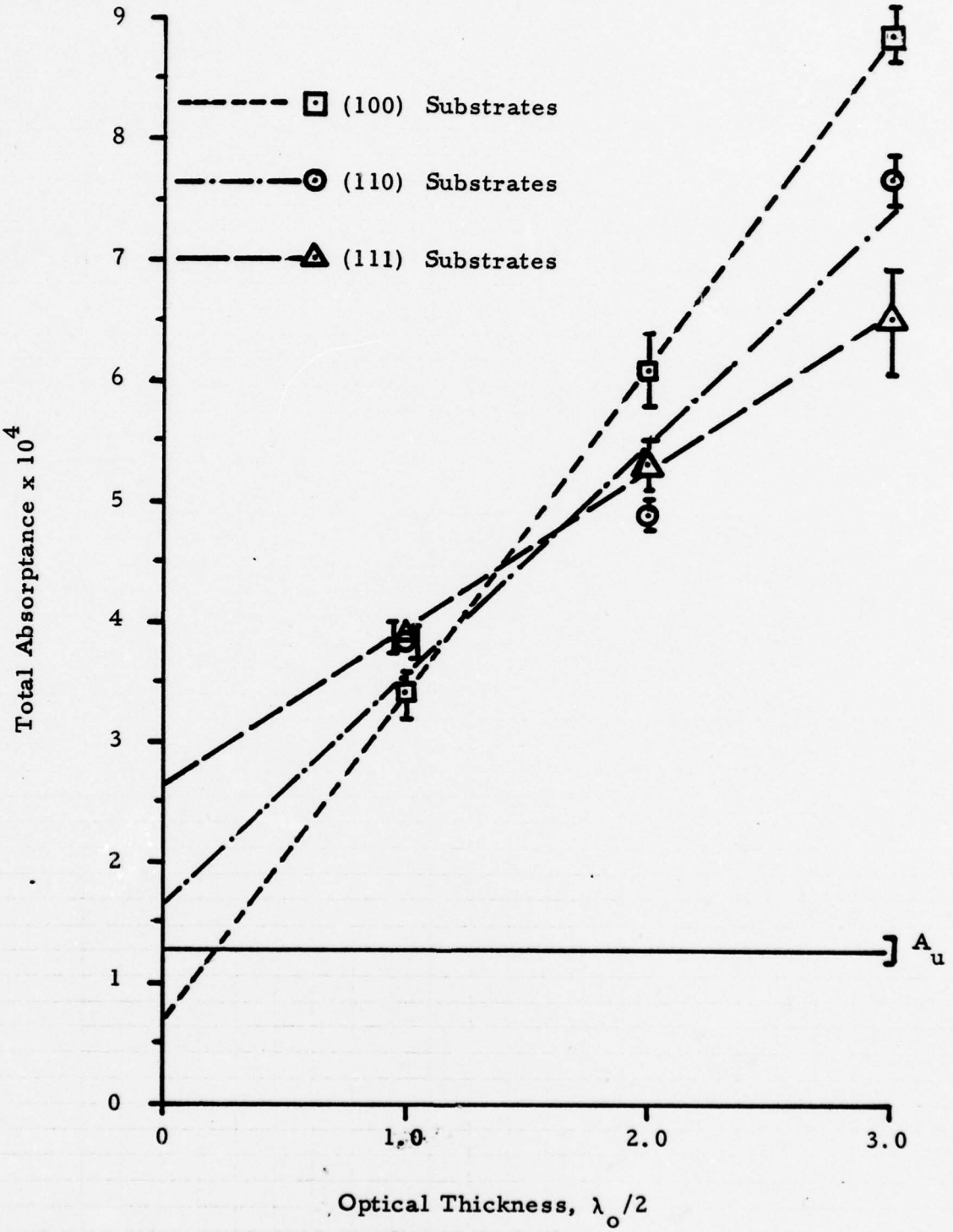

Fig.14 Total Optical Absorptance at 3.8 μm vs. Film Thickness for Si O on $Ca F_2$ Substrates.

indicating that the method of comparing film thickness with total absorptance can produce meaningful, consistent, results.

3.4.3 Absorptance and Structure of Single Layer Films on Polycrystalline Substrates.

Since it has been established that significant differences in absorption coefficient and structure of optical coatings arise from differences in the crystallographic orientation of single crystal substrates, it was necessary to determine these properties for films on polycrystalline substrates, where orientation of individual grains may vary.

Polycrystalline CaF_2 substrates produced by press forging were employed to test this effect. Grain size in this material, produced by Harshaw, is large (~ 1 cm), but birefringlace effects are minimal. Preferred orientation in a central area of approximately 2 cm^2 was determined by x-ray diffraction before coating the substrates (1 inch diameter) and absorptance of the same area was measured using DF laser calorimetry. A majority (seven of ten) substrates exhibited strong (110) preferred orientation, with minor (311), (111), and (331) peaks. Two substrates showed predominant (111) orientation with subequal (110) and one showed an indeterminate high index orientation. Total absorptances (surface and bulk) at DF wavelengths were generally high, of the order of 10^{-3} cm^{-1} for samples ~0.5 cm thick. No systematic variation of absorptance with preferred orientation of the substrate grains was established.

Results of this investigation are presented in Table XLV. Four coating materials showing particular promise for the DF laser wavelength region were selected; they are listed in the first column of the table. The preferred orientation of the substrate is given in the second column. A single set of Miller indices, e.g. (1110), indicates that the substrate

TABLE XLV. Comparison of Single Layer Film ($\lambda_o/2$ at 3.8 μm) Absorption Coefficients on Single and Polycrystalline CaF_2 Substrates.

Coating Material	Polycryst. Subst. Pref. Orient.	Film Struct. & Pref. Orient on Polycryst. Substrate	Film Abs. Coef. (cm^{-1}) Poly Cryst. Substrate	Singl. Cryst. Substrate *
PbF_2	(110)	Cubic (β) (110); Minor (111), Pb_2O_3	2.64	3.03
ThF_4	(110)/(311)	Microcrystalline Monocl. (220)/(103)	1.07	1.65
SiO	(110)	Amorphous	5.37	1.58
ZnSe	(110)/(111)	Cubic (111); Minor $ZnSeO_4$	1.58	1.55**

* Absorption Coefficient for a coating of the same material deposited in a separate coating run on a single crystal CaF_2 substrate having the same orientation as the dominant preferred orientation in the polycrystalline substrate.

**ZnSe coatings on single and polycrystalline substrates deposited in the same coating run.

grains had a common orientation parallel to only one crystallographic plane. Where two sets of indices are given, e.g. (110) / (311), the first set indicates the dominant orientation with the second set denoting a less strongly preferred set of planes (i. e. lower intensity of diffracted x-rays). Predominant features of the structure and preferred orientation of the half-wave film on the ploycrystalline substrate are summarized in the third column. and its absorption coefficient at the DF wavelength is given in the fourth column. For purposes of comparison, an absorption coefficient of the film material deposited on a single crystal CaF_2 substrate having the same orientation as the dominant orientation of the polycrystalline sample is listed in the fifth column. (In all cases except that of ZnSe, this number is generated from material deposited during a different coating run).

Agreement between the absorption coefficients of the films on single and polycrystalline substrates is reasonable for three of the four materials, with differences ranging from 2% to about 35%, the value for the polycrystalline substrates being lower, in most cases. Since the total experimental error in the film absorption measurements ranges from 5% to 15%, this degree of agreement is satisfactory and indicates that there are no special problems in extending results on single crystal substrates to the polycrystalline case.

For SiO, the absorption coefficient on the polycrystalline substrate is about 2.5 times that on the corresponding single crystal substrate. Differences in film structure cannot account for this, since all SiO films on single or polycrystalline CaF_2 substrates oriented parallel to (110) have been found amorphous to x-ray in the present work. An absorption coefficient of 5.74 cm^{-1} was reported under this program in September, 1977 for SiO on a (110) SrF_2 substrate; x-ray diffraction analyses of that material indicated small amounts of well crystallized SiO_2 (Tridymite) in addition to microcrystalline and amorphous material, suggesting that the film was

oxygen-rich. Evidence supporting this explanation of the high absorption coefficient of the SiO film on the polycrystalline substrate is lacking in the present case. If excess oxygen is present in the latter film, x-ray diffraction provides no indication that it is incorporated in a crystalline or microcrystalline form.

3.4.4 Effect of HF Vapor Environment Upon Coatings.

Since the ultimate applications of the coating materials being investigated here are in multilayer coatings for use in HF/DF lasers, the compatibility of these materials with HF vapor must be established. While actual life testing in an HF laser is most representative of service conditions, it is too time-consuming and cost-ineffective for screening and ranking a variety of coating materials. To accomplish such a screening and ranking in in the present program, a simple, rapid, cost-effective, but quite severe test was devised.

Thirty-five samples comprising single layer coatings on CaF_2 and SrF_2 substrates (1 inch diameter) were placed in a vinyl container approximately 14 inches in diameter and 7 inches high (approximate volume 17,000 cm^3) with plexiglas cover, maintained in the ambient atmosphere of a fume hood at 21.2°C. A polypropylene beaker (65 mm. diameter x 35 mm. height) containing 50 cm^3 of semi-conductor grade HF was placed in the center of the container above the level of the samples at commencement of the test. A second polypropylene beaker (70 mm. diameter x 90 mm. height) containing 100 cm^3 de-ionized water (initial pH 4.5) was also placed in the large vinyl container prior to the test to provide a pH reference and constant humidity during the test. Final pH of the water was 2.9 at a temperature of 19.5°C. Initial hydrogen ion concentration in the water was thus 3.16×10^{-5} changing to a final value of 1.26×10^{-3}, or an increase by a factor of 40 within 1.25 hours. Samples were observed

continuously through the plexiglas cover throughout the test; the cover was removed for approximately 2 minutes every 15 minutes to permit close examination and removal of failed samples. The criterion for failure was destruction of the physical integrity or optical uniformity of the coating either by crazing and cracking, fogging (general attack), or localized attack at defects or edges. An optical transmission or absorption criterion was not used due to the time required for performance of the test itself.

The coating materials chosen for testing included PbF_2, ThF_4, Al_2O_3, SiO, ZnS, and ZnSe. All but one of these materials (Al_2O_3) exhibits moderate absorptance at 3.8 μm and is thus a preferred candidate coating material. Al_2O_3 was tested in spite of its high 3.8 μm absorptance due to its potential usefulness in the HF laser band (2.7 μm) and in the ultraviolet.

Results of the HF vapor tolerance test are summarized in figure 15. In general, it appears that the oxides are most resistant to outright destruction in the humid HF environment, while the selenides are least resistant. Fluorides and zinc sulfide fall into an intermediate category, with the sole exception of a single quarterwave PbF_2 coating on SrF_2 (100). The latter result was probably fortuitous. With respect to the oxides, the solid lines indicate the time elapsed during formation of a very thin film at the exposed surface; this film exhibited interference rings in the visible and was not removable by solvent cleaning, but microscopic examination showed no evidence of attack of the coating so that it was not considered to have failed at this point. The dashed lines indicate the time elapsed from formation of the thin interference film until destructive effects became evident under the microscope. Here a criterion for failure involving optical transmission or absorption in the 3.8 μm wavelength region would have been more useful.

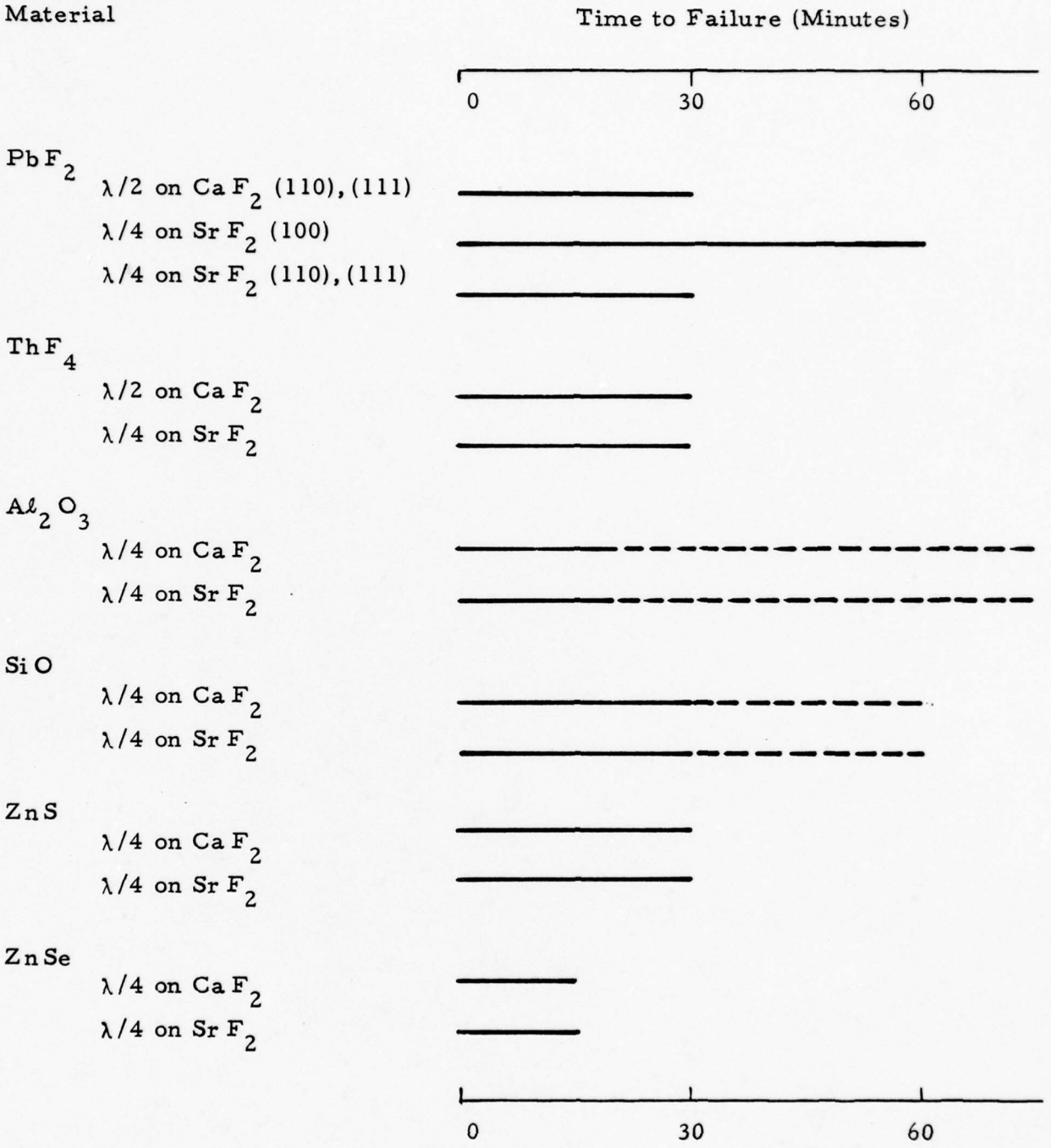

Figure 15. Summary of HF Vapor Tolerance Test Results For Coatings on CaF_2 and SrF_2 Substrates.

Modes of failure differed widely among the various coating materials and thicknesses, from general attack (ZnSe, ZnS, SiO, PbF_2) to selective attack at coating defects only (Al_2O_3 and $\lambda/4$ ThF_4 on SrF_2) or characteristic crazing patterns ($\lambda/2$ ThF_4 on CaF_2). Typical damage to PbF_2 films on CaF_2 and SrF_2 surfaces is illustrated in figures 16 and 17 respectively. The nature of the damage is etch pitting resulting from general chemical attack. Note the surficial expression of a substrate grain boundary in 16 (a) and the undisturbed appearance of the uncoated substrate surface in the lower half of figure 16 (b). Figure 17 (a) illustrates typical morphology of the damaged PbF_2 surface on (110) and (111) SrF_2 substrates after 30 minutes exposure to the humid HF environment. Figure 17 (b) shows the coating on (100) SrF_2 after 60 min. in the identical environment. The attack in the latter case is just as extensive, but not nearly as severe.

Damaged ThF_4 films are shown in Figures 18 and 19 after 30 minutes exposure to the HF vapor. A characteristic spiral crazing pattern which develops on ThF_4 films of halfwave thickness (at 3.8 or 5.3 μm) on (100) and (110) CaF_2 surfaces is illustrated in Figure 18 (a) while more general attack typical of the (111) surface is illustrated in figure 18 (b). HF damage to ThF_4 films of $\lambda/4$ thickness on SrF_2 is shown in figure 19. Crazing is conspicuously absent in all cases, the damage comprising pits and blisters, probably initiating at defects in the original coating. Thus there is an apparent substrate material and/or film thickness dependence for damage to ThF_4 films by wet HF vapor.

Damage to quarterwave thickness (at 3.8 μm) Al_2O_3 films is similar for all orientations of CaF_2 and SrF_2 substrates, comprising highly localized attack at film defects, surrounded by altered surficial material exhibiting a concentric ring interference pattern, similar to the microscopic pattern described above in connection with the onset of damage to these films. Typical examples are shown in Figure 20. Apparently, the mechanism of

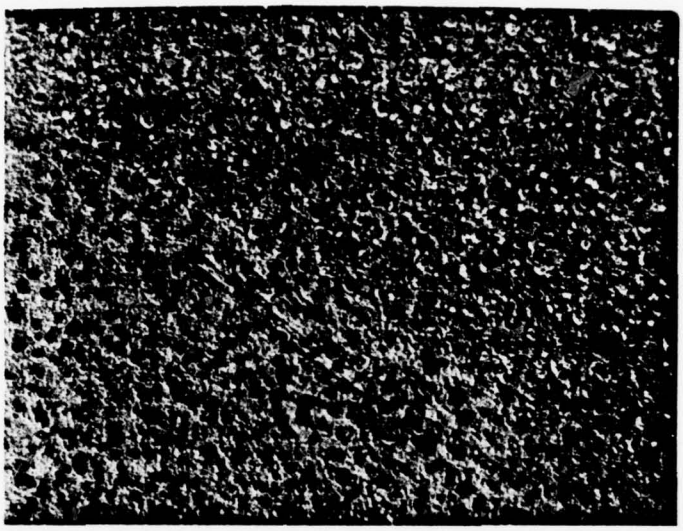

a) (110) Surface

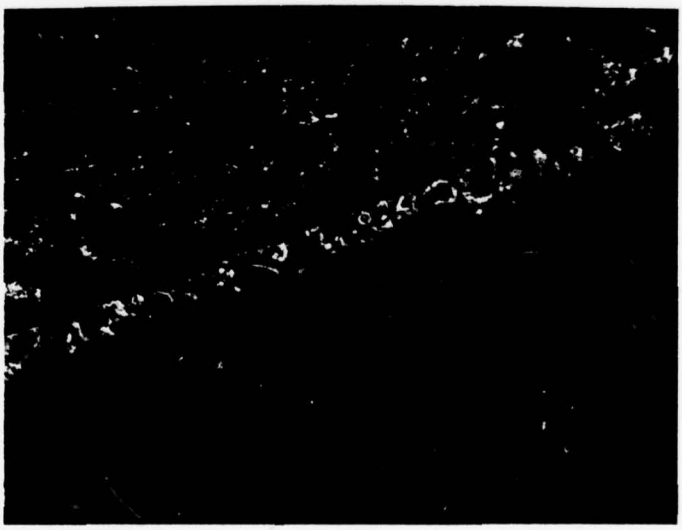

b) (111) Surface, Coating Edge.

Figure 16. PbF_2 ($\lambda/2$) on CaF_2 • HF vapor, 30 Min. 167X.

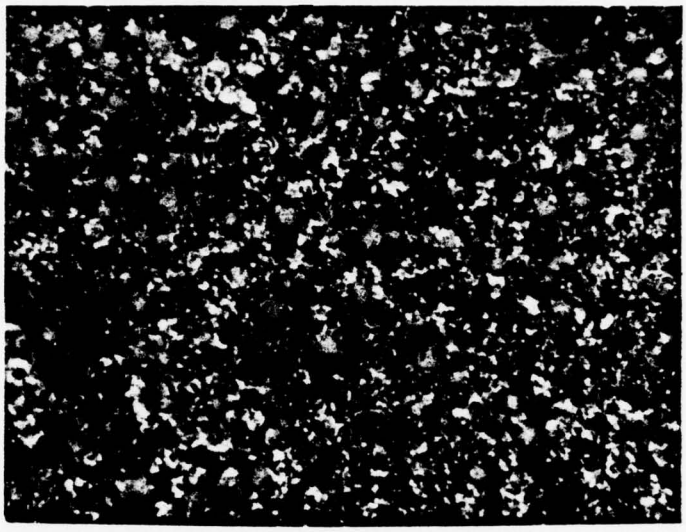

a) (110) Surface 30 Min.

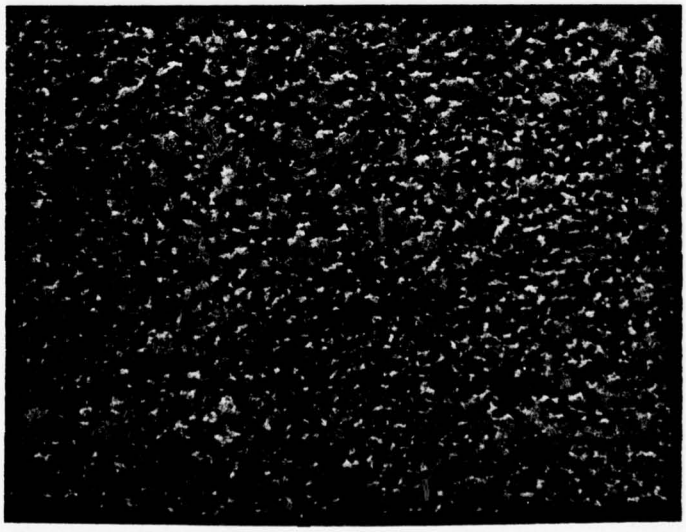

b) (100) Surface 60 Min.

Figure 17. PbF_2 ($\lambda/4$) on SrF_2 · HF vapor, 305X

a) (100) Surface

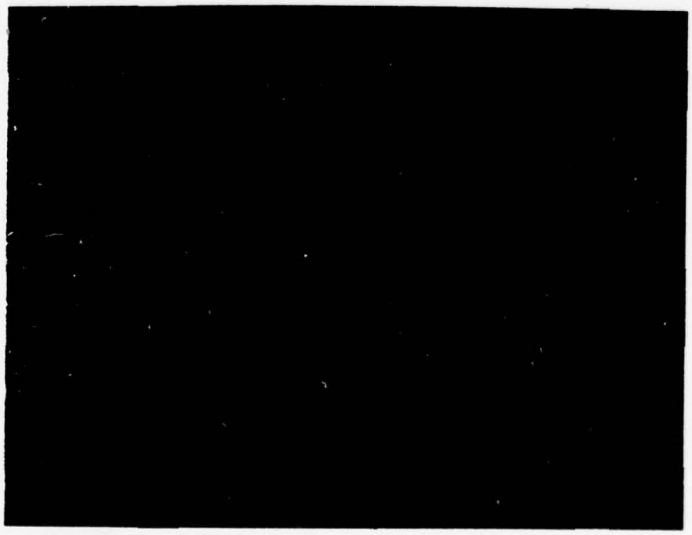

b) (111) Surface

Figure 18. ThF_4 ($\lambda/2$) on CaF_2 · HF vapor, 30 Min. 167X.

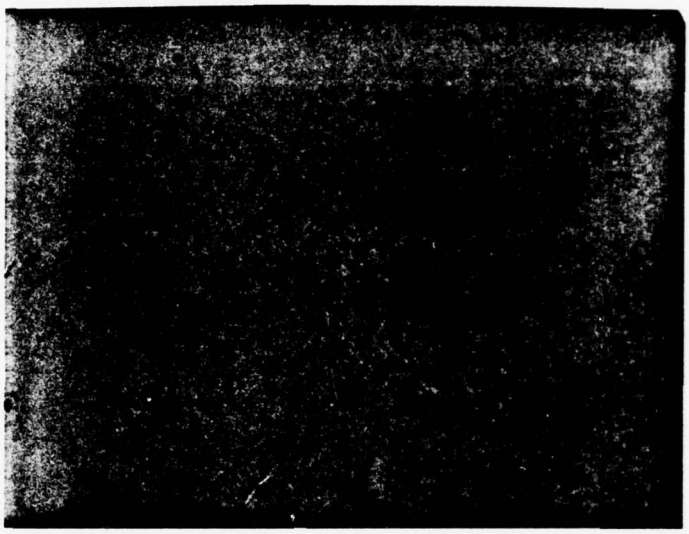

a) (110) Surface, Center, Typical.

b) (110) Surface, Near Edge, Atypical Area.

Figure 19. ThF_4 ($\lambda/4$) on SrF_2 · HF vapor, 30 Min. 167X.

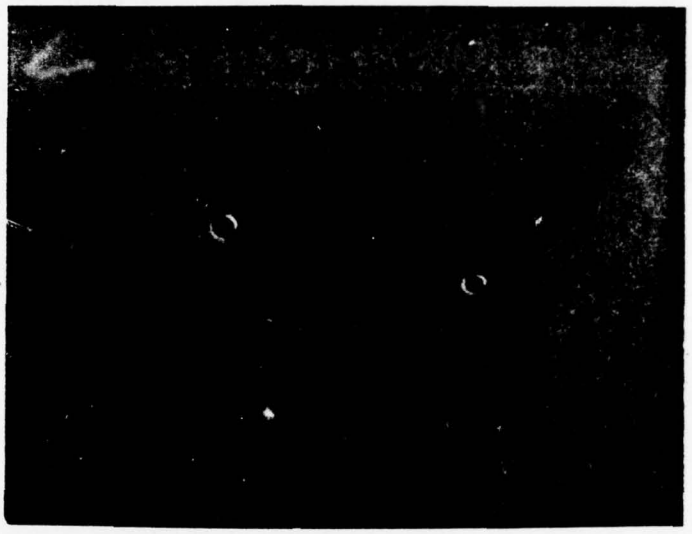

a) CaF_2 (100) Substrate

b) SrF_2 (111) Substrate

Figure 20. Al_2O_3 ($\lambda/4$) Typical HF vapor damage, 167X.

damage remains the same throughout the exposure period, simply progressing more rapidly at certain widespread defects.

A comparison of morphology and severity of HF vapor damage to SiO films on three orientations of CaF_2 and SrF_2 is given in figures 21 and 22. The least severely damaged SiO films appear on (111) CaF_2 surfaces and on (100) SrF_2 surfaces. The SiO films are most amorphous on these substrate orientations, exhibiting no diffraction peaks attributable to well crystallized SiO_2. Also, probably fortuitously, SiO films have their lowest absorption coefficients on (111) CaF_2 substrate surfaces. Thus we may tentatively conclude that amorphous SiO films are more resistant to HF vapor attack than films composed of measurable amounts of crystalline SiO_2.

Typical HF damage morphology in ZnS and ZnSe quarterwave films is shown in figures 23 and 24. The damage mechanism appears to be relatively uniform chemical attack, with no systematic differences correlating with substrate composition or orientation.

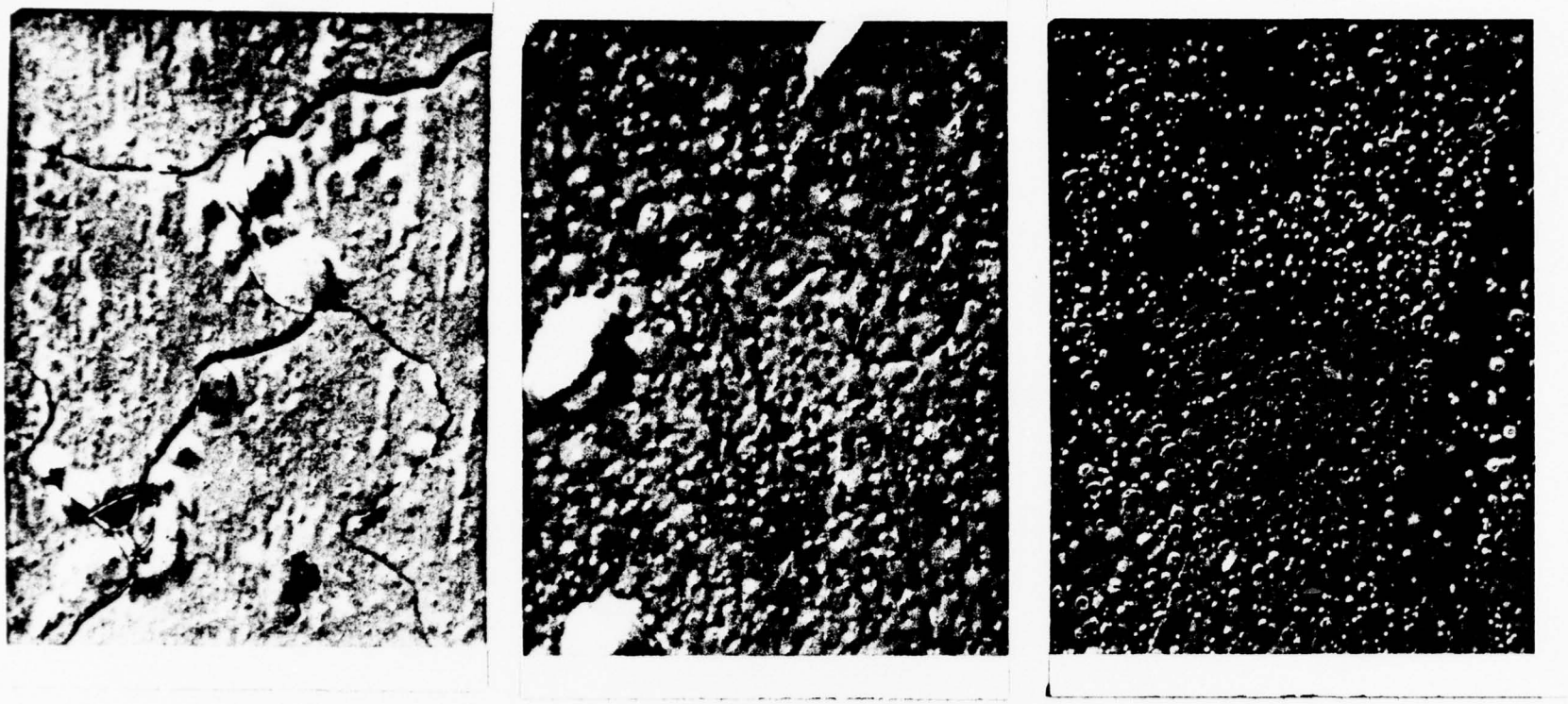

a) (100) b) (110) c) (111)

Figure 21. Si O ($\lambda/4$) on CaF_2. Typical HF Vapor Damage on Three Substrate Orientatations. 60 Min. 167X.

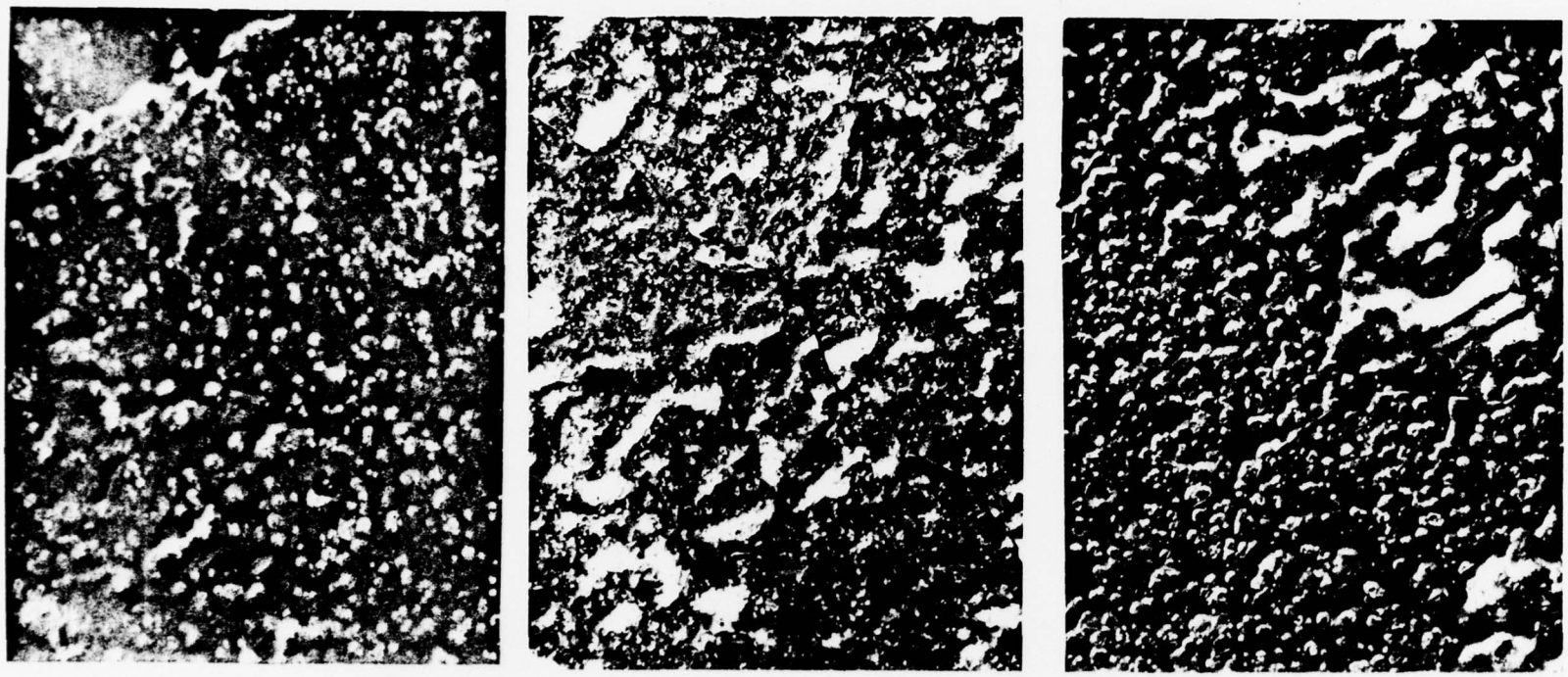

a) (100) b) (110) c) (111)

Figure 22. Si O ($\lambda/4$) on SrF_2. Typical HF Vapor Damage on Three Substrate Orientations. 167X.

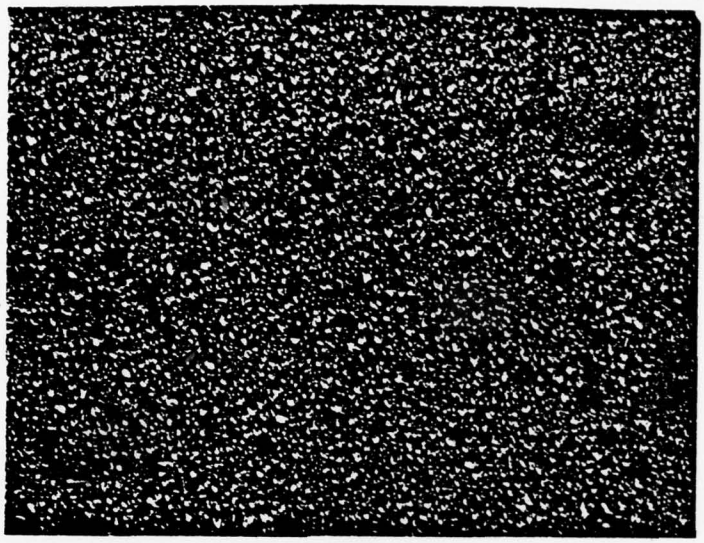

a) CaF_2 (111) Substrate.

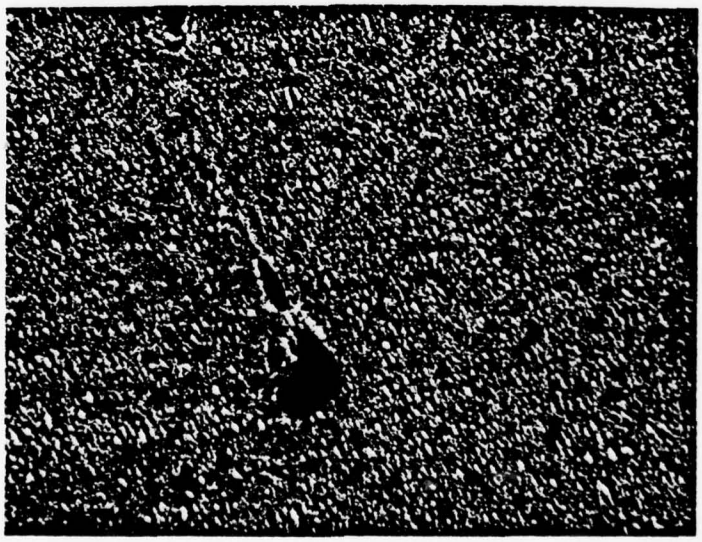

b) SrF_2 (111) Substrate.

Figure 23. ZnS ($\lambda/4$) Films. Typical HF Damage 30 Min. 167X.

a) CaF_2 (110) Substrate.

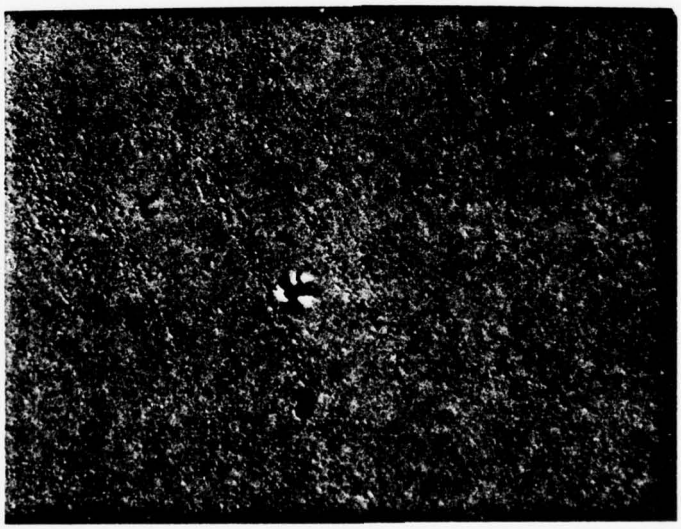

b) SrF_2 (110) Substrate.

Figure 24. ZnSe ($\lambda/4$) Films. Typical HF Damage 15 Min. 167X.

3.5 MULTILAYER ANTIREFLECTION COATINGS.

The intended application of most of the thin film material properties generated under this program is in the design of multilayer coatings for use on laser optics. In such multilayer applications, the surface encountered by the depositing material of the layer nearest the substrate is essentially identical to that in the single layer case, from which properties and structure were determined. The depositing material of the second layer (and any succeeding layers) encounters the surface of the first coating as its substrate, giving rise to possible differences in coating structure or properties. Thus it is necessary to determine absorptance and coating structure for multilayer coatings to establish similarities and differences in behavior in comparison with single layer coatings.

3.5.1 Absorptance of Multilayer Coatings

Absorptance values for coatings on window samples coated on both sides with a quarterwave-quarterwave design composed of ThF_4 and either PbF_2 or SiO are listed in Table XLVI for the DF laser wavelength region. The absorptance of the substrates ($\sim 1 \times 10^{-4}$) has been subtracted out in all cases so that the tabulated numbers represent the absorptance of two (2) coated surfaces. Mean values for each coating/substrate combination are listed at the far right; mean values for each coating pair and substrate orientation are also given for pusposes of comparison. Approximate bandwidth for both coating designs is 0.5 μm.

Some general observations to be drawn from the data include the relatively high absorptance and strong variation with substrate orientation of the ThF_4/PbF_2 coatings as compared to ThF_4/SiO and the small differences between average values for a given coating pair on CaF_2 or SrF_2 substrates. The last observation is in accord with single layer data as is

Table XLVI. Absorptance of Antireflection Coatings on Single Crystal CaF_2 and SrF_2 Substrates (2 coated surfaces) at 3.8 μm.

Materials & Design	Coating Absorptance for Various Substrate Orientations (x 10^4).			Mean Coating Absorptance
	(100)	(110)	(111)	(x 10^4)
ThF_4/PbF_2 on CaF_2	9.62	7.00	7.48	8.03
ThF_4/PbF_2 on SrF_2	9.30	5.54	7.15	7.33
ThF_4/PbF_2 Mean	9.45	6.27	7.32	7.68
ThF_4/SiO on CaF_2	4.30	3.60	3.12	3.67
ThF_4/SiO on SrF_2	3.60	4.00	3.44	3.68
ThF_4/SiO Mean	3.95	3.80	3.28	3.68

the stronger variation with substrate orientation. The lower mean sbsorptance of the ThF_4 / SiO pair as compared to the ThF_4 / PbF_2 pair is also in accord with single layer data, but the difference is much more pronounced. In the single layer case the difference amounts to only 10 to 20%, depending upon whether the absorptance values are those for halfwave coatings only or were determined as a function of coating thickn (βL vs. L). For the present set of antireflection coatings the difference in mean absorptance between the two designs is almost exactly a factor of two. This last observation is generally not in accord with experience on the LWTVP program, where differences between the same two coating designs averaged less than 10%, over a large number of single and polycrystalline samples of CaF_2 and SrF_2.

Comparing the overall magnitude of the AR coating absorptances in Table XLVI with averages for the LWTVP program reveals that the present results for ThF_4 / PbF_2 are consistently higher than the former results by a factor of four; those for ThF_4/ SiO are higher by a factor of two in the present case. Overall agreement between single layer absorptance results for ThF_4 and PbF_2 and AR results for the pair obtained under the present program is within 10%, the single layer results being higher. Single layer absorption coefficients for ThF_4 and SiO lead to a calculated mean absorptance for the AR coating which is about double the actual measured value obtained under the present program.

These problems, taken together with the inconsistencies in the results of the absorptance vs. film thickness studies for ThF_4 indicate strongly that the raw materials presently available from Balzers and Cerac differ from those purchased in the initial phase of the LWTVP program. Impurities such as oxides, oxyfluorides, or hydrated fluorides of Thorium would increase the absolute level of absorptance in coating designs involving ThF_4 and could lead to inconsistencies in absorptance based on interaction

of these impurities with other coating materials in a multilayer design.

Comparison of mean absorptance of ThF_4 / PbF_2 antireflection coatings on polycrystalline CaF_2 (8.91×10^{-4} for two coated surfaces) with the mean for the same pair on three orientations of single crystal CaF_2 substrates (Table XLVI) shows a difference of only 10%, with the polycrystalline substrate values being higher. Comparison of the coating absorptance on polycrystalline substrates with the mean calculated value using single layer (halfwave) data (9.60×10^{-4} for two coated surfaces) shows a difference of 7.5%, with the single layer calculated value being the higher. Thus, it appears that both the single layer and multilayer coating absorptances have practical value in predicting performance of coatings in systems of interest for real devices. However, much work is still required to achieve higher degrees of correlation and to understand the underlying phenomena responsible for the results.

3.5.2 Structure and Preferred Orientation in Multilayer Coatings.

In order to ascertain whether differences in coating structure or preferred orientation in multilayer and single layer coatings are associated with observed differences in coating absorptance, both coating pairs (ThF_4/ PbF_2 and ThF_4 / SiO) were subjected to x-ray diffraction analysis on all three single crystal substrate orientations. Results of these analyses are summarized in Tables XLVII and XLVIII for ThF_4 / PbF_2 and ThF_4/SiO, respectively.

Considering first the results in Table XLVII for ThF_4/PbF_2, we see that the structure and preferred orientation of the PbF_2 component film of the two-layer pair (deposited first on the uncoated substrate surface) is similar in most respects to that of the single layer film on a similarly

TABLE XLVII. Structures and Preferred Orientation in Component Films of the ThF_4/PbF_2 Quarterwave-Quarterwave Coating on CaF_2 and SrF_2 Substrates.

Substrate Material	Substrate Orient.	PbF_2 Structure and Orientation	ThF_4 Structure and Orientation
CaF_2	(100)	β(cubic) (100) ≧ (111) α (orthorh) (012)	Monoclinic, (110) > $(44\bar{3})$
	(110)	β (110) ; α (100)	Microcrystalline, (110) ≅ $(32\bar{1})$
	(111)	β (111), Minor (110) α (001)	Monoclinic (110) ; Minor μcryst.
SrF_2	(100)	β (100) ; Minor α (012) > (035).	Amorphous to X-Ray.
	(110)	β (110).	Monoclinic $(52\bar{1})$ > $(43\bar{1})$
	(111)	β (111)	Amorphous to X-Ray.

oriented substrate (compare with Sect. 3.3.3 and 3.3.5). The only major difference is the presence of a considerable amount of (100) oriented PbF_2 on (100) CaF_2, in addition to the (111) oriented PbF_2 which was the predominant orientation in the single layer case on (100) CaF_2. All other differences in the PbF_2 structure and orientation on CaF_2 or SrF_2 are quite minor, involving presence or absence of the orthorhombic α-phase (a minor constituent) or details of its preferred orientation.

On the other hand, the ThF_4 component film of the ThF_4/PbF_2 pair, which is deposited on top of the PbF_2 film in the AR coating, shows very little similarity of structure or preferred orientation with the single layer ThF_4 films deposited on the bare substrate. On (100) CaF_2, the ThF_4 component film is crystalline with a predominant (110) preferred orientation; single layer films (quarterwave or halfwave) on corresponding substrates were crystalline with a (270)≅ $(21\bar{3})$ preferred orientation. On (110) CaF_2 substrates, the ThF_4 film of the AR coating is microcrystalline as in the single layer case, but with subequal (110) and $32\bar{1}$) preferred orientation. The single layer films had subequal (110) and (103) orientation. On (111) CaF_2, the ThF_4 in the AR coating is well crystallized with a (110) preferred orientation, whereas the single layer films exhibit a strong $(32\bar{1})$ orientation. On SrF_2 substrates the ThF_4 of the AR coating is amorphous to x-ray on (100) and (111); single layer films on SrF_2 substrates of these orientations were microcrystalline and well crystallized with strong (010)/(322) orientation, respectively. The structure and orientation of ThF_4 films on (110) SrF_2 is similar in both the ThF_4/PbF_2 coating and the single layer film, having a strong $(52\bar{1})$ orientation with minor amounts of less strongly oriented material.

Structure and preferred orientation of component films of the ThF_4/Si O pair (Table XLVIII) is similar to the single layer films in four of the six

Table XLVIII Structures and Preferred Orientation in Component Films of the ThF_4/SiO Quarterwave-Quarterwave Coating on CaF_2 and SrF_2 Substrates.

Substrate Material	Substrate Orient.	SiO Structure and Orientation	ThF_4 Structure and Orientation
CaF_2	(100)	Amorphous to X-Ray	Amorphous to X-Ray
	(110)	Amorphous/Microcrystalline SiO_2 (α-Quartz) (100)	Microcrystalline, Monoclinic (110) + $ThF_4 \cdot nH_2O$ (211).
	(111)	Crystalline, α-Quartz (311) + Minor Tridymite (105)	Crystalline, Monoclinic ($32\bar{1}$), Minor (332).
SrF_2	(100)	Amorphous/Microcrystalline	Crystalline, Monoclinic (252)
	(110)	Amorphous to X-Ray	Microcrystalline, Monoclinic (102)
	(111)	Crystalline, α-Qtz. (110) + Microcrystalline (6.30Å)	Crystalline, Monoclinic (322)

substrate/coating combinations studied here (see Sec. 3.3.5 & 3.3.8). On (100) CaF_2 both Si O and ThF_4 are amorphous to x-ray. For Si O, this structure is similar to the single layer case; for ThF_4, the single layer films on this substrate orientation had been consistently crystalline with strong, subequal (270) and (21$\bar{3}$) preferred orientations. On (110) CaF_2, the structure and orientation of both films of the pair is similar to the single layer case; the only significant difference is the presence of a diffraction peak attributable to the(211) spacing of ThF_4. nH_2O[81] in the two-layer coating. On (111) CaF_2, Si O is crystalline with α-quartz and minor tridymite; in the single layer case it was amorphous or microcrystalline. The ThF_4 structure and preferred orientation in the multilayer and single layer films on (111) CaF_2 are essentially identical.

On (100) SrF_2, Si O and ThF_4 films of the multilayer coating have structure and orientation similar to single layer films of the same materials. The only notable difference is the absence of diffraction peaks attributable to hydrated ThF_4 in the multilayer case. On (110) SrF_2 the structure and orientation of both Si O and ThF_4 differ from the single layer cases with Si O being amorphous rather than crystalline or microcrystalline and ThF_4 being microcrystalline with a (102) preferred orientation rather than crystalline with a strong (52$\bar{1}$) orientation, as in the single layer case. Finally, on (111) SrF_2, Si O and ThF_4 component films are both crystalline, as in the single layer case. However, the Si O yields diffraction peaks for α-Quartz and some microcrystalline material with spacings near 6.30 A, rather than for Tridymite, as in the single layer case. The ThF_4 of the multilayer coating has a (322) preferred orientation, as compared to the (010) orientation of single layer films. In addition, no diffraction peaks attributable to hydrated ThF_4 are evident in the multilayer case, whereas a minor peak was observed in the single layer case.

In summary of the multilayer coating structure and orientation results, it appears that the PbF_2 structures are nearly identical to the single layer films in all cases, which is exactly as expected. Although the structure and orientation of the ThF_4 films of the ThF_4/PbF_2 coating pair differed from the single layer films in most cases, it is apparent that these differences did not significantly affect absorption, as noted in the previous subsection. In the ThF_4/Si O pair on the other hand, differences in both the Si O and ThF_4 film structures were observed, on comparison with the single layer cases. The absence of hydrated ThF_4 material in the multilayer case is significant and may explain the markedly reduced absorption in comparison with the single layer films. The difference in the Si O component of the multilayer are in the direction of less crystallinity and identification of α - quartz rather than Tridymite as the crystalline $Si O_2$ phase, when $Si O_2$ is present. These characteristics are difficult to identify with reduced absorptance at 3.8 μm, except that it is possible the multilayer films are less rich in oxygen than was the case with the single layer films.

4.0 SUMMARY

The major experimental results generated under the contract comprise the structures, preferred orientations, refractive indices, absorptance and relative growth rates of the ten thin film materials. This information is summarized here in a tabular or matrix format.

The results of the investigations of structure and preferred orientation of coating materials are summarized in three tables in this section. The materials are grouped by chemical composition (i. e. fluorides, oxides, sulfides and selenides). In these tables, the crystal structure and predominant crystallographic orientation of the coating material paralleling the substrate surface are given for each substrate material and orientation. Less strong preferred orientations are also given, along with any impurities indicated by one or more x-ray diffraction peaks.

Abbreviations used in the tables are self-explanatory, for the most part. Specific phases are designated by α or β where customary. Structures having orthorhombic symmetry are abbreviated "Orth". Monoclinic phases are designated "Monocl." and hexagonal structures are abbreviated "hexag." Microcrystalline material is abbreviated "μ cryst." and amorphous material is designated "amorph." Numbers enclosed in parentheses are always Miller indices of specific crystallographic planes, with strongest preferred orientation first, followed by lower intensity lines.

Considering the fluorides (Table XLIX), we see that several of them take strong perferred orientations paralleling the substrate, while others apparently have a preferrential growth direction which is independent of substrate orientation. Examples of the former behavior are provided by MgF_2, PbF_2 (on SrF_2), and ThF_4. Examples of a preferrential growth

TABLE XLIX

Summary of Structure and Preferred Orientation in Fluoride Coating Materials on CaF_2 and SrF_2 Substrates

Coating Material	Substrate Material and Orientation	Coating Structure and Orientation	Impurities, Remarks
LaF_3	CaF_2 (100)	Hexagonal: (111), (100), (110)	LaOF
	(110)	(100), (302)	La_2O_3
	(111)	(001), (110)	La_2O_3
	SrF_2 (100)	Hexagonal: (111), (100), (110)	
	(110)	(110)	
	(111)	(001)	$La(OH)_3$
MgF_2	CaF_2 (100)	Tetragonal: (001) α (100)	
	(110)	(211) $\approx$ (112) ; (110)	
	(111)	α (800)	Distorted α ?
	SrF_2	Amorphous to X-ray, all substrate orientations	Crazing; Defects
PbF_2	CaF_2 (100)	β (cubic) (111) ; α (Orth.) (001)	
	(110)	(111) $\approx$ (110)	
	(111)	(111) ; α (Orth.)	
	SrF_2 (100)	β (cubic) (100) α (Orth.) (010), (012)	
	(110)	(110) ; Minor (111)	Pb_2O_3
	(111)	(111) ; α (001)	PbO

TABLE XLIX (Cont'd.)

Summary of Structure and Preferred Orientation in Fluoride Coating Materials on CaF_2 and SrF_2 Substrates

Coating Material	Substrate Material and Orientation	Coating Structure and Orientation	Impurities, Remarks
SrF_2	CaF_2 (100)	Cubic (111), (100)	Sr, SrO
	(110)	(111), (110)	Sr, $Sr(OH)_2$
	(111)	(111)	Sr, SrO_2
ThF_4	CaF_2 (100)	Monocl. (270) ≈ $(21\bar{3})$	
	(110)	μ cryst. 3.8Å (220); 2.01Å (103)	
	(111)	Monocl. $(32\bar{1})$; (332)	
	SrF_2 (100)	Monocl. (132); (252) μcryst. 5-9Å	Cerac
		μ cryst. (512); (103), (220)	Balzers
	(110)	Monocl. $(52\bar{1})$ + Minor μcryst. & Hydrates	Balzers + Cerac
	(111)	Monocl. (030); (332) Minor Hydrates (Cerac) 2.45Å	Balzers + Cerac

direction independent of substrate preferred orientation are PbF_2 and SrF_2 on CaF_2, both of which show a strong (111) film preferred orientation irrespective of substrate orientation. The relationship of PbF_2 films to SrF_2 substrates suggests near perfect epitaxy or at least a "fiber" axis orientation of certain planes of βPbF_2 to corresponding planes of the SrF_2 substrate. These materials are iso-structural and the mismatch between corresponding interplanar spacings in the two materials is 2.4%. LaF_3 exhibits rather weak, but consistent film orientation, with appreciable randomness in the orientation of the less strongly diffracting planes.

Among the oxides studied, epitaxial growth is rare on fluoride substrates (Table L). The only strong preferred orientation in the thin films occurs in MgO films deposited on (100) and (110) CaF_2. The MgO structure is cubic (NaCl type) and the mismatch between (111) MgO and (100) or (110) CaF_2 is about 9%. The Al_2O_3 structure has hexagonal symmetry, but deposits as an amorphous or microcrystalline thin film on most orientations of CaF_2 and SrF_2 substrates. SiO is generally thought to be amorphous but the structure of thin films on various substrates is not well known. In the present studies, utilizing cubic fluoride substrates, the material is generally microcrystalline, with spacings corresponding to tridymite, a monoclinic or hexagonal form of SiO_2. On (100) CaF_2, the material is amorphous to X-ray. The presence of diffraction maxima attributable to forms of SiO_2 and none corresponding to elemental Si indicates an oxygen-rich film.

Zinc sulfide and selenide films deposit with strong preferred orientation on CaF_2 and SrF_2 (Table LI). In zinc selenide, there is apparently a preference for the cubic phase and a $[11\bar{1}]$ growth direction on CaF_2 and SrF_2 substrates oriented parallel to (100) and (110), while on the (111)

TABLE L

Summary of Structure and Preferred Orientation in Oxide Coating Materials on CaF_2 and SrF_2 Substrates

Coating Material	Substrate Material and Orientation		Coating Structure and Orientation	Impurities; Remarks
Al_2O_3	CaF_2	(100)	α (Hexagonal) (018), μ cryst.	
		(110)	μ cryst/amorph. 1.8-2.1Å	
		(111)	μ cryst/amorph. 6-7Å; α (012)	
	SrF_2	(100)	Amorph. to X-ray	
		(110)	Amorph. to X-ray	
		(111)	μ cryst. ≈ 6Å; 3.69Å	
MgO	CaF_2	(100)	Cubic (111), (110)	d_{111} (obs) > d_{111} (ASTM)
		(110)	Cubic (111), (100), (110)	d_{111} (obs) > d_{111} (ASTM)
		(111)	Amorphous to X-ray	$Mg(OH)_2$, MgO_2 (3.5Å)?
	SrF_2	(100)	μcryst.; Minor cubic (111)	Mg ?
		(110)	μcryst.	α - MgF_2?
		(111)	μcryst	

TABLE L (Cont'd.)

Summary of Structure and Preferred Orientation in Oxide Coating Materials on CaF_2 and SrF_2 Substrates

Coating Material	Substrate Material and Orientation	Coating Structure and Orientation	Impurities; Remarks
SiO	CaF_2 (100)	Amorphous to X-ray	
	(110)	μcryst. (1.9Å)	
	(111)	μcryst. (1A, 6.3Å); Minor cryst. Tridym. Monocl. 3.49Å	
	SrF_2 (100)	μcryst. 1.41Å, 1.46Å	Spacings corres. to Tridymite Monocl. or Hex.
	(110)	μcryst. 4Å, 2.28Å	
	(111)	μcryst. 4-9Å, 3.7Å	

TABLE LI

Summary of Structure and Preferred Orientation in Zinc Selenide and Sulfide Coating Materials on CaF_2 and SrF_2 Substrates

Coating Material	Substrate Material and Orientation	Coating Structure and Orientation	Impurities Remarks
ZnSe	CaF_2 (100)	Cubic (β ZnS) (111)	$ZnSeO_4$
	(110)	Cubic (β ZnS) (111)	$ZnSeO_4$
	(111)	Hexag. (100)	d(obs) > d(ASTM)
	SrF_2 (100)	Cubic (β ZnS) (111)	ZnO, $Zn(OH)_2$,
	(110)	Cubic (β ZnS) (111); μcryst. 3-4Å	$ZnSeO_4$
	(111)	Hexag. (103), (105); μcryst. 5-7Å	
ZnS	CaF_2 (100)	Hexag. α ZnS (8H) (001), (110), (100).	$Zn(OH)_2$?
	(110)	Hexag. α ZnS (8H) (001), (10 10), (10 13), (110).	
	(111)	Hexag. α ZnS (212)	Superstruct(?) 3.377Å
	SrF_2 (100)	Hexag. α ZnS (101); ZnS (10H)	
	(110)	Hexag. α ZnS (102); ZnS (10H)	
	(111)	Hexag. α ZnS (10H) (10 14)	

substrate orientation, the hexagonal phase is preferred with the (100) orientation of CaF_2 and the (103) orientation on SrF_2.

Zinc sulfide, on the other hand, exhibits a preference for polytypes of the hexagonal phase on all three orientations of the two substrate materials. On CaF_2 these take a basal (001) orientation on (100) and (110) and a higher index orientation on (111). The 8H polytype (c-axis unit spacing is 8 times the fundamental value for the phase) occurs on (100) and (110), while the fundamental polytype occurs on (111). On SrF_2, prismatic orientations of the 10H polytype of ZnS occur on all substrate orientations.

Structural mismatch criteria between the substrate and film do not appear to govern the choice of structure and orientation in these ZnS films. These criteria would predict a cubic (sphalerite or β-ZnS) structure for films on CaF_2, with a strong preferred orientation paralleling the substrate. On SrF_2, these same criteria would predict α - ZnS on all three orientations with (101) ZnS paralleling (100) SrF_2, (102) ZnS on (110) SrF_2 and (100) ZnS on (111) SrF_2. The first two of these relationships are in fact observed.

The measured refractive indices and coating absorption coefficients obtained in this study are presented in Tables LII-LV, along with information on relative growth rates obtained from spectrophotometer transmission scans in the visible region (600 to 800 nm), where interference effects are more pronounced. The absorption coefficient, β, is tabulated rather than the absorption index, k, for convenience. The absorption index can be obtained from the tabulated β using the realtion (equation 11, Section 2.7)

$$k_1 = \frac{\lambda_o \beta_1}{4\pi}$$

TABLE LII. ABSORPTION COEFFICIENTS OF FLUORIDE COATING MATERIALS MEASURED BY DF LASER CALORIMETRY ON COATINGS OF HALFWAVE OPTICAL THICKNESS AT A DESIGN WAVELENGTH OF 3.8 μm

COATING MATERIAL	REFRACTIVE INDEX	COATING ABSORPTION COEFFICIENT, β (cm^{-1}) CaF_2 SUBSTRATE (100)	(110)	(111)	SrF_2 SUBSTRATE (100)	(110)	(111)
LaF_3	1.52	41.49	28.43	24.88	36.61	24.53	29.49
MgF_2	1.36	19.06	21.70	21.17	17.56	18.33	19.20
PbF_2*	1.73	4.24	3.03	7.16	1.63**	2.01**	1.94**
SrF_2	1.34	39.81	44.71	29.24	--	--	--
ThF_4***	1.49	2.86	1.65	3.58	4.43	2.76	3.59

* ON CaF_2 THE GROWTH RATE OF PbF_2 ON (110) > (111) > (100), WHILE ON SrF_2, (110) ≥ (100) > (111).

** ABSORPTANCE VALUES DETERMINED FROM βL VS. L EXPERIMENT.

*** COATINGS ON ALL SUBSTRATES EMPLOYED CERAC RAW MATERIAL. GROWTH RATES OF ThF_4 ARE INDISTINGUISHABLE ON THE THREE ORIENTATIONS OF TWO SUBSTRATE MATERIALS.

TABLE LIII. ABSORPTION COEFFICIENTS OF OXIDE, SULFIDE, AND SELENIDE COATING MATERIALS MEASURED BY DF LASER CALORIMETRY ON COATINGS OF HALF-WAVE OPTICAL THICKNESS AT A DESIGN WAVELENGTH OF 3.8 μm.

COATING MATERIAL	REFRACTIVE INDEX	COATING ABSORPTION COEFFICIENT, β (cm^{-1})					
		CaF_2 SUBSTRATE			SrF_2 SUBSTRATE		
		(100)	(110)	(111)	(100)	(110)	(111)
Al_2O_3	1.57	40.75	37.70	29.65	45.13	43.90	32.71
MgO	1.63	65.91	86.14	79.06	62.55	100.85	102.03
SiO	1.73	2.25*	1.58*	1.07*	3.67	5.74	2.22
ZnSe	2.42	3.67	1.59	1.41	1.08	3.73	4.69
ZnS	2.23	10.10	8.81	10.20	16.73	13.52	19.61

Al_2O_3: ON BOTH SUBSTRATE MATERIALS THE GROWTH RATE ON (100) $\cong$ (110) > (111).

MgO: REFRACTIVE INDEX GIVEN FOR COATINGS ON CaF_2; ON SrF_2 n(100) = 1.62, n(110) = 1.66, n(111) = 1.65. ON CaF_2, THE GROWTH RATE ON (100) > (110) $\cong$ (111), WHILE ON SrF_2, (110) $\geq$ (111) > (100).

SiO: ON CaF_2, THE GROWTH RATE ON (100) > (111) > (110), WHILE ON SrF_2, (110) $\cong$ (111) > (100).

ZnSe: ON CaF_2, THE GROWTH RATE ON (100) $\cong$ (110) > (111), WHILE ON SrF_2, (110) $\cong$ (111) > (100).

ZnS: ON CaF_2, THE GROWTH RATE ON (110) > (100) > (111), WHILE ON SrF_2, (110) > (111) > (100).

* ABSORPTANCE VALUES DETERMINED FROM βL VS. L EXPERIMENT.

TABLE LIV. ABSORPTION COEFFICIENTS OF FLUORIDE COATING MATERIALS MEASURED BY CO LASER CALORIMETRY ON COATINGS OF HALFWAVE OPTICAL THICKNESS AT A DESIGN WAVELENGTH OF 5.3 μm.

COATING MATERIAL	REFRACTIVE INDEX	COATING ABSORPTION COEFFICIENT, β (cm^{-1}) CaF_2 SUBSTRATE (100)	(110)	(111)	SrF_2 SUBSTRATE (100)	(110)	(111)
PbF_2*	1.72	1.69	2.14	3.34	--	--	--
SrF_2	1.33	17.67	16.16	13.41	--	--	--
ThF_4**	1.48	3.24	3.11	2.98	1.41	0.78	0.78

* THE GROWTH RATE OF PbF_2 ON (110) > (111) > (110).

** COATINGS ON CaF_2 SUBSTRATES UTILIZED CERAC RAW MATERIAL; THOSE ON SrF_2 EMPLOYED BALZERS MATERIAL. GROWTH RATES ARE INDISTINGUISHABLE ON THE THREE ORIENTATIONS OF TWO SUBSTRATE MATERIALS.

TABLE LV. ABSORPTION COEFFICIENTS OF OXIDE, SELENIDE, AND SULFIDE COATING MATERIALS MEASURED BY CO LASER CALORIMETRY ON COATINGS OF HALF-WAVE OPTICAL THICKNESS AT A DESIGN WAVELENGTH OF 5.3 μm.

COATING MATERIAL	REFRACTIVE INDEX	COATING ABSORPTION COEFFICIENT, β (cm^{-1})					
		CaF_2 SUBSTRATE			SrF_2 SUBSTRATE		
		(100)	(110)	(111)	(100)	(110)	(111)
SiO	1.78	38.59	41.17	39.16	--	--	--
ZnSe	2.41	3.98	0.96	1.69	1.76	2.10	2.04
Zns	2.22	9.65	11.49	10.94	6.68	6.85	8.26

SiO: THE GROWTH RATE ON (100) > (111) > (110).

ZnSe: ON CaF_2, THE GROWTH RATE ON (100) ≅ (110) > (111), WHILE ON SrF_2, (110) ≅ (111) > (100).

ZnS: ON CaF_2, THE GROWTH RATE ON (110) > (100) > (111), WHILE ON SrF_2, (110) > (111) > (100).

where λ_o is the laser (and coating design) wavelength in centimeters. All absorption coefficients were calculated from the raw data using the program of Loomis[32] for a single layer film on the exit surface of a transparent medium.

Some general features of the data are worth noting. It appears that the coating materials fall into three broad groups, based on absorption: (1) those having β values between ~ 1 and ~ 7 cm^{-1}, (the low absorption group); (2) those having β values between ~ 9 and ~ 20 cm^{-1} (the intermediate group); and (3) those having β values of 20 cm^{-1} or more, ranging to 100 cm^{-1} (high absorption group).

The sum of the standard deviation of the absorption measurements on the uncoated and coated substrate is a measure of the precision of the coating absorption determination. Since this determination involves the subtraction of two numbers with similar errors, the precision of the results will vary. The error in the coating absorption determination for the low absorption group is of the order of 10 to 15%; that for the intermediate and high absorption groups is 3 to 5%.

In general, differences among materials are greater than differences among substrate orientations for the same coating material. However, differences among substrate orientations for the same coating may amount to factors of 2 to 4 in absorption (e.g. ZnSe on SrF_2 at 3.8 μm, Table LIII or on CaF_2 at 5.3 μm, Table LV). Structural and growth rate data may be used to establish correlations among these properties, but further work is needed to determine repeatability and ascertain the effects of deposition variables. This work is presently being carried out and will be reported in the open literature.

5.0 CONCLUSIONS AND RECOMMENDATIONS

General conclusions and recommendations for further work based on the findings of this investigation are presented here.

5.1 CONCLUSIONS

1. Substrate Materials

CaF_2 and SrF_2 are essentially equivalent in absorptance for the DF wavelength region (3.9 μm ± 0.15 μm) with a mean total absorption coefficient of $(1.4 \pm 0.2) \times 10^{-4}$ cm^{-1} for three orientations of the two materials. There is a definite advantage to SrF_2 for the CO wavelength region $(8.3 \pm 1.4) \times 10^{-5}$ cm^{-1}; the mean total absorptance of CaF_2 is $(4.35 \pm 0.4) \times 10^{-4}$ cm^{-1}, a difference by more than a factor of five.

2. Substrate Surface Chemistry

Substrate (CaF_2) surface absorptance is strongly affected by cleaning procedures, especially glow discharge bombardment in vacuum. Effects vary significantly with substrate orientation (110) or (111), glow discharge medium (Argon or oxygen), and subsequent exposure to ambient atmosphere. Laser calorimetery is a more sensitive indicator of these changes than Auger electron spectroscopy. The effects are still not completely understood.

3. Coating Material Selection

On the basis of the optical properties information generated in this investigation, the most promising coating materials for the 3.8 μm region (DF) are PbF_2, ThF_4, SiO, ZnSe, and ZnS. Resistance of SiO and thin layers of ThF_4 to chemical attack by wet HF vapor is reasonably satisfactory;

the other three materials have poor survivability in this medium. Although LaF_3 was found to have very high absorptance at 3.8 μm, due to a high level of LaOF in the raw material, it could be a potential replacement for ThF_4 if a source of pure material could be located. Al_2O_3 has high absorptance at 3.8 μm but also has the best survivability in wet HF vapor and is thus still a candidate for use in the HF band (2.7 μm). The most promising coating materials for the CO laser wavelength region (5.3 μm) are PbF_2, ThF_4, ZnSe, and ZnS. SiO is a poor choice, based upon high absorptance in this region.

4. Variation of Coating Absorptance with Substrate Orientation

Differences in single layer coating absorptance correlating with substrate orientation have been documented. These differences amount to factors of two to four in some cases, which is outside the bounds of experimental uncertainty (10 to 20% as a worst case); these variations are strongest in LaF_3, PbF_2, ThF_4, MgO, SiO, and ZnSe at 3.8 μm and with PbF_2, ThF_4, and ZnSe at 5.3 μm. Variations with substrate orientations are least strong for MgF_2, Al_2O_3, and ZnS at 3.8 μm and for SrF_2 and ZnS at 5.3 μm. Systematic studies of absorptance vs. film thickness (βL vs. L) provide a sensitive and reliable method for establishing these variations in single layer films of most materials; ThF_4 provides a notable and important exception to this statement.

5. Variation of Coating Structure And/Or Preferred Orientation With Substrate Orientation

Differences in preferred orientation or structure of thin films correlating with substrate orientation have been documented for the majority of the materials studied. Variations in preferred orientation (of the same structure type) are by far the more common. An actual difference in crystal

structure has been documented for ZnSe, which is cubic on (100) and (110) CaF_2 and SrF_2, and hexagonal on (111) orientations of both materials. The most marked differences in preferred orientation and crystallinity are observed in LaF_3, PbF_2 on SrF_2 substrates, ThF_4, and ZnS. The smallest differences occur in MgF_2 on SrF_2 substrates, PbF_2 on CaF_2 substrates, SrF_2 on CaF_2 substrates, and Al_2O_3 on all substrates.

6. Effects of Polycrystalline Substrates on Coating Structure and Properties

In studies of single layer PbF_2, ThF_4, SiO, and ZnSe coatings on polycrystalline CaF_2 substrates having a strong preferred orientation, it is found that film structure is very similar to that on single crystal substrates of the same orientation in all cases. Absorptances of the films on polycrystalline substrates are equal to those on single crystal substrates within 30% or less in all cases except SiO, in which the difference is significant (a factor of 3). The behavior of PbF_2, ThF_4, and ZnSe is according to expectations; that of SiO is not. The latter difference in absorptance may be fortuitous.

7. Structure and Absorptance in Multilayer Coatings - Correlation With Single Layer Data

Good correspondence of structure and preferred orientation of the first layer (deposited on the bare substrate) of a multilayer coating with single layer structure on a similarly oriented substrate is observed, as expected. This degree of correspondence is not observed with the second layer in either ThF_4/PbF_2 or ThF_4/SiO antireflection coatings. The fact that the first-deposited layer forms a different effective substrate environment for the second layer provides an excellent physical reason for this observation. Correlation of measured absorptance in AR coatings with values calculated from single layer data is not as close as expected. It is not clear at this

point whether the observed structural differences are responsible for these results or whether they arise from other sources such as raw material impurities or deposition conditions.

5.2 RECOMMENDATIONS

1. Substrate Chemistry

Further work is sorely needed to elucidate the effects of glow discharge cleaning of (100), (110), and (111) orientations of SrF_2 substrates. Laser calorimetry at HF, DF, and CO wavelengths, combined with judicious use of X-Ray and electron diffraction, Auger electron spectroscopy, and/or attenuated total reflection spectroscopy (ATR) would provide the most sensitive indications of changes in the near-surface impurity spectrum.

2. ThF_4

Absorptance of this material as presently available from suppliers exceeds values measured prior to initiation of this investigation, at both 3.8 μm and 5.3 μm. In addition, the behavior of the material in βL vs. L experiments is erratic, unlike that of PbF_2 and SiO. These problems have given rise to excessive absorptance in multilayer coatings utilizing ThF_4. An investigation of fabrication, purification, or pre-coating treatment of the raw material or the selection of a substitute (e.g. pure LaF_3) and location of a suitable source is recommended.

3. Absorptance vs. Film Thickness

It is recommended that this method of determining the absorption coefficient of thin film materials be extended to ZnSe and ZnS, and to other wavelengths such as CO, CO_2, and HF laser bands. Although the method requires acquisition and reduction of a fair amount of data, it has one advantage in

providing a more firm statistical base than measurements on single, half-wave films and another in the capacity for separating out substrate surface contributions and spotting erratic values for a certain material or in a specific coating run.

4. Extensions; Further Work

It is recommended that systematic investigations of this type be applied to other wavelength regions (e.g. HF) additional substrate materials (e.g. Al_2O_3 and ZnSe), and alternative coating deposition methods and conditions (e.g. sputtering, ion beam deposition). Effects of substrate orientation, for example, would be expected to be much stronger with Al_2O_3, which exhibits strong optical anisotropy; although this material is a candidate substrate for the HF wavelength region, this effect has not been investigated.

6.0 REFERENCES

1. M. Sparks and H. C. Chow, "High Power 2 to 6 μm Window Materials Figures of Merit with Edge Cooling and Surface Absorption Included," J. Appl. Phys., Vol. 45, p. 1510 (1974).

2. S. K. Dickerson, Infrared Laser Window Materials Property Data for ZnSe, KCL, NaCl, CaF_2, SrF_2, and BaF_2, AFCRL-TR-75-0318 (1975).

3. R. T. Newberg and J. Pappis, "The Fabrication of Fluoride Laser Windows by Fusion Casting," presented at the Fifth Conference on Infrared Laser Window Materials, Las Vegas, Nevada, Dec. 1-4, 1975.

4. P. Kraatz, S. J. Holmes, and A. Klugman, "Absorptance of Alkaline Earth Fluoride Windows at CO Laser Wavelengths," presented at the Fifth Conference on Infrared Laser Window Materials, Las Vegas, Nevada, Dec. 1-4, 1975.

5. M. Monsler, "High Power Optics," in W. R. Sooey, Ed., "Optical Design Problems in Laser Systems," Proc. of Seminar, Society of Photo-Optical Instrumentation Engineers, Vol. 69, pp. 95-106, San Diego, 1975.

6. S. J. Holmes and P. Kraatz, "Investigation of Crystal Orientation Influence on Thin Film Coatings for CaF_2 Laser Windows" AFML Technical Report TR-75-188, Air Force Materials Laboratory, Wright-Patterson Air Force Base, Ohio 45433, (1975).

7. D. A. Brine and R. A. Young, "X-Ray Diffraction Studies of Crystal Orientations in Thin Films", in Seventh National Symposium on Vacuum Technology, Transactions, C. R. Meissner, Editor, American Vacuum Society (Pergamon Press, N. Y.) pp. 250-259, (1960).

8. E. Bauer, "Reflection Electron Diffraction" in Techniques of Metals Research, R. F. Bunshah, Ed., Vol. 11, part 2, Chap. 15, pp 501-509, (1969).

9. Rowe, J. M., Kraatz, P., and Holmes, S. J., "Calorimetric Absorptance Measurements of CaF_2 and SrF_2 at DF and CO Wavelengths," Proc. Eighth Symposium on Optical Materials for High Power Lasers, NBS, Boulder, Colorado, (1976).

10. J. T. Cox and G. Hass, "Antireflection Coatings for Germanium and Silicon in the Infrared", J. Opt. Soc. Amer., Vol. 48, p. 677 (1958).

11. G. Hass, and E. Ritter, "Optical Film Materials and Their Applications", J. Vac. Sci. and Tech., Vol. 4, p. 71 (1966).

12. Electron-Beam Technology, Airco-Temescal, Berkeley, California (1973).

13. M. G. Inghram, "Detection of Impurities", in Solid State Physics, L. Marton, Editor, Vol. 6, Chap. 2, Academic Press, N.Y., (1959).

14. J. F. Hall and W. F. C. Ferguson, "Optical Properties of Cadmium Sulfide and Zinc Sulfide from 0.6 microns to 14 microns", JOSA, Vol. 45, p. 714 (1955).

15. R. J. Mattauch, "A Simple Vacuum Substrate Heater", Rev. Sci. Inst., Vol. 43, p. 148, (1972).

16. M. M. Hanson, P. E. Oberg, and C. H. Tolman, "Substrate-Temperature Measurement and Control", J. Vac. Sci. and Tech., Vol. 3, p. 277, (1966).

17. G. Hass and C. D. Salzberg, "Optical Properties of Silicon Monoxide in the Wavelength Region from 0.24 to 14.0 Microns", JOSA, Vol. 44, p. 181 (1954).

18. W. Steckelmacher, in Thin Film Microelectronics, L. Holland, Editor, p. 193, John Wiley & Sons, Inc., New York (1965).

19. K. H. Behrndt, in Physics of Thin Films, G. Hass and R. E. Thun, Editors, Vol. 3, p. 1, Academic Press, New York, (1966).

20. A. P. Bradford, G. Hass, and M. McFarland, "Optical Properties of Evaporated Magnesium Oxide Films in the 0.22-8 μm Wavelength Region," Appl. Opt., Vol. 11, p. 2242 (1972).

21. G. Hass, J. B. Ramsey, and R. Thun, "Optical Properties of Various Evaporated Rare Earth Oxides and Fluorides," J. Opt. Soc. Amer. 49 , 116, (1959).

22. J. T. Cox, G. Hass, and J. B. Ramsey, "Improved Dielectric Films for Multilayer Coatings and Mirror Protection", J. Phys., Vol. 25, pp. 250-254, (1964).

23. M. Born and E. Wolf, Principles of Optics, 2nd Edition, p. 63, Macmillan Company, New York, (1964).

24. A. C. S. van Heel and W. van Vonno, "The Rapid and Precise Determination of the Optical Thickness of Thin Coatings in a Vacuum," Appl. Opt., Vol. 6, p. 793, (1967).

25. E. Ritter and R. Hoffmann, "Influence of Substrate Temperature on the Condensation of Vacuum Evaporated Films of MgF_2 and ZnS", J. Vac. Sci. and Tech., Vol. 6, p. 733, (1969).

26. O. S. Heavens, "Optical Constants of Thin Films", in Physics of Thin Films, G. Hass and R. Thun, Editors, Vol. 2, p. 231, Academic Press, New York (1964).

27. F. Abele's, "Optics of Thin Films," in Advanced Optical Techniques, A. C. S. van Heel, Editor, Chap. 5, p. 174, John Wiley & Sons, Inc., New York, (1967).

28. R. Weil, "Calculations of Small Absorption Coefficients From Calorimetric Experimental Data", Appl. Phys., Vol. 41, p. 3012, (1970).

29. J. S. Loomis, "Absorption in Coated Laser Windows", Appl. Opt. Vol, 12, p. 877, (1973).

30. P. Kraatz, and P. J. Mendoza, "CO Laser Calorimetry for Surface and Coating Evaluation", Proc. Fourth Conf. on Infrared Laser Window Materials, p. 77, (1975).

31. T. F. Deutsch, "Research in Optical Materials and Structures for High Power Lasers", Final Technical Report, Raytheon Research Division, ARPA Order 1180 (1973).

32. Loomis, J. S., "Computing the Optical Properties of Multilayer Coatings", Air Force Weapons Laboratory Technical Report No. AFWL-TR-75-202, September, 1975.

33. Gross, R. W. F., and Bott, J. F., Eds. Handbook of Chemical Lasers, Wiley, N. Y. pp. 236-237 (1976).

34. Spencer, D. J., Beggs, J. A., and Mirels, H., "Small Scale CW HF (DF) Chemical Laser", J. Appl. Phys., Vol. 48, pp. 1206-1211, (1977).

35. R. C. Evans, An Introduction to Crystal Chemistry, 2nd Ed., Cambridge University Press, London (1964).

36. A. F. Wells, Structural Inorganic Chemistry, 3rd Ed., Oxford University Press, London (1962).

37. C. S. Barrett and T. B. Massalski, Structure of Metals, McGraw-Hill, New York (1966).

38. R. W. G. Wyckoff, Crystal Structures, Vol. 1, 2nd Ed. (1963).

39. E. G. Chernevskaya and G. V. Ananeva, "Structure of Mixed Crystals Based on CaF_2, SrF_2 and BaF_2, "Soviet Physics-Solid State," Vol. 8, pp. 169-171 (1966).

40. J. F. Nye, Physical Properties of Crystals, Oxford University Press, Press, London (1957).

41. W. L. Phillips, Jr., "Deformation and Fracture Processes in Calcium Fluoride Single Crystals," J. Amer. Cer. Soc. 44, 499-506, (1961).

42. E. Schmid and W. Boas, Plasticity of Crystals, Hughes, London (1950).

43. T. S. Liu and C. H. Li, "Plasticity of Barium Fluoride Single Crystals," J. Appl. Phys., Vol. 35, pp. 3325-3330 (1964).

44. J. J. Gilman, "Direct Measurements of the Surface Energies of Crystals, "J. Appl. Phys., Vol. 31, pp, 2208-2218 (1960).

45. P. Kraatz and T. Zoltai, "Cleavage Surface Energy of the ((111)) Plane of Strontium Fluoride," J. Appl. Phys., Vol. 45, pp. 4741-4750 (1974).

46. M. J. Soileau, "Surface Preparation and Characterization of HEL Components," Third Conference on High Power Infrared Laser Window Materials, AFCRL-TR-0085 (111), 841 (1974).

47. R. W. G. Wyckoff, Crystal Structures, 2nd Ed, Vol. 2, Wiley, N. Y. (1964).

48. ASTM Powder Diffraction File: Card No. 6-0290.

49. ASTM Powder Diffraction File: Card No. 16-160.

50. P. W. Black and J. Wales, "Materials for Use in the Fabrication of Infrared Interference Filters," Infrared Physics, Pergamon Press Ltd., Great Britain, Vol. 8, pp. 209-222 (1968).

51. E. Ritter, "Dielectric Film Materials for Optical Applications," in Physics of Thin Films, edited by G. Hass, M. H. Francombe and R. W. Hoffman, Vol. 8, pp. 1-49, Academic Press, N. Y. (1975).

52. A. E. Ennos, "Stress Developed in Optical Film Coatings," Appl. Opt., Vol. 5, p. 51 (1966).

53. M. A. Gisin, "Optical Constants of Thin Strontium Fluoride Films," Optics and Spectroscopy, Vol. 27, p. 194 (August 1969).

54. ASTM Powder Diffraction File Card Nos. 23-1423 and 23-1426.

55. M. Braunstein and J. E. Rudisill, "Polishing and Coating of Large Diameter High Energy ZnSe Windows and Coatings for Alkali-Halide Windows," Proc. Fourth Annual Conf. on Infrared Laser Window Materials, 1975.

56. W. Heitmann and E. Ritter, "Production and Properties of Vacuum Evaporated Films of Thorium Fluoride, "Appl. Opt., Vol. 7, p. 307 (1968).

57. M. O. Aboelfotoh, K. C. Park, and W. A. Pliskin, "Infrared and High-High-Energy Electron Diffraction Analyses of Electron-Beam-Evaporated MgO Films" J. Appl. Phys. V. 48, pp. 2910-2917, 1977.

58. A. P. Bradford, G. Hass, and M. McFarland, "Optical Properties of Evaporated Magnesium Oxide Films in the 0.22 - 8 μm Wavelength Region," Appl. Opt. V l. 11, -. 2242 (1972).

59. S. S. Ballard and K. A. McCarthy, Optical Materials for Infrared Instrumentation," University of Michigan Press, 1961.

60. C. S. Sahagian and C. A. Pitha, "Compendium on High Power Infrared Laser Window Materials," AFCRL-72-0170 (1972).

61. G. Hass and C. D. Salzberg, "Optical Properties of Silicon Monoxide in the Wavelength Region from 0.24 to 14.0 Microns," JOSA, Vol. 44, p. 181 (1954).

62. K. H. Behrndt, "Influence of the Deposition Conditions on Growth and Structure of Evaporated Films," Vacuum, Vol. 13, pp. 337-347 (1963). Pergamon Press Ltd., Great Britain.

63. ASTM Powder Diffraction File Card Nos. 18-1170, 14-260.

64. ASTM Powder Diffraction File Card No. 5-0565.

65. ASTM Powder Diffraction File Card No. 5-0522.

66. ASTM Powder Diffraction File Card. No. 15-105.

67. K. H. Behrndt and D. W. Doughty, "High-Reflectance Multilayer Dielectric Mirrors," J. Vac. Sci. and Tech., Vol. 4, p. 199 (1966).

68. Optical Material Bulletin," Raytran ZnSe, "Raytheon Research Division, Waltham, Mass., 1975.

69. ASTM Powder Diffraction File Card No. 5-0492.

70. ASTM Powder Diffraction File Card No. 5-0566.

71. ASTM Powder Diffraction File Card No. 12-688.

72. A. R. Verma and P. Krishna, "Polymorphism and Polytypism in Crystals" Wiley, NY, 1966.

73. ASTM Powder Diffraction File Card No. 20-1437.

74. ASTM Powder Diffraction File Card No. 4-0864.

75. ASTM Powder Diffraction File Card No. 6-0262.

76. J. F. Hall and W. F. C. Ferguson," Optical Properties of Cadmium Sulfide and Zinc Sulfide from 0.6 Microns to 14 Microns," JOSA, Vol. 45, p. 714 (1955).

77. R. J. Scheuman, "Stresses in Dielectric Films," Thin Film Dielectrics, Edited by F. Vratny, p. 714, The Electrochemical Society, Inc., New York, 1969.

78. P. A. Young, "Thin Films for Use on Sodium Chloride Components for Carbon Dioxide Lasers," Thin Solid Films, Vol. 6, p. 423, (1970).

79. J. T. Cox, J. E. Waylonis, and W. R. Hunter, "Optical Properties of Zinc Sulfide in the Vacuum Ultraviolet," JOSA, Vol. 49, p. 807 (1959).

80. ASTM Powder Diffraction File Card No. 23-1426.

81. ASTM Powder Diffraction File Card No. 9-304.

82. ASTM Powder Diffraction File Card No. 12-96.

83. ASTM Powder Diffraction File Card No. 2-29.

7.0 APPENDIX: Surface Chemistry and Absorptance of CaF_2 at HF, DF, and CO Wavelengths.

SURFACE CHEMISTRY AND ABSORPTANCE OF CaF_2 AT HF, DF AND CO WAVELENGTHS*

P. KRAATZ AND S. J. HOLMES

NORTHROP CORPORATION
Northrop Research and Technology Center
Hawthorne, California 90250

ABSTRACT

The relative importance of bulk and surface contributions to absorptance in transmitting optics at DF and CO wavelengths has recently been discussed, with the observation that the surface contribution may be as much as 15 times that of the bulk.[1] The nature of changes in surface absorption and surface chemistry associated with such processes as cleaning with organic solvents or vacuum glow discharge have not been fully explained.[1,2] To elucidate some aspects of these problems, we report results of some investigations employing Auger electron spectroscopy (AES) in conjunction with HF, DF, and CO laser calorimetry. It has been found that the effects of vacuum glow discharge cleaning and subsequent exposure to ambient atmosphere vary markedly with the nature of the gas employed (reactive, e.g. Oxygen, or inert, e.g. Argon) and with the crystallographic orientation and specific surface free energy of the sample surfaces, as well with the laser wavelength employed in calorimetric measurements. Results of experiments in which these parameters are varied are discussed in the light of parallel AES studies.

*Work supported by DARPA under Navy Contract No. N00123-76-C-1321.

INTRODUCTION

Processes contributing to changes in the surface component of absorptance of the alkaline earth fluorides in the middle infrared region of the spectrum are not well understood.[1,2] Various solvent cleaning procedures, as well as vacuum glow discharge and exposure to the ambient atmosphere may profoundly influence this property in wavelength regions of interest for high power chemical (HF, DF) and CO lasers operating nominally at 2.8, 3.8, and 5.3 μm, respectively. In the present work, elucidation of some effects of glow discharge cleaning in an Argon or Oxygen medium, with subsequent exposure to the ambient atmosphere is attempted, utilizing laser calorimetry at HF, DF, and CO wavelengths and Auger electron spectroscopy. In addition, the influence of crystallographic orientation of sample surfaces upon response to these processes is illustrated. Results are discussed in terms of elemental composition of surfaces, their atomic configuration, and specific surface free energy.

2. EXPERIMENTAL METHODS

The laser absorption vacuum calorimeter used to obtain the present Absorptance data was constructed following the general design of Deutsch[3] and has been described in detail elsewhere.[4] The only change in the apparatus since the

previous description has been the addition of a CW HF/DF chemical laser and suitable AR coated windows for the calorimeter box when working at the chemical laser wavelengths. The chemical laser itself has also been described in detail elsewhere.[5] Maximum available DF power is 11 Watts, but 1 to 3 Watts was sufficient for calorimetric measurements on the small (1 in. diameter x 1/4 in. thick) samples employed in this study. An irradiation time of 2 to 3 minutes at these power levels was adequate for absorptance measurement. The calorimeter is liquid nitrogen trapped and was evacuated to a pressure of 0.08 to 0.15 Torr during measurements. Samples were irradiated at 3 different wavelengths in succession without breaking vacuum, in an absorptance determination comprising irradiation with HF, DF, and CO lasers.

Auger electron spectroscopy (AES) analyses were carried out in a Physical Electronics unit equipped with a sputter ion gun capable of sputter etching a specimen while simultaneously monitoring the AES signal. Since this system must operate in a vacuum of 10^{-9} to 10^{-10} Torr, pumpdown times are substantial, placing a practical lower limit of about 12 hours on the interval between analyses of samples exposed to different environmental conditions. Samples for Auger analysis were subjected to the various surface processing operations simultaneously with those samples

prepared specifically for absorptance measurements and were exposed to the ambient (laboratory) atmosphere for comparable total times following these operations.

All AES analyses were carried out with a primary 2 keV electron beam to avoid problems of surface charge buildup on the insulating CaF_2 samples. Even at this low beam energy, simultaneous sputter etching and AES profiling could be carried only to depths of a few hundred Ångstroms due to charge build-up and resultant peak displacement. Auger peaks for Calcium and Fluorine and common surface contaminants such as Oxygen, Nitrogen and Sulfur were monitored. The carbon peak, which is of intense interest in a study of this nature, unfortunately could not be resolved due to its proximity to the large calcium peak on CaF_2 surfaces. Repetition of the experiments on SrF_2 surfaces would be useful in this regard.

Surface cleaning processes investigated in the present work are similar to those employed previously.[1,2] They comprise a solvent cleaning procedure and glow discharge cleaning procedure. These may be described briefly as follows:

Solvent Cleaning Procedure

(1) Soak in acetone (30 minutes).
(2) Rinse with warm tap water.
(3) Wash with warm tap water and liquid detergent.
(4) Rinse with distilled water.
(5) Rinse with reagent grade alcohol.
(6) Blow dry with nitrogen gas.

Glow Discharge Cleaning Procedure

(1) Solvent clean, as above, place in vacuum chamber.
(2) Pump out chamber to ~ 5×10^{-6} Torr (1 Hr.). Heater on (200°C).
(3) Glow discharge 3 minutes at 200 mA in 2×10^{-2} Torr of Argon.
(4) Heater off. Valve shut. (10^{-4} Torr range).
(5) Sample cools to ambient (1 Hr.).
(6) Remove sample from glow discharge chamber, place in laser calorimeter following equilibration to room temperature (20-30 min.).
(7) Pump out calorimeter

In a variation of the argon glow discharge procedure to test the effect of a reactive atmosphere, oxygen was substituted for argon, with all other parameters held constant.

The basic experiments reported here involved solvent cleaning of two groups of samples, followed by calorimetric absorptance measurement and Auger electron spectroscopy. One group of samples was subsequently glow discharge cleaned in an argon medium and the other in an oxygen medium. Following these processes, changes in

absorptance with exposure to ambient atmosphere were monitored at HF(2.8 μm), DF(3.8 μm) and CO(5.3 μm) wavelengths. Elemental composition of sample surfaces was monitored with AES. Argon ion milling within the Auger system was utilized to determine the depth of coverage and tenacity of contaminant species upon CaF_2 surfaces. Each group of samples was composed of equal numbers of (111) and (110) orientations to determine the influence of crystallographic orientation upon contaminant composition and optical absorption.

RESULTS

Effects of Argon glow discharge cleaning upon optical absorptance are illustrated in Table I and figures 1 and 2. In these figures, each symbol represents the mean of 5 or more absorptance measurements with error bars representing the experimental dispersion (standard deviation). Symbols lacking error bars represent results in which experimental dispersion plots within the size of the symbol employed.

At 5.3 μm, total absorptance (β_T) of samples with surfaces oriented parallel to (111) decreases approximately 25% relative to the solvent-cleaned value after 0.5 and 4.5 hours exposure to ambient atmosphere. The apparent decrease is approximately 31% following 22 hours exposure, but this difference is not significant due to experimental dispersion. At 3.8 μm, the initial decrease is approximately 43% going to 38% in 4.5 hours and 57% in 22 hours. The latter decrease is statistically significant. At 2.8 μm, we see a 20% decrease, relative to the freshly glow discharge cleaned value, in 4.5 hours remaining constant over 22 hours exposure to ambient atmosphere.

For samples with surfaces oriented parallel to (110), behavior is quantitatively and qualitatively different. At 5.3 μm, glow discharge cleaning produces an immediate decrease of 12%, followed by an increase of 21% after 6 hours

exposure, relative to the value for the solvent cleaned sample. After 24 hours, the absorptance is within 9% of the solvent cleaned value. At 3.8 μm, an initial decline of 47% is followed by an increase of 41% after 6 hours exposure relative to the solvent cleaned sample. At 24 hours, the absorptance is 7% below the value for the solvent cleaned sample, which is within the standard deviation of the measurements. At 2.8 μm, the absorptance increases by 86%, relative to the freshly glow discharged condition, within 6 hours. The absorptance subsequently decreases to within 57% of this value after 24 hours exposure. For both crystallographic orientations, highest absorptances are at 5.3 μm and 2.8 μm, while the lowest absolute values and greatest initial decreases are seen at 3.8 μm, for glow discharge cleaning in an inert gas.

Results for a similar series of experiments, utilizing a reactive glow discharge medium (oxygen) are shown in Table II and figures 3 and 4. It is clear that these results differ radically from those in which an inert glow discharge medium was employed and again the response of (111) and (110) surfaces differs markedly. In all cases absorptance at 2.8 μm is greatest, followed by 5.3 μm, while that at 3.8 μm is a minimum.

On (111) surfaces of CaF_2, 5.3 μm absorptance decreases approximately 21%, relative to the solvent cleaned value, after oxygen glow discharge and 3 hours exposure to ambient. This decrease is essentially constant at 26% after 20 hours. At 3.8 μm, the corresponding values are 46% and 50% decreases, respectively. At 2.8 μm, absorptance values after 3 hours and 20 hours ambient exposure are indistinguishable, within experimental precision.

On (110) surfaces of CaF_2, the situation is entirely different: At 5.3 μm, absorptance increases by 11% within 20 minutes after oxygen glow discharge cleaning and remains 3% higher than the solvent cleaned value after 20 hours. At 3.8 μm, an initial decrease of 3% becomes 27% after 20

hours exposure to ambient. At 2.8 μm, values are again high and essentially indistinguishable after 20 minutes or 20 hours.

Auger results are most conveniently expressed in terms of the ratio of oxygen to calcium peak heights, since oxygen is probably the most directly related to mid IR absorptance of the elements monitored. (As noted previously, Carbon could not be monitored due to masking by the calcium peak.) In general, all AES traces showed sulfur, nitrogen, oxygen, and strontium in addition to calcium and fluorine in scans of surfaces which were either solvent or glow discharge cleaned with Argon before insertion in the system. Nitrogen was absent from samples exposed to oxygen glow discharge. Argon ion milling to a depth of a few hundred Ångstroms within the AES system removed sulfur and nitrogen in all cases and significantly changed the relative peak height of oxygen in some cases, to be discussed later. The strontium peak height was unchanged by ion milling, indicating that it is a bulk impurity in the CaF_2.

Oxygen to calcium ratios are shown in table III for solvent cleaned samples and those subjected to Argon or oxygen glow discharge. Results for Argon glow discharge cleaning are plotted in figure 5 and for oxygen glow discharge in figure 6. Error bars represent the approximate ± 10% expected precision in the experimental O/Ca ratios. Comparison with absorptance results plotted in figures 1 - 4 shows poor correlation, except in isolated cases; e.g. the 20% reduction in O/Ca ratio on (111) CaF_2 following oxygen glow discharge cleaning is similar to the 21% reduction in absorptance at 5.3 μm shown in table II. In general, the trend of the Auger results is toward increasing O/Ca ratio with time of exposure to ambient, except in the case of (110) CaF_2 surfaces subjected to Argon glow discharge cleaning, which show a decrease. Most changes, howevever, are not significant relative to the solvent cleaned or initial glow discharge values, when experimental dispersion is taken into account.

On the other hand, the results of profiling surfaces using Argon ion milling within the Auger system are more interesting. Results of this operation are illustrated in Table IV. Due to the highly insulating character of the CaF_2 surfaces, monitoring of AES peaks during ion milling was precluded by static charging effects in all but the single case noted in table IV. Hence, it was necessary to take an initial and final scan following the milling operation. The final scan thus does not accurately represent the uncontaminated CaF_2 surface, since some oxygen is redeposited in the time (5-10 minutes) required for stabilization of the charged surface. However, the amount of oxygen redeposited apparently differs markedly with the nature of the crystal surface and its history.

For example, we see that for (110) surfaces subjected to Argon glow discharge cleaning and 1/2 hour in the ambient atmosphere, the final O/Ca ratio after milling is reduced by a factor of four below the initial value. On the other hand for (111) surfaces treated similarly, the reduction is by a factor of ten. For Argon glow discharged (110) surfaces exposed to the ambient for 26 hours, a net increase in O/Ca ratio follows ion milling on (110) and a reduction by a factor of two occurs on (111). For oxygen glow discharged (110) surfaces with 1/2 hour ambient exposure, the decrease is by a factor of only 1.6, while for (111) there is a slight, but insignificant increase. For oxygen glow discharged surfaces exposed to ambient for 30 hours, the maximum decrease is only 36% on a scan taken during milling. A final scan for the (111) surface could not be obtained.

DISCUSSION

Optical absorptance of CaF_2 in the middle infrared, as determined by laser calorimetry at 2.8, 3.8, and 5.3 μm, is found to vary significantly with the nature of the glow discharge medium (reactive or inert), time of subsequent exposure to the ambient atmosphere, and the crystallographic orientation of the optical surfaces tested. These changes show no real correlation with surficial O/Ca ratios

determined by AES, indicating either that the differences arise from contaminants other than oxygen (e.g. hydrocarbons) or that they arise from variations in the state of aggregation of oxygen atoms on the surfaces. Ion milling experiments provide tentative evidence favoring the latter hypothesis.

Differences in behavior with crystallographic orientation are most readily examined in relation to the details of structure and physical properties of those surfaces. The arrangement of atoms in the (111) and (110) surfaces of CaF_2 is illustrated in figure 7, taken from Phillips.[6] In this figure, the large circles represent fluorine ions and the small circles represent calcium ions. The (111) surface is the natural cleavage plane of CaF_2 and is thus electrically neutral.[7] Examination of experimentally determined electron density distributions in CaF_2 shows overlap between F^- ions in the [100] and [110] directions, but none in the [111] direction,[8] indicating that the breaking of bonds in the former two directions gives rise to free charges while breaking of [111] bonds does not. In addition, consideration of the specific surface free energy (i.e. the energy required to create new surface of unit area by a reversible process of cutting) of (111) and (110) surfaces of CaF_2 indicates that the surface energy of the (110) surface is approximately double that of the (111) surface.[9] Hence, we may conclude that the (110) surface of CaF_2 is more reactive than the (111) surface. This is also supported by the ion milling results reported in Table IV.

Time dependence of absorptance upon exposure to ambient atmosphere may be explained using these properties of the surfaces involved. Following Argon glow discharge cleaning, (111) CaF_2 surfaces are covered with an oxygen-rich layer which is not too tightly bound, as indicated by the AES results in Tables III and IV. Due to their electrical neutrality, they do not react rapidly with oxygen of the ambient atmosphere. As a consequence, they show no significant increase in absorptance with exposure to ambient atmosphere (fig. 1).

On the other hand, (110) CaF_2 surfaces subjected to an identical process are covered with a more tenacious oxygen-rich layer and react more rapidly with oxygen, as indicated by the data of tables III and IV. Thus, their surfaces are apparently activated by the glow discharge cleaning and react rapidly with oxygen of the ambient atmosphere. Hence, the optical absorptance of these samples increases to a maximum at some point within less than 24 hours following glow discharge cleaning and then decreases to a value approaching that of the solvent cleaned sample in 24 hours. This phenomenon could arise from the formation of more tightly bound and stable oxygen-rich complexes with prolonged exposure of the activated (110) surfaces to the ambient atmosphere. The data of table IV would tend to support this.

An explanation of the oxygen glow discharge effects upon absorptance at (111) and (110) surfaces may be made following similar reasoning. On (111), the process produces an initial decrease in absorptance which remains constant with exposure to ambient, reflecting the relatively non-reactive nature of the surface and the stability of the oxygen-rich complexes formed there (Table IV). On (110), no significant initial decrease in absorptance is produced by the glow discharge, due to the immediate saturation of available bonding sites at the surface and rapid formation of relatively tightly bound and stable oxygen-rich complexes. This is again supported by the data of Table IV. The high absorptance at the 2.8 μm wavelength in the oxygen processed sample also tends to support this hypothesis, due to its usual association with absorption by hydrogen-oxygen complexes (OH or "water-band").

CONCLUSIONS

1. Surface absorptance of CaF_2 in the mid-infrared is influenced by the amount and state of aggregation of impurities (particularly oxygen) absorbed at the surfaces.

2. The (110) surface is more reactive than (111) and exhibits profound positive and negative changes in absorptance when subjected to glow discharge cleaning in an inert atmosphere (Argon) and subsequent exposure to ambient air. Changes following identical processing of (111) surfaces are less marked, involving only an initial decrease in absorptance followed by relative stability with exposure to ambient atmosphere.

3. Glow discharge cleaning of the reactive (110) surface in a reactive medium (oxygen) produces no marked changes in absorptance at any of the three wavelengths monitored. Identical processing of (111) surfaces produces an initial decrease followed by relative stability, as in the case of Argon glow discharge cleaning noted above.

4. Auger electron spectroscopy is apparently not as sensitive to these changes as is laser calorimetry. However, in combination with ion milling, it can provide useful information on the thickness, stability, and tenacity of surficial contaminants.

5. The role of hydrocarbon contaminants, if any, in these surface chemical reactions remains unknown since carbon could not be monitored in the present work due to overlap with the calcium peak on CaF_2.

ACKNOWLEDGEMENTS

The authors wish to thank Mr. T. Remmel and Mr. J. Schifando for the Auger measurements and Dr. J. M. Rowe for helpful discussions of the methodology, particularly the sensitivity of laser calorimetry as an analytical tool.

References

1. Rowe, J. M., Kraatz, P., and Holmes, S. J., "Calorimetric Absorptance Measurements of CAF_2 and SrF_2 at DF and CO Wavelengths," Proc. Eighth Symposium on Optical Materials for High Power Lasers, NBS, Boulder, Colorado, (1976).

2. Kraatz, P., Holmes, S.J., and Klugman, A., "Absorptance of Coated Alkaline Earth Fluoride Windows at CO Laser Wavelengths." Proc. Fifth Conf. on IR Laser Window Materials, DARPA, 1975.

3. T. F. Deutsch, "Research in Optical Materials and Structures for High Power Lasers," Final Technical Report, Contract No. DAAH 01-72-C-0194, ARPA Order No. 1180, Raytheon Research Division, 1973.

4. P. Kraatz and P. J. Mendoza, "CO Laser Calorimetry for Surface and Coating Evaluation," Proc. Fourth Conference on Infrared Laser Window Materials, ARPA, 1974.

5. J. A. Harrington, Final Technical Report, Contract No. DAAH 01-74-C-0438, U. S. Army Missile Command, Redstone Arsenal, Alabama, 1975.

6. W. L. Phillips, Jr. "Deformation and Fracture Processes in Calcium Fluoride Single Crystals" J. Amer. Ceramic Soc. 44, 499-506, 1061.

7. L. G. Berry and Brian Mason, MINERALOGY, Freeman, San Francisco, 1959.

8. H. Witte and E. Wölfel, "Electron Distributions in NaCl, LiF, CaF_2, and Al" Rev. Mod. Phys. 30, 51-55, 1958.

References

9. G. C. Benson and T. A. Claxton, "Calculation of the Surface Energy of the {110} Face of Some Crystals Possessing the Fluorite Structure" Canadian Journal of Physics 41, 1287-1293, (1963).

Table I . Optical Absorptance (β_T) of CaF_2 as affected by Solvent Cleaning and Glow Discharge Cleaning with Argon.

SAMPLE ORIENTATION	λ (μm)	$\beta_T(10^{-4}cm^{-1})$ SOLVENT CLEANED	$\beta_T(10^{-4}cm^{-1})$ FOLLOWING ARGON GLOW DISCHARGE CLEANING & EXPOSURE TO AMBIENT ATMOSPHERE				
			0.5 HR.	4.5 HR.	5.7 HR.	22.0 HR.	24.0 HR.
(111)	5.3	5.81 ± 0.27	4.33 ± 0.17	4.32 ± 0.29	---	3.99 ± 0.17	---
	3.8	3.19 ± 0.20	1.83 ± 0.05	1.97 ± 0.07	---	1.37 ± 0.14	---
	2.8	---	4.90 ± 0.45	3.95 ± 0.30	---	3.91 ± 0.09	---
(110)	5.3	4.77 ± 0.07	4.18 ± 0.19	---	5.77 ± 0.27	---	4.33 ± 0.17
	3.8	1.81 ± 0.06	0.96 ± 0.02	---	2.55 ± 0.12	---	1.68 ± 0.09
	2.8	---	2.67 ± 0.11	---	4.96 ± 0.28	---	4.20 ± 0.13

TableII . Optical Absorptance (β_T) of CaF_2 as Affected by Solvent Cleaning and Glow Discharge Cleaning with Oxygen.

SAMPLE ORIENTATION	λ (μm)	$(10^{-4}cm^{-1})$ SOLVENT CLEANED	$\beta_T 10^{-4}cm^{-1}$) Following Oxygen Discharge Clean & Exposure to Amb. Atm.		
			0.3 HR.	3.3 HR.	20.5 HR.
(111)	5.3	4.42 ± 0.42	---	3.48 ± 0.21	3.28 ± 0.15
	3.8	3.05 ± 0.18	---	1.66 ± 0.12	1.54 ± 0.17
	2.8	---	---	4.06 ± 0.47	4.37 ± 0.27
(110)	5.3	4.26 ± 0.17	4.74 ± 0.19	---	4.39 ± 0.14
	3.8	4.12 ± 0.18	4.00 ± 0.26	---	3.01 ± 0.08
	2.8	---	6.30 ± 0.28	---	6.12 ± 0.31

Table III. Auger O/Ca Ratio (Peak to Peak) Following Solvent and Glow Discharge Cleaning.

SAMPLE ORIENTATION	O/Ca SOLVENT CLEANED	GLOW DISCHARGE MEDIUM	O/Ca FOLLOWING GLOW DISCHARGE AND EXPOSURE TO AMBIENT ATMOSPHERE		
			0.5 HR.	26.0 HR.	30.0 HR.
(110)	0.3704	ARGON	0.4173	0.2926	---
(111)	0.3576	ARGON	0.3090	0.3963	---
(110)	0.3704	OXYGEN	0.2959	---	0.4230
(111)	0.3576	OXYGEN	0.3128	---	0.5390

TABLE IV. EFFECT OF ARGON ION MILLING
UPON OXYGEN CONCENTRATION ON CaF_2 SURFACES

Surface Orientation	Glow Discharge Medium	Exposure to Ambient (Hr)	O/Ca Initial Scan	O/Ca After Ion Milling
(110)	Argon	0.5	0.4173	0.1016
		26.0	0.2926	0.3282
	Oxygen	0.5	0.2959	0.1853
		30.0	0.4230	0.3097*
(111)	Argon	0.5	0.3090	0.0370
		26.0	0.3963	0.1975
	Oxygen	0.5	0.3128	0.3466
		30.0	0.5390	--

*Scan taken during ion milling.

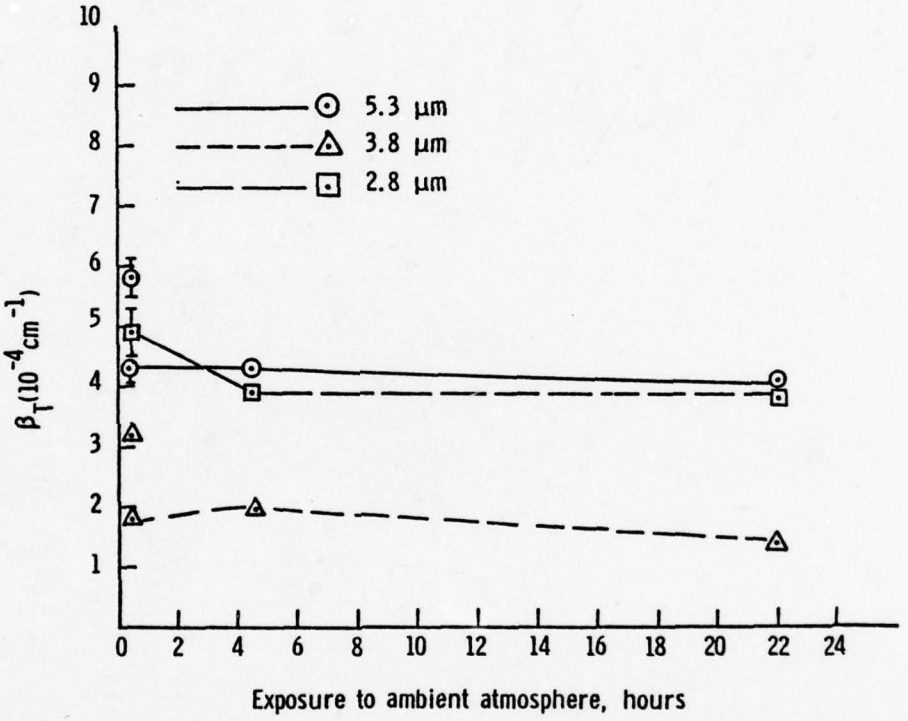

Figure 1 . Changes in Optical Absorptance of (111) CaF_2 Following Argon Glow Discharge Cleaning.

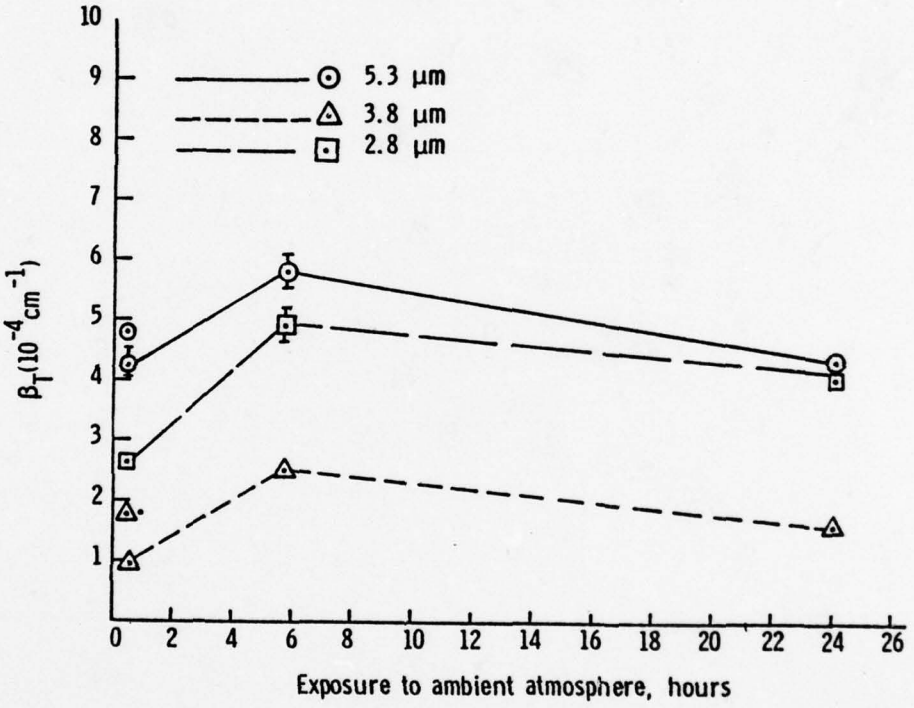

Figure 2. Changes in Optical Absorptance of (110) CaF_2 following Argon Glow Discharge Cleaning.

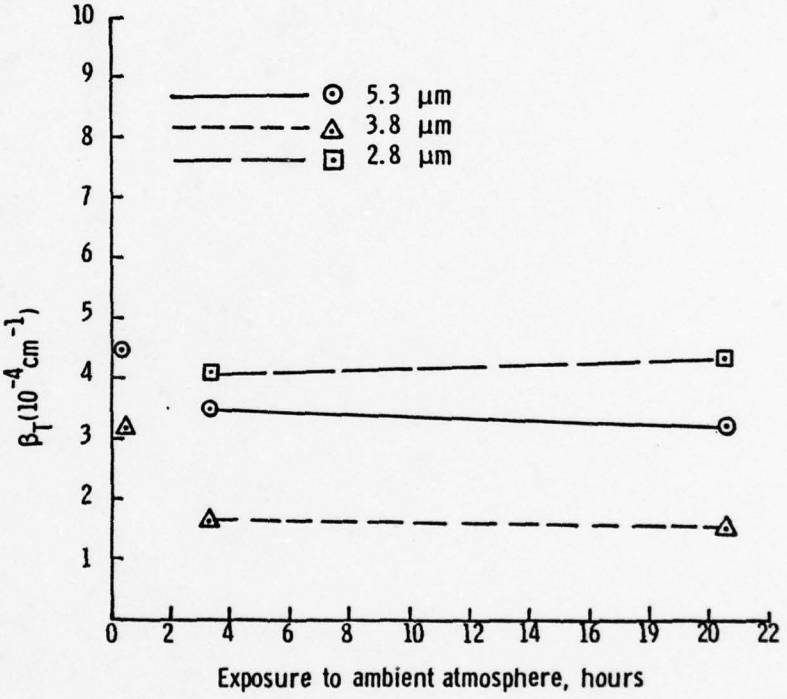

Figure. 3 Changes in Optical Absorptance of (111) CaF_2 Following Oxygen Glow Discharge Cleaning.

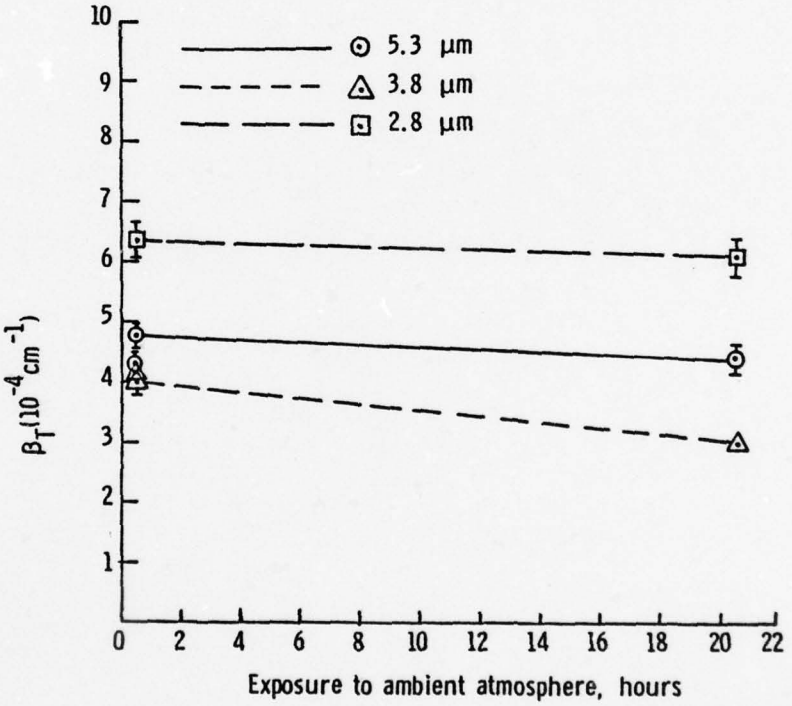

Figure 4. Changes in Optical Absorptance of (110) CaF_2 Following Oxygen Glow Discharge Cleaning.

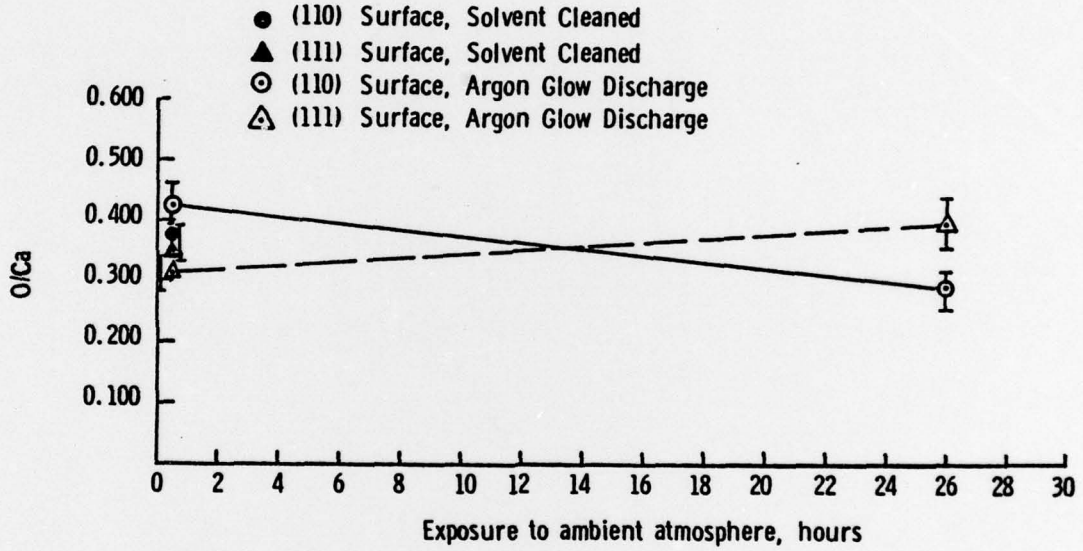

Figure 5. Changes in Auger O/C_a Ratio (Peak to Peak) with Exposure of CaF_2 Surfaces to Ambient Atmosphere Following Argon Glow Discharge Cleaning.

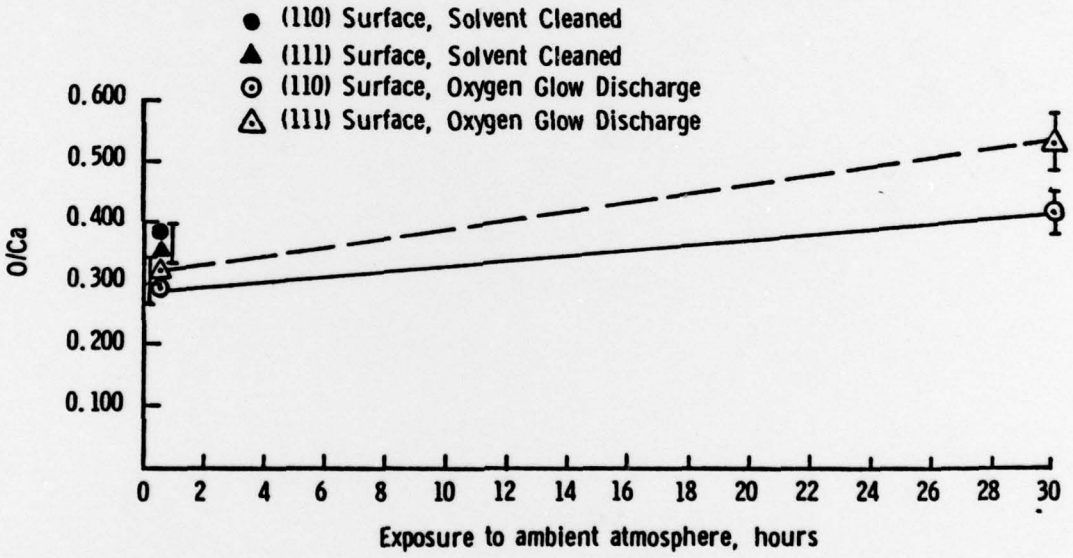

Figure 6. Changes in Auger O/Ca Ratio (Peak to Peak) with Exposure of CaF_2 Surfaces to Ambient Atmosphere Following Oxygen Glow Discharge Cleaning.

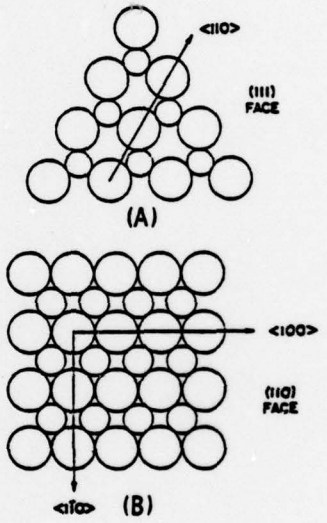

Figure 7. Atomic Configuration of Two Crystallographic Planes of Calcium Fluoride.

(A) - (111), (B) - (110)